GEOLOGICAL SURVEY OF CANADA
COMMISSION GÉOLOGIQUE DU CANADA

BULLETIN 324

This document was produced
by scanning the original publication.

Ce document est le produit d'une
numérisation par balayage
de la publication originale.

STRUCTURE AND METAMORPHISM OF THE APHEBIAN PENRHYN GROUP AND ITS ARCHEAN BASEMENT COMPLEX IN THE LYON INLET AREA, MELVILLE PENINSULA, DISTRICT OF FRANKLIN

J.R. HENDERSON

Canada

1983

BULLETIN 324

STRUCTURE AND METAMORPHISM OF THE APHEBIAN PENRHYN GROUP AND ITS ARCHEAN BASEMENT COMPLEX IN THE LYON INLET AREA, MELVILLE PENINSULA, DISTRICT OF FRANKLIN

J.R. HENDERSON

1983

© Minister of Supply and Services Canada 1983

Available in Canada through

authorized bookstore agents
and other bookstores

or by mail from

Canadian Government Publishing Centre
Supply and Services Canada
Ottawa, Ontario, Canada K1A 0S9

and from

Geological Survey of Canada
601 Booth Street
Ottawa, Ontario, Canada K1A 0E8

A deposit copy of this publication is also available
for reference in public libraries across Canada

Cat. No. M42-324 Canada: $8.00
ISBN 0-660-11485-2 Other countries: $9.60

Price subject to change without notice

Critical Readers

A.V. Okulitch
Peter Nielsen

Scientific Editor

Peter J. Griffin

Original manuscript submitted 1978-06
Final approved for publication 1979-09-15

Preface

During the 1960s as a result of a helicopter reconnaissance of the northern Canadian Shield, an extensive belt of Aphebian metasediments extending from western Melville Peninsula to eastern Baffin Island, was outlined. The presence of these rocks suggests that the area may contain economic mineral occurrences and that it should be considered as a site for base metal and uranium exploration.

This report on the Lyon Inlet area describes the stratigraphy, metamorphism, and structure of early Proterozoic sediments and their Archean basement, and illustrates the complex structural interaction of basement and cover rocks during intense deformation and high grade metamorphism. It is the first of several publications which will describe this entire belt of rocks. By providing a comprehensive understanding of the geology of these metasediments the Geological Survey is able to aid in the discovery and estimation of the potential resources available to Canada from this area.

D.J. McLaren
Director General
Geological Survey of Canada

Ottawa, September 1979

CONTENTS

Tables

Figures

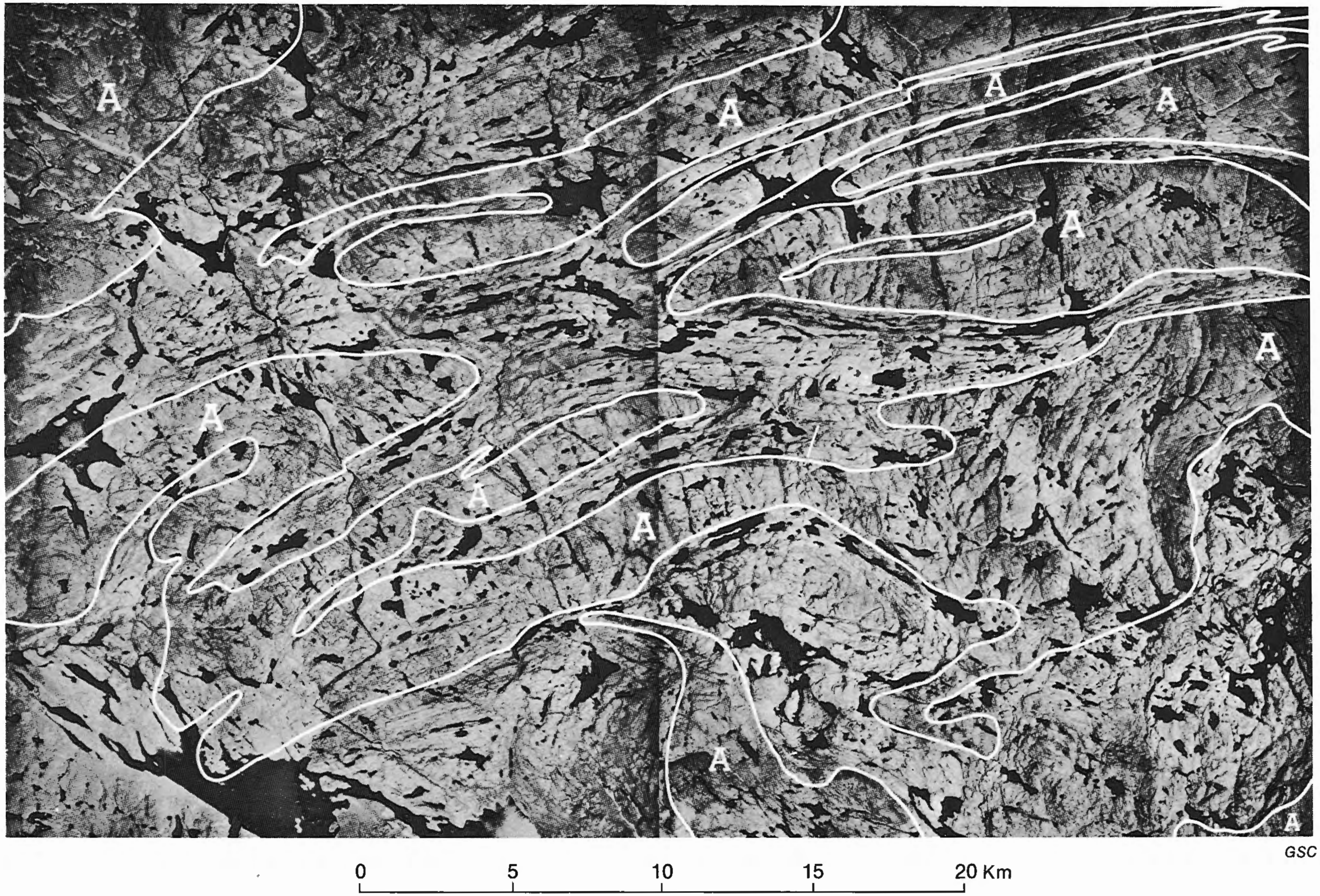

Figure 1. *Frontispiece: Photomap of part of the area north of Lyon Inlet (map areas 46 N/1,2). Note the linear belts of Aphebian Penrhyn Group paragneiss, and the Archean granitoid gneiss massifs (A).*

STRUCTURE AND METAMORPHISM OF APHEBIAN PENRHYN GROUP AND ITS ARCHEAN BASEMENT COMPLEX IN THE LYON INLET AREA, MELVILLE PENINSULA, DISTRICT OF FRANKLIN

Abstract

Southern Melville Peninsula near the head of Lyon Inlet consists mainly of Archean (+2500 Ma old) and Aphebian (1800-2500 Ma old) plutonic and supracrustal rocks that were regionally metamorphosed during the Hudsonian Orogeny about 1800 Ma ago.

The Prince Albert Group comprises the oldest rocks identified in the map area; they formed more than 2900 Ma ago on an unidentified crust. Metagreywacke and metavolcanic rocks compose most of the group; lean siliceous iron formation is a minor component in the Lyon Inlet area. Prince Albert Group rocks were intruded by granitoid batholiths about 2700 and 2500 Ma ago.

During the Aphebian Era Penrhyn Group clastic and chemical sediments accumulated in a shallow, stagnant, hypersaline (?) basin on the Archean crust. At the base of the group a quartz-rich blanket sand was deposited on a discontinuous carbonaceous regolith; it was intercalated in places with some mafic volcanic rocks. A mixed succession of carbonaceous pelitic, psammitic and carbonate sediments formed the remainder of the lower Penrhyn Group. The upper part of the Aphebian sedimentary succession was mainly carbonaceous shale and arkosic wacke. Small amounts of disseminated iron, zinc, and nickel sulphides occur in Penrhyn Group carbonaceous metapelitic rocks.

The earliest documented deformation (D_1) involved recumbent folding and thrusting of Archean basement rocks over Aphebian supracrustal rocks. The Penrhyn Group rocks in the region occur in the breached core of a synclinal nappe. In the northeastern Lyon Inlet area Aphebian supracrustal rocks dip beneath a folded sheet of Archean basement gneiss preserved on the inverted limb of the nappe.

The terminal phase of Hudsonian deformation (D_2) occurred before the time of the regional metamorphic climax when rocks now exposed were buried more than 17 km beneath the surface, and were heated to more than 700°C. In this environment the rocks in the D_1 nappe underwent intense subhorizontal elongation, possibly in response to gravity-induced flowage of rock material out of the deep-seated Lyon Inlet region towards rising crustal diapirs located farther northeast and southwest of Melville Peninsula.

Numerous granitic plutons intruded the region mainly after D_2 ended although small palingenetic granite laminae, sills and dykes formed in metapelitic rocks before the end of penetrative deformation. Some of the postkinematic plutons show anomalously-high levels of uranium radioactivity.

During the Helikian or Hadrynian (between 1100 and 700 Ma ago) the crust in the region was fractured, faulted, and intruded by diabase dykes along vertical northwest-southeast-striking surfaces. By late Middle Ordovician (about 460 Ma ago) the region was denuded to nearly the present level and carbonate sediments of the Bad Cache Rapids Formation were deposited on an erosion surface with several hundred metres of local relief.

The present climate of the region promotes oxidation and leaching of most base metal sulphides from exposed rocks. Abundant limonite-capped gossans in Penrhyn Group pelitic gneiss contain relatively insoluble secondary iron sulphide veins and granular quartz. Lake waters and sediments in the vicinity of the gossans are enriched in Zn, Ni, and Cu.

Résumé

La partie sud de la Péninsule de Melville, en amont de l'Inlet de Lyon, consiste principalement en roches plutoniques et supracorticales de l'Archéen (2500 Ma) et Aphébien (1800-2500 Ma) qui furent métamorphisées pendant l'orogénie hudsonienne il y a environ 1800 Ma.

Le groupe du Prince Albert comprend les roches les plus anciennes identifiées dans cette région; elles furent formées il y a plus de 2900 Ma au-dessus d'une croûte non-identifiée. Des roches métagrauwackeuses et métavolcaniques forment la majeure partie de ce groupe; une étroite formation de fer est une composante peu importante dans la région de l'Inlet de Lyon. Des batholites granitiques datant de 2700 à 2500 Ma pénètrent les roches du groupe du Prince Albert.

Pendant l'Aphébien Era, les sédiments clastiques et chimiques du groupe de Penrhyn s'accumulèrent dans un bassin peu profond, stagnant, hypersalin, sur la croûte archéenne. A la base du groupe, une couverture de sable riche en quartz fut déposée sur un régolithe riche en carbone discontinu, des roches volcaniques mafiques s'y intercalant par endroit. Une succession

mélangée de sédiments pélitiques riches en carbone, psammitiques et carbonatés forme le reste du groupe de Penrhyn inférieur. La partie supérieure de la succession sédimentaire aphébienne est formée surtout de schiste argileux riche en carbone et d'arkose. De petites quantités de sulfures de fer, zinc et nickel disséminés sont présents dans les roches métapélitiques riches en carbone du groupe de Penrhyn.

La plus ancienne période de déformation documentée (D_1) comprit le plissement couché et charriage de roches du socle archéen sur les roches supracorticales aphébiennes. Les roches du groupe de Penrhyn dans la région, sont situées dans le centre mis à nu d'une nappe synclinale. Au nord-est de la région de l'Inlet de Lyon, les roches supracorticales aphébiennes plongent sous une nappe plissée de gneiss du socle archéen préservée dans le flanc renversé de la nappe.

La phase finale de déformation hudsonienne (D_2) est antérieure au maximum de métamorphisme regional, lorsque les roches affleurant à l'heure actuelle étaient enterrées plus de 17 kilomètres sous la surface et atteignirent une température de plus de 700°C. Dans cet environnement, les roches de la nappe D_1 subirent une forte élongation horizontale, provoquée peut-être par l'écoulement induit par gravité, de matériel rocheux provenant de zone profonde, vers des diapires s'élevant plus au nord-est et sud-ouest de la Péninsule de Melville.

De nombreux plutons granitiques sont intrusifs dans la région, surtout après l'épisode D_2, bien que de petites intercalations, sills et dykes de granite palingénétique furent formés dans les roches métapélitiques avant la fin de la déformation pénétrante. Certains plutons post-cinématiques montrent des niveaux anormaux de radioactivité due à la présence d'uranium.

Pendant l'Hélikien et le Hadrynien (il y a de 1100 à 700 Ma), la croûte terrestre de cette région fut fracturée, faillée et pénétrée par des dykes de diabase suivant des surfaces verticales de direction nord-ouest à sud-est. A la fin de l'Ordovicien moyen (environ 460 Ma), la région fut dénudée presque jusqu'au niveau actuel et les sédiments carbonatés de la formation de Bad Cache Rapids furent déposés sur la surface d'érosion, avec un relief local de plusieurs centaines de mètres.

Le climat actuel de la région favorise l'oxydation et lessivage de la plupart des sulfures de métaux de base des roches affleurantes. Des chapeaux de fer couverts de limonite dans les gneiss pélitiques du groupe de Penrhyn contiennent des veines secondaires de sulfure de fer relativement insoluble et du quartz granulaire. Les eaux et les sédiments des lacs à proximité des chapeaux de fer sont enrichis en Zn, Ni et Cu.

INTRODUCTION

The rocks described in this report are mainly Archean and Aphebian gneisses that were intensely deformed and regionally metamorphosed more than 1750 Ma ago. Subsequent uplift and erosion of more than 17 km has exposed the gneisses as low ridges and valleys extending across southern Melville Peninsula. The Lyon Inlet area includes about 8300 km^2 covering parts of the Mierching Lake (46 N), Hurd Channel (46 K), and Barrow River (46 O,P) topographic map sheets. The Inuit village of Repulse Bay is the nearest settlement to the map area. The village receives year-round, weekly air-service from Churchill, Manitoba; ships deliver supplies annually during late August and September. The area may be reached also by air from Hall Beach, a village to the northeast.

Larger lakes and Lyon Inlet are ice-free for approximately eight weeks from mid-July to September. From June to September, air temperatures range from 0° to 25°C. Highest daily temperatures may be reached in July and early August when a four to six week period of predominantly clear skies may occur. No permanent snow cover exists in the area, and the ground may be snow free by late June.

The map area is nearly 1000 km north of the treeline, well within the Arctic tundra. White heather, grasses, and mosses are the principal ground covers; small arctic willows are found in sheltered locations near sea level. Groups of caribou, probably totalling several thousand individuals, live in the area, but other mammals are not common. Lakes and rivers abound with two to three pound arctic char and lake trout. Gulls, ducks, snow geese, jaegers, ravens, terns, plovers, longspurs, horned larks, and snow buntings are common summer residents; rough legged hawks and rare peregrine falcons nest in the region also. Mosquitoes are a minor nuisance during late July and August.

Local relief attains 100 m, and is greatest in areas underlain by mixed lithologies. Massive granitoid gneiss and marble generally form ridges, whereas highly fractured and layered rocks form valleys. Large uplands of granitoid rocks commonly are covered by featureless felsenmeer. Valley walls may be drift-free near their tops due to solifluction of loose material downhill where it has accumulated on lower slopes and valley floors. Regions underlain by Penrhyn Group metasedimentary rocks are characterized by northeast-southwest-trending ridge-and-valley topography expressing differential erosion parallel to limbs of upright, gently plunging macroscopic folds characteristic of the Foxe Fold Belt (Fig. 1). The granitoid gneiss upland terrane northeast of Mierching Lake displays narrow northwest-southeast-trending valleys resulting from erosion along a prominent set of fractures in the rocks.

The last ice sheet came from Baffin Island, and laid down a thin veneer of ground moraine. Near the coast of Lyon Inlet ice disintegration features such as outwash plains, deltas, and eskers are numerous suggesting that a large stagnant ice mass melted on southern Melville Peninsula. Presently the region is undergoing postglacial isostatic rebound which is most apparent around Lyon Inlet. There, old beaches have been raised more than 100 m above present sea level and shallow coastal inlets have become shallow lakes. Sim (1960) reported as much as 137 m of postglacial isostatic uplift in northern Melville Peninsula and predicted that an additional 198 m would occur. Drainage in the map area is southeast into Lyon Inlet except in the northeast where the headwaters of Barrow River flow east to Foxe Basin.

The bedrock geology of the region was investigated first in 1964-65 under the direction of W.W. Heywood, using helicopter traverses spaced at six-mile intervals (Heywood, 1967). His work has formed a basis for the present study which was proposed and initiated by J.E. Reesor. Reesor conducted about a month's field work north of Lyon Inlet in July 1971. He resumed work in the area in 1973 with

J.R. Henderson and I.D. Hutcheon, and in 1974 with Henderson, Hutcheon, A.N. LeCheminant, and A. Miller. The north half of 46 J/13 (the southeast corner of the Lyon Inlet area) was mapped by J.R. Henderson and M.N. Henderson in 1977.

Most of the mapping was done by tracing lithological boundaries on foot. A Bell 47 G-4A helicopter was used for spot landings, aerial reconnaissance, and logistical support. Rubber boats provided transportation around Lyon Inlet.

In the field geology was traced on 1:50 000 scale photomosaics and aerial photographs, and transferred to 1:50 000 scale topographic maps (Henderson et al., 1976). Field notes were recorded in the system proposed by Lambert and Reesor (1974) and computer processed.

Special objectives attempted in the field work were:

(a) to describe the lithological variations, and determine the stratigraphic succession within the Prince Albert and Penrhyn groups;

(b) to determine the relative ages of the Prince Albert and Penrhyn groups;

(c) to describe the structural geometry and determine the deformational history of the Foxe Fold Belt (in particular the basement-cover structural relations);

(d) to describe the metamorphic geology and determine the metamorphic conditions of the region; and

(e) to appraise the mineral potential of the region.

Acknowledgments

The following geology students are acknowledged for providing willing and able assistance in the field: Clint Tippett, Ken Andrews, and Monty Smith (1973); Larry Lane, John Dudley, and Joe White (1974). Terry Hutcheon served ably and cheerfully as our cook in 1973 and 1974.

Thin section petrography was done by Al Miller, Jack Henderson, and Ian Hutcheon. Gordon Pringle and Maurizio Bonardi did the microprobe analyses. Peter Nielsen and Peter Thompson kindly read the section on metamorphism, and considerably aided my attempts to interpret the petrographic and chemical data.

I especially thank John Reesor for giving me the opportunity to work with him on this research project. He conceived the project, directed the field work, and carried out the initial stages of data compilation and reduction. This report would have benefited greatly from his experience and intelligence if the demands of administrative work had not forced him to yield final responsibility to me.

GENERAL GEOLOGY

All rocks in the region mapped are Precambrian with the exception of two small erosional remnants of Lower Paleozoic limestone exposed near the west shore of Hoppner Inlet. The rocks assigned to the Prince Albert group found in the northwest of the region are the oldest rocks recognized in the map area, and are Archean in age. The age is based on a 2953 Ma concordia zircon date (Table 15) obtained from zircons separated from leucocratic quartzofeldspathic gneiss interpreted as a felsic metavolcanic unit within the group. Other principal lithologies of the Prince Albert Group are: plagioclase-hornblende-quartz-biotite paragneiss with lenses of biotite-quartz-plagioclase-microcline paragneiss; quartz-magnetite-grunerite iron formation, and fine grained amphibolite. Several episodes of deformation, metamorphism, and granitic intrusion render it impossible to determine the stratigraphic succession or original thicknesses of Prince Albert Group rocks in the region mapped.

Granitoid gneisses of various compositions and textures occur throughout the area. These gneisses appear to intrude Prince Albert Group rocks and seem also to be overlain unconformably by Penrhyn Group rocks. Radiometric studies of granitoid gneisses from the region suggest a minimum intrusive age of about 2500 Ma for some of them, and on this basis they are all assigned an Archean age. Three compositional and textural varieties of granitoid gneiss were distinguished in the mapping: layered granitoid gneiss, quartz monzonite augen gneiss, and quartz diorite augen gneiss. Augen gneisses are common in the north of the region, but elsewhere equigranular, layered gneiss is most common.

The Penrhyn Group, the youngest sequence of metasedimentary rocks in the region, is given an Aphebian age on the basis of the group's apparent unconformable relationship with Archean granitoid gneiss and its subsequent metamorphism and deformation during the Hudsonian orogeny. An 1804 Ma Rb-Sr whole rock isochron obtained from Penrhyn Group pelitic gneiss is interpreted as a minimum age for the group. The Penrhyn Group is an interbedded succession of quartzite, pelitic and psammitic gneiss, calcium-silicate gneiss, marble, and minor amphibolite. Several periods of isoclinal folding and high grade metamorphism have completely obliterated all primary facing-indicators, and made determination of the stratigraphic succession and original thickness of the group conjectural. However, an orthoquartzite or a sillimanite-graphite-quartz-biotite schist commonly forms the basal unit of the succession, and in some localities an amphibolite occurs above the orthoquartzite. Gossans formed in rusty-weathering graphite-pyrite-biotite-quartz paragneiss are well developed near the base of the group in the centre of the region, but they occur elsewhere and throughout the succession. The total thickness of the Penrhyn Group in the region mapped is probably less than 2000 m. Pelitic and psammitic gneiss makes up about 60 per cent of the total thickness; marble and calcium-silicate gneiss makes up the bulk of the remainder of the group.

A small swarm of west-northwest-striking amphibolite dykes intrude Prince Albert Group rocks and Archean granitoid gneiss in the northwest part of the area, but were not observed cutting Penrhyn Group rocks. These narrow, discontinuous, weakly-foliated dykes may be late Archean or early Aphebian.

A few lenses of coarse grained mafic and ultramafic rocks occur within the Penrhyn Group near the centre of the map area and near the south border at Norman Inlet. These bodies, mainly containing pyroxene and hornblende, are emplaced near the Penrhyn Group-granitoid gneiss contact. Their mode of emplacement and age relative to the Penrhyn Group supracrustal rocks is not known; they are assumed to be Aphebian intrusions.

Numerous late-stage biotite granite dykes, sills, and plutons occur throughout the region, but most commonly intrude marble and pelitic gneiss where they may make up most of the outcrop. Although many of the granites are unfoliated pegmatite or aplite, deformed gneissic granite occurs also, and suggests that there may have been several granite-forming episodes in the fold belt.

The youngest igneous rocks in the region are northwest-striking diabase dykes. The dykes, up to 30 m wide and 10 km long, may be Helikian or Hadrynian.

Two remnants of horizontally-bedded Ordovician limestone that occur on the steep slope west of Hoppner Inlet are the youngest rocks in the region mapped.

TABLE OF FORMATIONS

AGE	ROCK UNIT	MAP UNIT*	ROCK TYPE
ORDOVICIAN	Bad Cache Rapids Formation	Ob	Thinly bedded limestone
	Angular unconformity		
NEOHELIKIAN OR HADRYNIAN	Mackenzie or Franklin Intrusions	NHd	Diabase dykes
	Intrusive contact		
APHEBIAN	Granite	Ag	Massive aplitic to pegmatitic granitic dykes, sills, and plutons
	Intrusive contact		
	Ultrabasic rocks	Aub	Hornblende peridotite, pyroxenite, metagabbro
	Intrusive contact		
	Penrhyn Group	APqb	Quartzofeldspathic psammitic gneiss
		APn	Pelitic gneiss
		APnc	Massive calcium-silicate gneiss
		APcs	Laminated calcium-silicate gneiss and marble
		APc	Marble
		APm	Massive amphibolite
		APq	Massive quartzite
	Angular unconformity		
ARCHEAN OR APHEBIAN		AAm	Amphibolite dykes
	Intrusive contact		
ARCHEAN	Granitoid gneisses	Aqdn	Quartz diorite augen gneiss
		Aqmn	Quartz monzonite augen gneiss
		Agdn	Layered granite to granodiorite gneiss
	Intrusive contact		
	Prince Albert Group	AAif	Oxide, silicate, and sulphide iron formation
		AAln	Leucocratic quartzofeldspathic gneiss
		AAm	Fine grained amphibolite gneiss
		AAn	Hornblende-rich paragneiss
	Rocks older than Prince Albert Group were not identified		

GSC

*Map 1510A (in pocket)

Prince Albert Group

Prince Albert Group rocks are found in the northwest part of the area, mainly southwest of Mierching Lake, and as northeast-trending inclusions in granitoid gneiss northwest of the lake. The rocks assigned to the group are metamorphosed to amphibolite grade, and have been intruded by granite and penetratively deformed several times. Their internal structure is characterized by northeast-striking, tight, upright folds with locally variable plunges, except in the southwest where broadly warped recumbent folds occur.

Lithologies characteristic of the Prince Albert Group in the area are: banded iron formation, hornblende-bearing paragneiss, fine grained amphibolite, and leucocratic quartzofeldspathic gneiss. Average mineral compositions based on modal analyses of 43 thin sections of Prince Albert Group rocks are given in Table 1. Protoliths of these rocks may have been chert-magnetite iron formation, greywacke, shale, and mafic and felsic volcanic rocks. The sequence and thickness of Prince Albert Group rocks in the region mapped are unknown. The relative abundances of the lithologies mapped decrease in the sequence: hornblende paragneiss, fine grained amphibolite, leucocratic quartzofeldspathic gneiss, and iron formation. A few lenses of biotite-rich paragneiss are found in the much more abundant hornblende paragneiss. Correlation of these rocks with the Prince Albert Group in the type region of the Prince Albert Hills (Heywood, 1967) is based on lithological similarities.

Hornblende Paragneiss (AAn)

Hornblende paragneiss (map unit AAn), the principal lithology of the Prince Albert Group in the area, is exposed in scattered small outcrops of low relief throughout the region of occurrence of the group. Exposures commonly are covered by black lichens. The paragneiss weathers dark grey or dark green; fresh surfaces have a fine grained, granular texture, and may show black and grey laminae a few centimetres wide. Mafic minerals generally are aligned in a secondary foliation which is crenulated and isoclinally folded. Less commonly small hornblende prisms have a linear parallelism. In places layers and lenses of biotite paragneiss occur which may contain cordierite, garnet, and sillimanite; because these more aluminous rocks have a similar weathered appearance to the hornblende paragneiss they were not mapped separately.

Average modes based on eleven thin sections of hornblende paragneiss and three modes of biotite paragneiss are given in Table 1. The major mineral assemblage in hornblende paragneiss is plagioclase (An_{49} avg.), hornblende, and quartz; biotite and microcline occur also in many rocks. Accessory minerals observed are sphene, apatite, and zircon. The major mineral assemblage in the biotite paragneiss is biotite, quartz, and plagioclase (An_{30} avg.); garnet, cordierite, sillimanite, and microcline also occur as major components in some rocks. Accessory minerals observed in biotite paragneiss are apatite and zircon. Both hornblende paragneiss and biotite paragneiss commonly show some retrograde alteration in the form of sericitization and saussuritization of plagioclase, and chloritization of biotite and hornblende.

Table 1

Estimated Mineral Compositions (Modal Analysis*) of Prince Albert Group Rocks

Rock Type	Hornblende Paragneiss (map unit AAn)			Biotite Paragneiss (map unit AAn)			Banded Iron Formation (map unit AAif)			Silicate Iron Formation (map unit AAif)			Amphibolite Gneiss (map unit AAm)			Leucocratic Quartzofeldspathic Gneiss (map unit AAln)		
Number of Thin Sections	11			5			12			3			7			5		
	Average	Range	S.D.†	Average	Range	S.D.	Average	Range	S.D.	Average	Range	S.D.	Average	Range	S.D.	Average	Range	S.D.
Quartz	18	7-27	6.9	25	8-38	13.2	48	24-63	9.7	14	9-20	4.5				28	22-37	5.0
Plagioclase	42	27-54	7.9	17	5-24	7.2							36	31-42	3.3	50	34-63	10.9
(Per cent Anorthite)	(49)	(31-64)	(12.2)	(30)	(28-43)	(12.5)							(46)	(38-60)	(7.4)	(26)	20-35	(5.7)
Microcline	3	0-28	8.0	3	0-10	3.7										11	0-38	14.8
Biotite	10	0-26	8.8	31	21-45	8.9	trace						1	0.5	1.8	10	5-22	6.2
Hornblende	23	6-40	11.2										54	31-64	12.1			
Grunerite							16	8-29	5.8	7	0-15	6.2						
Anthophyllite							4	0-31	9.3									
Diopside													10	0-26	10.3			
Garnet				12	0-32	12.6				7	0-18	7.9						
Cordierite				4	0-12	5.2												
Sillimanite				3	0-8	3.3												
Orthopyroxene										53	39-61	9.9						
Fayalite										12	1-26	10.5						
Magnetite							32	27-42	4.8	7	3-11	3.3	trace					
Epidote	trace			4	0-18	7.0							trace					
Chlorite	3	0-17	5.5	1	0-4	1.6	trace											
Muscovite				2	0-8	3.1												
Apatite	trace			trace			trace						trace			trace		
Zircon	trace			trace									trace			trace		
Sphene	1	0-4	1.2										trace			trace		
Total	100			102			100			100			101			99		

*Volume percentages of major constituents are estimated from traverses averaging 100 mm.

†In the tables of modal mineral abundances the standard deviation (S.D.) of each mineral is calculated by the expression $\left[\frac{\Sigma(X_i-\bar{X})^2}{N}\right]^{1/2}$

Hornblende paragneiss contains layers and lenses of other Prince Albert Group lithologies, such as fine grained amphibolite (map unit AAm). Contact relations with granitoid gneisses (map units Agdn, Aqmn and Aqdn) are locally concordant, but isolated thin lenses of hornblende paragneiss found within the granitoid gneisses suggest that the gneisses either have intruded the group or have been derived from Prince Albert Group rocks. Numerous bodies of granite (map unit Ag), characterized by textures ranging from aplitic to pegmatitic, intrude Prince Albert Group paragneiss.

The abundance of metamorphic hornblende and the high calcium content of plagioclase, as well as the uncommon occurrence of potassium feldspar in the hornblende paragneiss suggest that its protolith was a greywacke derived from intermediate to mafic igneous source rocks. The biotite paragneiss probably was originally a pelite.

Amphibolite Gneiss (AAm)

Fine grained amphibolite gneiss (map unit AAm) is common in the Prince Albert Group in the map area. Amphibolite layers vary from less than 1 m to 10 m wide. Weathered exposures are black and dark brown; fresh surfaces are black. Most amphibolite gneiss shows thin alternating hornblende- and plagioclase-rich laminations 0.5-1 cm wide. Within the laminae, the hornblende grains ordinarily show some degree of planar or linear parallelism. The common assemblage observed in seven thin sections (Table 1) is hornblende and plagioclase (An_{46} avg.); other principal minerals are diopside and biotite. Accessory phases observed are apatite, zircon (in biotite), and opaque minerals. Some retrogressive saussuritization of plagioclase and chloritization of biotite is evident in most of the thin sections.

Contacts of amphibolite with other Prince Albert Group lithologies appear concordant although the tight folding of the rocks would have obscured any slight discordances. Chemical analyses of three samples of Prince Albert amphibolite gneiss are given in Table 2. The average major element compositions of tholeiitic basalt (Nockolds, 1954) and average para-amphibolite (after Preto, 1970) are presented also in the table for comparison. Oxidation ratios of the three amphibolites range from values typical of para-amphibolite (2.74 and 4.26) to a value more similar to ortho-amphibolite (18.98). On the basis of field appearance and rock associations a mafic volcanic origin for the Prince Albert amphibolites is preferred.

Table 2

Chemical Analyses of Melville Peninsula Amphibolites compared to Average Tholeiite and Para-amphibolite

Chemical Composition	Prince Albert Group 1	2	3	Penrhyn Group 1	2	Average Tholeiite (Nockolds, 1954)	Average Grand Forks Para-amphibolite (Preto, 1970)
Weight per cent							
SiO_2	48.3	49.7	49.9	45.3	47.3	50.83	48.6
Al_2O_3	15.0	15.9	13.6	14.0	13.2	14.07	15.03
Fe_2O_3	0.3	2.5	0.5	1.6	1.7	2.88	1.24
FeO	9.6	9.6	10.1	12.9	13.2	9.06	8.79
MgO	5.75	6.18	5.85	6.37	5.71	6.34	7.86
CaO	14.7	10.0	13.8	11.2	9.82	10.42	10.26
Na_2O	2.8	2.2	2.9	2.6	3.3	2.23	3.34
K_2O	0.38	0.63	0.88	0.66	0.59	0.82	0.96
$H_2O(T)$	1.6	1.3	0.8	1.3	1.2	0.91	1.5
TiO_2	0.92	0.91	0.80	2.12	2.30	2.03	1.37
P_2O_5	0.08	0.09	0.07	0.22	0.27	0.23	0.22
MnO	0.23	0.23	0.25	0.24	0.24	0.18	0.20
CO_2	0.1	0.0	0.5	0.1	0.0	-	0.25
Cr_2O_3	0.04	0.06	0.03	0.05	0.03		0.03
S	0.08	0.04	0.11	0.17	0.04		
Zr	0.000	0.000	0.000	0.005	0.005		
Sr	0.017	0.012	0.022	0.042	0.044		
Rb	0.000	0.000	0.000	0.000	0.000		
Zn	0.003	0.006	0.003	0.004	0.006		
Ni	0.011	0.021	0.013	0.006	0.004		
Ba	0.005	0.007	0.012	0.005	0.012		
Total	99.8	99.5	100.2	98.9	99.0	100.00	99.6
Oxidation Ratio*	2.74	18.98	4.26	10.04	10.39	22.21	11.35

Chemical analyses by Geological Survey of Canada Laboratories.

*mols $\frac{2Fe_2O_3 \times 100}{2Fe_2O_3 + FeO}$

Leucocratic Quartzofeldspathic Gneiss (AAln)

Southwest of Mierching Lake lenses of grey leucocratic quartzofeldspathic gneiss (map unit AAln) up to 1 km wide and several kilometres long compose a significant proportion of the Prince Albert Group. Typically the rock is homogeneous, medium grained, and granular with a weak foliation defined by aligned, scattered biotite flakes.

Principally the leucocratic gneiss contains plagioclase-quartz-microcline-biotite or plagioclase-quartz-biotite. The average composition of plagioclase in 5 thin sections examined is An_{26} (range An_{20} to An_{35}). Accessory minerals observed are apatite, zircon, and sphene.

Although granite intrusion and folding have obscured original contact relationships, the leucocratic gneiss appears to be conformable with Prince Albert Group paragneiss. Zircons extracted from the gneiss yielded a 2953 ± 52 Ma concordia age (Table 15) which may be either the primary age or a maximum age for the Prince Albert Group.

Iron Formation (AAif)

Discontinuous beds of oxide, silicate, and sulphide iron formation (map unit AAif) form a small but characteristic component of the Prince Albert Group in the area. Banded iron formation is most common; it averages 3-4 m wide and may extend several hundred metres along strike. The dark-weathering rock consists of black and white laminae 1-5 mm wide containing aligned poikiloblastic laths of amphibole enclosing medium grained, granular magnetite and quartz. Rusty-brown-weathering, massive, silicate and sulphide iron formation occur in a few localities near the southwest limit of the Prince Albert Group in the map area. The silicate iron formation contains coarse grained mixtures of iron-rich silicates, quartz, and magnetite; the sulphide iron formation contains massive pyrite-pyrrhotite-quartz mixtures.

The estimated mineral compositions of 12 thin sections of banded iron formation and three thin sections of silicate iron formation are given in Table 1. Magnetite averages 32 per cent, quartz 48 per cent, and amphibole 20 per cent in the banded iron formation. Both grunerite and anthophyllite co-exist in several rocks. None of the banded iron formation observed was of sufficient iron content or extent to excite economic interest. Silicate iron formation contains the assemblage orthopyroxene-quartz-fayalite-almandite-magnetite or orthopyroxene-quartz-grunerite-fayalite-almandite-magnetite. In these rocks the iron silicates form coarse symplectic intergrowths with scattered inclusions of magnetite and quartz.

Rocks typically enclosing iron formation are fine grained amphibolite (map unit AAm) and hornblende paragneiss (map unit AAn). Thin layers of brown-weathering sillimanite and garnet schist were observed in contact with banded iron formation at several localities.

Granitoid Gneiss

Medium- to coarse-grained granitoid gneisses are widespread in the region, and comprise the predominant lithologic type. In the southern part of the map area east of Ross Bay granitoid gneiss occurs as semi-concordant sheets isoclinally folded with Penrhyn Group rocks. In the centre of the map area deformed granitoid gneiss bodies of various shapes and sizes occur separated by narrow screens of steeply dipping paragneiss. In the region north of Penrhyn Group rocks granitoid gneisses form a large continuous domain in which scattered lenses of Prince Albert Group rocks occur.

Table 3

Estimated mineral compositions (modal analysis*) of Archean granitoid gneiss

Rock Type		Layered Granitoid Gneiss (map unit Agdn)			Quartz Monzonite Augen Gneiss (map unit Agmn)			Quartz Diorite Augen Gneiss (map unit Agdn)		
Number of Thin Sections		22			5			8		
		Average	Range	Standard Dev.	Average	Range	Standard Dev.	Average	Range	Standard Dev.
Major Constituents	Quartz	31	11-42	7.3	21	14-29	4.8	19	14-23	3.2
	Plagioclase	39	13-54	12.6	39	18-52	11.4	46	37-52	4.9
	(Per cent Anorthite)	(24)	(12-38)	(5.7)	(28)	(20-35)	(5.5)	(37)	(30-45)	(5.8)
	Microcline	15	0-44	11.6	23	2-51	16.0	6	0-11	4.6
	Hornblende	7	0-44	11.3	7	0-11	4.0	16	7-30	7.5
	Biotite	7	3-17	3.7	9	2-16	4.7	12	6-16	3.2
	Total	99			99			99		
		Per cent of thin sections			Per cent of thin sections			Per cent of thin sections		
Minor Constituents	Apatite	100			100			100		
	Zircon	100			100			100		
	Sphene	59			0			87		
	Allanite	23			40			13		
	Epidote	23			0			63		
	Opaque	36			20					

*Volume percentages of major constituents are estimated from traverses averaging 150 mm.

The granitoid gneisses present a relatively flat upland surface commonly covered by a thin veneer of large, angular boulders which make walking difficult. Outcrop abundance varies considerably from place to place, but generally is good. Exposures tend to be massive, smooth joint or glaciated surfaces covered by black lichens which obscure the foliation and layering.

Three varieties of granitoid gneisses were distinguished: layered granitoid gneiss (map unit Agdn), quartz monzonite augen gneiss (map unit Aqmn), and quartz diorite augen gneiss (map unit Aqdn). Average modal analyses of 35 thin sections of granitoid gneiss are listed in Table 3. Relative proportions of modal quartz, plagioclase, and microcline in each section are plotted in Figure 2, and relative proportions of modal quartz, feldspar, and mafic minerals are plotted in Figure 3. From the table and figures it appears that the quartz diorite augen gneiss is the most mafic and compositionally homogeneous variety. The layered gneiss seems to have a wider range of mineral proportions than the augen gneisses.

Boundaries between the gneiss units are gradational and their relative ages are not apparent on the basis of contact relations. Compositionally and structurally the augen gneisses appear to be the least varied and complex, and they may intrude the layered unit.

Inclusions of hornblende paragneis, amphibolite, and iron formation typical of the Prince Albert Group are found in various stages of assimilation within both layered and augen gneisses in the northwest of the region. However, only the layered granitoid gneiss was mapped in contact with Penrhyn Group rocks, and small inclusions of lithologies characteristic of the group (marble, calcium-silicate gneiss, and quartzite) are conspicuously absent. All of the granitoid gneiss units are intruded by unfoliated aplitic to pegmatitic granite plutons (map unit Ag). These granitic masses are especially common along and adjacent to contacts between granitoid gneiss and Penrhyn or Prince Albert group rocks. They decrease in abundance in the gneisses towards the north margin of the area mapped.

Radiometric studies (Table 16) of zircons from granitoid gneisses indicate that the layered gneiss may be about 2727 Ma old, quartz diorite augen gneiss may be about 2584 Ma and quartz monzonite augen gneiss may be about 2527 Ma old. A whole rock Rb-Sr isochron suggests that some granitoid gneiss was intruded or metamorphosed about 2493 Ma ago during the Kenoran orogeny. K-Ar mineral dates from the gneiss appear to mainly reflect cooling of the rocks subsequent to Hudsonian metamorphism.

Layered Granitoid Gneiss (Agdn)

Layered gneiss (map unit Agdn) is the most widespread variety of granitoid gneiss mapped in the region (the two augen gneiss units occur only in the northwest part of the area). The layered gneiss is very heterogeneous: its composition varies from granite to quartz diorite, and it contains up to 50 per cent hornblende and biotite. Commonly the rock is differentiated into 2- to 10-cm wide felsic layers and 1- to 5-mm wide mafic layers. Some foliated, homogeneous granite occurs locally and may be intrusive into the layered gneiss.

The layered gneiss is mostly medium grained, xenomorphic granular. Hornblende and biotite commonly exhibit a weak preferred orientation parallel to the gneissic layering. Foliation is developed most strongly in gneiss bordering Penrhyn Group rocks and in the northwest of the area where blastocataclastic textures occur.

Modal analyses of 22 thin sections of layered gneiss are summarized in Table 3. The principal minerals observed are plagioclase (An_{24} avg.) quartz and microcline (less than 10 per cent perthite). Embayments of myrmekite commonly intrude microcline adjacent to plagioclase. Brown biotite

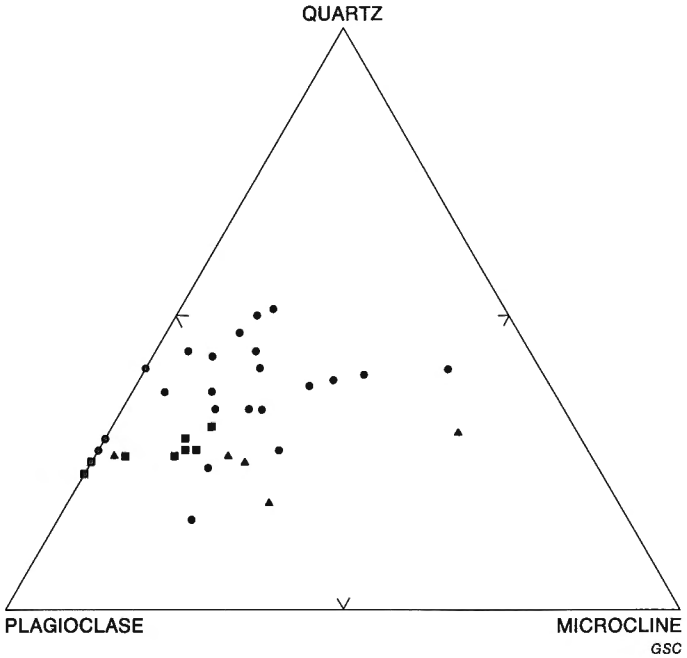

Figure 2. *Triangular graph showing modal proportions of quartz, plagioclase and microcline in 35 thin sections of granitoid gneiss. Circles are layered granitoid gneiss (map unit Agdn), squares are quartz diorite augen gneiss (map unit Aqdn), and triangles are quartz monzonite augen gneiss (map unit Aqmn).*

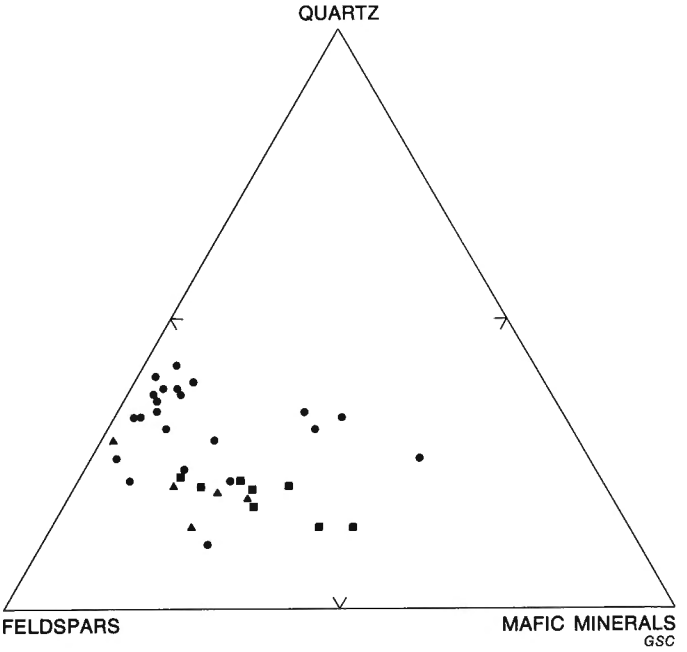

Figure 3. *Triangular graph showing modal proportions of quartz, feldspars, and mafic minerals in 35 thin sections of granitoid gneiss. Circles are layered granitoid gneiss (map unit Agdn), squares are quartz diorite augen gneiss (map unit Aqdn), and triangles are quartz monzonite augen gneiss (map unit Aqmn).*

occurs in amounts up to 15 per cent and green hornblende occurs in variable amounts up to 45 per cent. The average colour index of the sections examined is 14. Apatite and zircon appear to be ubiquitous accessory minerals in layered gneiss; sphene (commonly mantling ilmenite or magnetite) and allanite (yellow metamict) are widespread also. Most rocks examined showed minor effects of retrograde alteration in the form of sericitization of plagioclase and chloritization of biotite and hornblende.

Amphibolite schlieren and lenses are a characteristic component in many exposures of the layered gneiss. Marble and calcium-silicate gneiss inclusions were rarely observed; where they do occur (e.g. between Lyon Inlet and Ross Bay) the paragneiss and the granitoid gneiss both appear to have been folded isoclinally in several directions giving rise to isolated bodies of paragneiss within the granitoid gneiss. On the other hand, small bodies of Prince Albert hornblende paragneiss, amphibolite, and iron formation found in the granitoid gneiss in the northwest of the region may be unassimilated xenoliths rather than infolded inclusions. In general, contacts between granitoid gneiss and Penrhyn Group paragneiss are abrupt and straight, whereas contacts with Prince Albert Group rocks are gradational and interlayered. Granitic plutons commonly occur along the contact between granitoid gneiss and both Prince Albert and Penrhyn Group rocks, and locally obscure contact relations with the supracrustal rocks.

Quartz Monzonite Augen Gneiss (Aqmn)

The north part of the map area is underlain mostly by coarse grained feldspar-augen gneiss (map unit Aqmn). The augen gneiss ranges from quartz monzonite to granodiorite; it contains feldspar megacrysts as long as 5 cm and hornblende megacrysts as long as 2 cm. Colour index averages about 16. The rock is massive and weathers deep orange.

The modal mineral compositions of 5 thin sections of quartz monzonite augen gneiss are summarized in Table 3. The average proportion of microcline to total feldspar indicated by the data in the table (37%) may be too low because a significant amount of microcline is concentrated in large megacrysts which may not be adequately represented in thin section. The rock probably is mainly quartz monzonite: its designation is based on field estimates of feldspar ratios. The average colour index of the sections examined is 18. Textures consist of large ovoid microcline and plagioclase megacrysts surrounded by medium grained xenomorphic granular aggregates of plagioclase, quartz, and microcline. Biotite and hornblende commonly occur in clusters of subparallel grains that wrap around the feldspar megacrysts. Plagioclase compositions range from 20-35 per cent anorthite (An_{28} avg.) in the sections examined. Myrmekite embayments into plagioclase grains adjacent to microcline are not common. Microcline has less than ten per cent bead, string and patch perthite. Hornblende is pleochroic green, and biotite is pleochroic brown. Quartz commonly occurs in lenticular aggregates of grains parallel to foliation or lineation. Larger quartz grains are subdivided by deformation bands.

Foliation and lineation are characterized in most outcrops by aligned ellipsoidal feldspar augen and mafic clots. Both foliation and lineation commonly are uniformly oriented over large domains in distinct contrast to locally variable foliation attitudes in layered gneiss (map unit Agdn) to the south. The average strike of foliation in the augen gneiss is northeast-southwest and dips are generally shallow to the northwest. Local zones of more intense cataclasis each a few kilometres apart are characterized by steep dips. Lineations plunge northwest except near the southwest border of the augen gneiss where lineations plunge southwest.

Quartz monzonite augen gneiss is interlayered with medium grained granitoid gneiss (not separately mapped) containing rare augen. Inclusions of hornblende paragneiss and amphibolite are especially abundant near contacts with Prince Albert Group rocks. Amphibolite dykes (map unit AAm) and unfoliated granitic bodies (map unit Ag) cut the augen gneiss near its southwest margin.

Quartz Diorite Augen Gneiss (Aqdn)

A single body of quartz diorite augen gneiss (map unit Aqdn) was mapped in the north of the region. It is about 26 km long by 2 km wide with its long dimension trending northeast-southwest parallel to the regional trend of foliation. The quartz diorite is a mafic-rich gneiss with plagioclase megacrysts less than 1 cm long.

In outcrop the quartz diorite augen gneiss resembles the quartz monzonite augen gneiss (map unit Aqmn) except for a generally higher colour index. This superficial resemblance is because plagioclase augen in the quartz diorite weather pale orange due to extensive sericitization. On fresh surfaces the plagioclase augen are pale green where sericitized or light grey where unaltered. In general the plagioclase augen in the quartz diorite also are smaller than the microcline augen in the quartz monzonite gneiss.

The average modal composition of eight thin sections is given in Table 3. The average mineral composition of the rocks examined is quartz diorite with a colour index of 28. The average anorthite content of plagioclase in the sections is 37 per cent (range An_{30}-An_{45}). Textures consist of ovoid plagioclase glomeromegacrysts surrounded by medium grained xenomorphic granular plagioclase-quartz-microcline aggregates. Green hornblende and brown biotite occur in lenticular clusters parallel to foliation or lineation. Quartz grains exhibit undulose extinction and commonly are divided into parallel deformation bands. Secondary alteration of plagioclase into patches of fine grained decussate sericite is widespread but without apparent pattern. Some specimens contain secondary epidote and chlorite after biotite and hornblende. Apatite, zircon, and sphene are ubiquitous accessory minerals.

Plagioclase augen in the quartz diorite commonly resemble triaxial ellipsoids, and define a uniformly oriented foliation and lineation. The foliation strikes east-northeast and dips 40° northwest; the lineation defined by the long axes of the augen plunges at about 25° towards west-northwest.

Abundant inclusions of hornblende paragneiss and amphibolite occur in the quartz diorite augen gneiss, suggesting that it intruded or was derived in part from Prince Albert Group rocks. The quartz diorite gneiss grades laterally and along strike into equigranular layered gneiss (map unit Agdn).

Amphibolite Dykes (AAm)

A small swarm of northwest-striking black amphibolite dykes (map unit AAm) cuts Prince Albert Group rocks and granitoid gneiss west of Mierching Lake. The dykes are 5-50 m wide and up to 4 km long. They are not folded, but appear to have been boudinaged into isolated short segments. Commonly the dykes contain a weakly developed foliation parallel to their margins which is offset 10-15° from the adjacent country rock foliation.

A single thin section examined contains 68 per cent hornblende, 27 per cent plagioclase (An_{62}), and 5 per cent iron oxide, as well as trace amounts of apatite and sphene. The section is medium grained and differentiated into felsic and mafic laminae 1-2 mm wide. Iron oxide occurs as disseminated inclusions in hornblende.

The relative age of the amphibolite dykes is uncertain; they were not observed cutting Penrhyn Group rocks in the map area, and may be either Archean or Aphebian.

Penrhyn Group

The sequence of supracrustal rocks composing the Penrhyn Group occurs mainly in northeast-southwest-trending bands separated by belts of Archean gneiss. The group is a lithologically varied sequence of pelitic and psammitic gneiss, calcium-silicate gneiss, marble, quartzite, and amphibolite. The contrasted mineralogy of pelitic, psammitic, and calcium-silicate gneiss is illustrated in Figure 4: Modal QF, AFM, and CS from 89 thin sections of Penrhyn Group paragneiss. In the triangular graph the three components show the strong separation of pelitic and calcium-silicate gneiss mineralogies, as well as the transitional mineralogy of psammitic gneiss. In the field, considerable difficulty was experienced in distinguishing psammitic gneiss from similar-looking calcium-silicate or pelitic gneiss.

The structure of the Penrhyn Group is complex. Bedding or differentiated layering is folded isoclinally and mineral foliation (defined by aligned platy minerals) parallels the layering. The earliest folds recognized were originally recumbent; later, upright and overturned subhorizontal folds give the group its characteristic northeast-southwest regional grain. Contacts between various units of the Penrhyn Group and the Archean basement gneiss vary from nearly concordant to discordant, and indicate that basement-cover rock relations range from autochthonous to allochthonous.

Textures and mineral assemblages show that Penrhyn Group paragneiss was subjected to upper amphibolite grade regional metamorphism after the last penetrative deformation. Partial replacement of higher-grade minerals occurred later in some areas. Late syntectonic and posttectonic granitic pegmatite and aplite plutons commonly intrude Penrhyn Group rocks, but no granitic bodies of batholithic size were found.

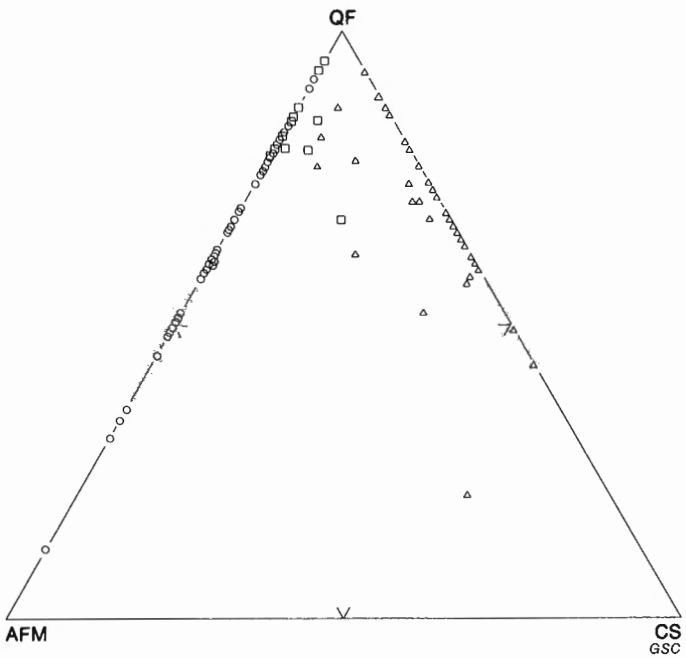

Figure 4. *Triangular graph showing modal proportions of quartz + scapolite + feldspars (QF), biotite + chlorite + garnet + cordierite + sillimanite (AFM) and diopside + tremolite/actinolite + calcite (CS) in 89 thin sections of Penrhyn Group paragneiss. Circles are pelitic gneiss (map unit APn), squares are psammitic gneiss (map unit APqb), and triangles are calcium-silicate gneiss (map units APcs, APnc).*

The Penrhyn Group appears to be an ensialic miogeoclinal accumulation of medium-to fine-grained clastic and chemical sediments. Coarse clastic materials are absent from the group, and mafic volcanic rocks are very rare. The original extent and thickness of the group is unknown; Heywood (1967) mapped Penrhyn Group rocks in a triangular-shaped area with an apex west of Rae Isthmus, and widening northeast to the Foxe Basin between Cape Wilson and Amitioke Peninsula. He assigned the group an Aphebian age and tentatively correlated it with the Chantry and Hurwitz groups in Central District of Keewatin on the basis of their common lithologic characteristics. In a comprehensive review of the relationships between various Aphebian rock units and fold belts in the northeastern Canadian Shield, Jackson and Taylor (1972) correlated the Penrhyn Group on Melville Peninsula with the Piling Group on central Baffin Island. Both groups occur in the Late Aphebian (Hudsonian) Foxe Fold Belt, but the Piling Group, in contrast to the Penrhyn Group, is mainly a thick pile of monotonous metaturbidites and amphibolites with a very thin quartzite and carbonate sequence at the base. The authors suggested that more rapid sedimentation occurred in the Piling Basin to produce the thicker accumulation of Aphebian clastic sediments (Jackson and Taylor, 1972).

Within the map area the Penrhyn Group unconformably overlies late Archean granitoid gneiss and was regionally metamorphosed during the Hudsonian orogeny thus placing the time of Penrhyn sedimentation between about 2500 and 1800 Ma ago. The base of the group commonly is marked by a massive pure quartzite about 10 m thick which may be underlain or interbedded near the top with a few metres of rusty-weathering graphite schist. In a few places massive amphibolite about 30 m thick overlies the basement gneiss or the basal quartzite.

Marble and calcium-silicate gneiss are widespread as well as abundant, but psammitic and pelitic gneiss is the most common lithology in the group. Total thickness of the Penrhyn Group rocks exposed in the map area is not great, perhaps about 2000 m. Tectonic thickening and thinning of more than ten times is apparent in individual units so original thickness estimates are very uncertain.

In several places macroscopic structural relations within the Penrhyn Group seem to be understood well enough to warrant reconstruction of local stratigraphic successions. In Figure 14 the Penrhyn rocks west of Tasers Lake are interpreted as forming an overturned, south-dipping homoclinal sequence overlying parautochthonous basement gneiss to the south, and in contact to the north with an allochthonous sheet of basement gneiss. It appears that the succession varies from west to east (Fig. 14) due to lateral changes in lithofacies. In the west an interbedded marble and calcium-silicate (map unit APcs) overlies the basal quartzite (APq) and underlies a massive calcium-silicate (map unit APnc). In the east pelitic gneiss (map units APn, APr) is abundant near the base of the group as well as above the interbedded marble and calcium-silicate unit.

In the region west of Aua River (Fig. 27) the group can be divided into two stratigraphic units: a lower sequence composed of discontinuous basal quartzite (map unit APq), rusty pelitic schist (map unit APr), and abundant marble and calcium-silicate gneiss (map units APc and APcs); and an upper unit consisting mostly of pelitic gneiss (map unit APn) with several psammitic gneiss lenses (map unit APqb) near

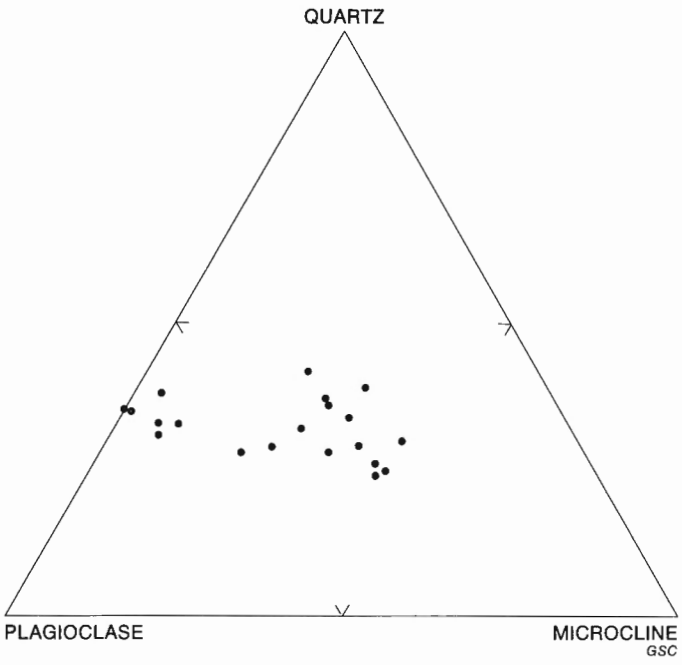

Figure 5. *Triangular graph showing modal proportions of quartz, plagioclase, and microcline in 20 thin sections of Aphebian granitic rocks (map unit Ag).*

the base. Very little marble or calcium-silicate gneiss occurs in the upper unit, and very little pelitic or psammitic gneiss occurs in the lower unit.

Elsewhere in the Lyon Inlet area folding is too tight and complicated to permit stratigraphic subdivision within the Penrhyn Group: this is especially so in the belt extending from southwest of Mierching Lake to the northeast corner of the area.

Quartzite (APq)

Coarse grained, vitreous, grey or white quartzite (map unit APq) commonly outcrops within a few metres of the contact between Penrhyn Group rocks and granitoid gneiss (map unit Agdn). The unit has been mapped continuously for more than 50 km along strike, but more commonly it occurs as a narrow band a few kilometres long. Typically the quartzite is found in a shallow valley with basement gneiss and marble exposed on opposite walls. Exposure of the quartzite is poor and actual contacts with adjacent rocks were rarely observed.

The quartzite generally is about 10 m thick but in places may be up to 100 m thick. Bedding is poorly-defined and is revealed by widely-spaced biotite-sillimanite laminae. Mineral foliation is defined by scattered parallel mica flakes and tabular quartz grains. Most outcrops are well jointed and relatively free of lichens. In places rusty-yellow-weathering graphite-sillimanite-biotite schist interbeds have imparted a surface stain on the quartzite.

In 11 thin sections examined quartz constitutes about 90 per cent of the rock. Quartz grains generally are coarse to very coarse; in some sections tabular shapes may be due to inhibited growth against adjacent foliated mica and graphite, but in other sections quartz grains up to 1 cm diameter have completely enclosed smaller scattered grains of mica, sillimanite, graphite, and feldspar. Retrograde alteration of aluminosilicates to chlorite, muscovite, and iron oxide is evident in nearly all of the sections examined.

The quartzite appears to be a unique lithologic unit found only near the base of the Penrhyn Group. Commonly it is underlain or overlain by a few metres of rusty-weathering biotite-graphite schist rich in sillimanite, garnet, and cordierite (map unit APr). Near the east margin of the map area quartzite is overlain and locally underlain by amphibolite (map unit APm). In many places the stratigraphic position of the quartzite above the granitoid gneiss is taken by another lithology; in fact any of the Penrhyn map units may be found in contact with the basement gneiss in one place or another.

Due to deformation and metamorphism the origin of the basal quartzite is uncertain; it may have been a quartz-rich regolith leached of other minerals, or it may have been a transgressive blanket of quartz sand.

Amphibolite (APm)

In the east-centre of the map area a stratiform amphibolite (map unit APm) was traced along strike for about 15 km. The amphibolite occurs above quartzite (map unit APq) and below pelitic gneiss (map unit APm). Near the easternmost limit of this occurrence another amphibolite layer underlies the quartzite for about 1 km. Close to the northeast corner of the map area amphibolite overlies quartzite in a refolded dome. Another occurrence is near the centre of the map area where amphibolite directly overlies granitoid gneiss (map unit Agdn) and underlies marble (map unit APc) on the crest and limbs of a doubly-plunging upright anticline.

Amphibolite averages about 30 m and may be as much as 100 m thick. It is well exposed generally and weathers dark brown or dark green; fresh surfaces are black. Gneissic layering is defined on many outcrops by laminae with variable proportions of medium grained hornblende and plagioclase. Most rocks display a well developed foliation and a poorly developed lineation defined by the degree of alignment of hornblende prisms.

The estimated mineral composition of amphibolite based on five thin sections examined is summarized in Table 4. On the average amphibolite appears to contain about 43 per cent green hornblende, 41 per cent plagioclase (An_{51} avg.), and about 11 per cent diopside, along with small amounts of biotite and magnetite (commonly mantled by sphene). One section contains grunerite rather than hornblende and seven per cent magnetite. Epidote, calcite, and sericite occur as alteration products of plagioclase; diopside was altered partially to pale green tremolite-actinolite in several sections.

Chemical analyses of two samples of Penrhyn amphibolite are given in Table 2. The Prince Albert amphibolite and the Penrhyn amphibolite appear chemically similar. Oxidation ratios of Penrhyn amphibolite (10.0 and 10.3) are closer to the average of supposedly para-amphibolite (11.35) from Grand Forks, British Columbia than to the average tholeiitic basalt (22.21).

Either a volcanic or sedimentary protolith may be favoured because of the consistent stratigraphic position of the Penrhyn amphibolite near the base of the group. Although the low oxidation ratios, if original, may argue for a sedimentary origin, the absence of interbedded or enclosing metasediments as well as the massive, homogeneous appearance of the amphibolite seems to support a basic volcanic origin for the rocks.

Pelitic Gneiss (APn and APr)

Biotite-rich paragneiss (map units APn and APr), the most common and widespread lithology within the Penrhyn Group in the region, occurs at several stratigraphic horizons and is found also as a subordinate component of psammitic

Table 4

Estimated Mineral Compositions (Modal Analysis*) of Penrhyn Group Rocks

Rock Type	Amphibolite (map unit APm)			Pelitic Gneiss (map unit APn)			Psammitic Gneiss (map unit APqb)			Diopside-poor Calcium-silicate Gneiss (map unit APnc)			Diopside-rich Calcium-silicate Gneiss (map unit APcs)		
Number of Thin Sections	5			42			11			11			25		
	Avg.	Range	S.D.	Avg.	Range	S.D.	Avg.	Range	S.D.	Avg.	Range	S.D.	Avg.	Range	S.D.
Quartz				32	2-62	12.0	44	33-50	7.8	26	1-37	10.7	15	0-35	11.1
Plagioclase	41	24-52	10.4	18	0-54	15.6	30	15-44	8.3	41	18-66	14.5	15	0-44	14.5
(Per cent Anorthite)	(51)	(37-60)	(6.7)	(33)	(20-52)	(9.3)	(38)	(25-53)	(10.9)	(36)	(30-44)	(4.0)	(60)	(20-86)	(18.1)
Scapolite							1	0-10	2.9	trace			12	0-42	14.5
Microcline				12	0-59	13.9	8	0-33	10.7	15	0-39	13.6	19	0-62	16.5
Biotite	trace	0-1		23	4-42	9.2	14	4-21	4.9	7	0-21	7.4	2	0-21	4.6
Hornblende	43	36-72	16.8	trace						trace			trace		
Diopside	11	0-37	13.6							4	0-12	3.6	15	0-40	8.7
Tremolite-Actinolite							1	0-6	1.9	6	0-17	5.3	10	0-37	11.1
Calcite				trace			trace	0-2		trace	0-1		8	0-43	11.6
Garnet				3	0-30	7.2							1	0-18	3.5
Cordierite				5	0-30	8.0									
Sillimanite				2	0-24	4.7									
Andalusite				trace	0-2										
Graphite				trace	0-3		trace	0-2		trace	0-2		trace	0-2	
Epidote	trace	0-1		trace	0-2		1	0-5	1.4	trace	0-3		3	0-17	4.6
Chlorite				2	0-42	7.4	trace			trace			trace	0-2	
Muscovite				3	0-26	5.8	1	0-4	1.6	trace			trace	0-2	
Sphene	1	0-2	0.7	trace			trace			trace	0-3		1	0-3	0.8
Apatite	trace			trace			trace			trace			trace		
Opaque	2.4	1-7	2.3	trace			trace			trace	0-1		trace		
Zircon	trace			trace			trace			trace			trace		
Total	98			100			100			99			101		

*Volume percentages of major constituents are estimated from traverses averaging 100 mm.

Figure 6. *Microfold in pelitic gneiss. Note that gneissosity and biotite foliation are deformed in the fold hinge. Width of photo area is 5 mm. (GSC 202949-I)*

gneiss (map unit APqb) and calcium-silicate gneiss (map unit APcs). The predominant major mineral assemblage observed in pelitic gneiss is biotite-quartz-feldspar. Where graphite attains a significant proportion the rock also contains iron sulphide. Upon oxidation these zones produce brilliant red and yellow gossans that are mapped separately as rusty paragneiss (map unit APr).

Where it is particularly biotite-rich and homogeneous pelitic gneiss is very resistant to erosion and underlies some of the highest hills in the region. Characteristically the unit contains 10 to 40 per cent quartozfeldspathic pegmatite as narrow laminae, veins, and sills. In the field, the presence of the white pegmatitic component of the pelitic gneiss is useful to distinguish it rapidly from rocks otherwise similarly covered by black lichens. Around Lyon Inlet pelitic gneiss contains abundant coarse grained microcline and garnet porphyroblasts set in a matrix of biotite, quartz, feldspar, cordierite, and sillimanite. Elsewhere occurrences of garnet-cordierite-sillimanite gneiss are more sporadic; they appear to be least abundant in the northeast of the region.

The microfabric of pelitic gneiss consists of medium grained, foliated biotite, and coarse grained, granular quartzofeldspathic laminae. Parallel platy and prismatic minerals define the mineral foliation. Not uncommonly both the differentiated layering and mineral foliation are folded isoclinally (Fig. 6). Quartz, feldspar, and cordierite are xenoblastic matrix minerals with no preferred morphological orientation. Sillimanite occurs as folded fibrolite mats or dense clusters of tiny prisms. Garnets vary from skeletal to inclusion-free idioblasts, but many are xenoblastic. Generally trails of finer grained minerals wrap around coarse, ovoid porphyroblasts, but in some rocks the matrix minerals are enclosed poikiloblastically by idioblastic garnet or microcline. Effects of postcrystallization strain are shown in several thin sections by garnet porphyroblasts that have been flattened parallel to the foliation and have been broken and separated across high angle fractures. Other effects of postcrystallization strain commonly observed are bent twin planes in plagioclase, kink bands in biotite cleavage, and undulose extinction bands in quartz. For the main, however, the microfabric of pelitic gneiss in the region appears to be the result of a period of syn- and post-kinematic grain growth under conditions where the assemblage quartz-biotite-plagioclase-microcline-cordierite-garnet-sillimanite was stable in rocks of appropriate composition.

Modal analyses of 42 thin sections of pelitic gneiss are summarized in Table 4. On the average the unit appears to contain about 32 per cent quartz, 23 per cent biotite, 18 per cent plagioclase (An_{33} avg.), and 12 per cent microcline (less than 10 per cent microperthite). The remainder consists mainly of cordierite, garnet, sillimanite, and retrograde alteration minerals such as muscovite (sericite, pinite) and chlorite. Minor phases commonly observed are graphite, zircon, apatite, pyrite, iron oxide, rutile (in chlorite after biotite), epidote (after plagioclase), and calcite. More rarely observed phases are andalusite (up to 2 per cent in the same thin section with sillimanite), tourmaline, spinel, amphibole, and chalcopyrite. Many rocks contain six major minerals; some contain seven, but one phase commonly is armoured by another.

Pelitic gneiss contains as much as 50 per cent granitic material as small deformed veins and lenses which are likely of local anatectic origin. The large discordant, unfoliated granites probably are allochthonous.

The mineralogy of the pelitic gneiss indicates that the protolith was a clay-rich sediment. The rusty-weathering zones (map unit APr) richer in graphite and pyrite may be lean, sulphide-facies iron formation. Very graphitic aluminous schist found in places adjacent to the basement gneiss and basal quartzite possibly was a bauxitic regolith. Within the group pelitic gneiss seems to occur mainly at two stratigraphic positions: a lower unit commonly overlies quartzite (map unit APq) and underlies marble and calcium-silicate gneiss (map units APc and APcs), and an upper, thicker unit commonly overlies marble and calcium-silicate gneiss. The relationship between pelitic gneiss and psammitic gneiss (map unit APqb) appears to be laterally and vertically gradational. Gradual variation in the relative proportions of the biotitic and quartzofeldspathic components of these two rocks occurs in many places.

Psammitic Gneiss (APqb)

Quartzofeldspathic paragneiss (map unit APqb) is most abundant in the belt of Penrhyn Group rocks extending from southwest of Mierching Lake to the northeast corner of the map area; it also occurs near the east edge of the area northwest of Aua River. Exposure of the gneiss is variable: where it is massive (layers up to 1 m thick) and gently dipping large expanses of bedrock are typical, but where it is flaggy and steeply dipping bedrock exposure is poor. Outcrops of

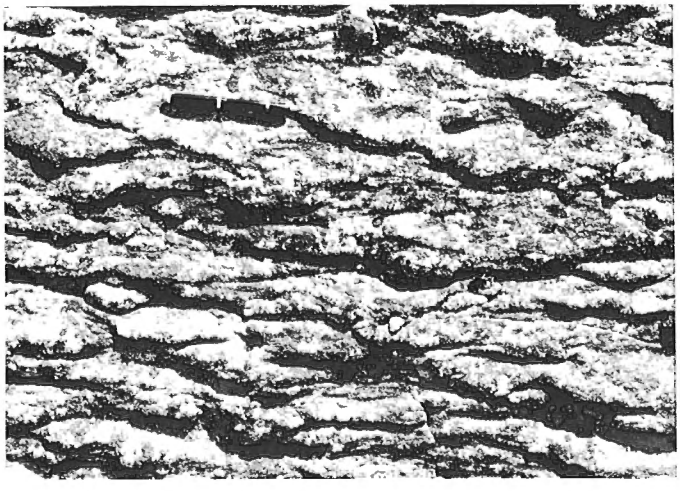

Figure 7. *Intersecting subparallel crêpe-like mullions on the surface of a calcium-silicate bed. Width of photo area is 1.4 m. (GSC 203251-A)*

psammitic gneiss are dark grey, fine- to medium-grained, granular, and covered by black lichens. Compositional layering generally is well defined and planar. Layers up to 100 cm thick are separated by 1- to 10-cm thick marble or biotite schist laminae. Commonly a thin calcium-silicate reaction rind forms a resistant lip at the contact between psammitic gneiss and marble. Weakly aligned or randomly oriented biotite flakes disseminated in the quartzofeldspathic matrix of the rock give it a salt-and-pepper appearance on fresh surfaces. Weathered exposures of massive psammitic gneiss closely resemble pelitic gneiss without its characteristic pegmatitic component. On the other hand psammitic gneiss with marble laminations superficially resembles massive calcium-silicate gneiss in outcrop.

Modal analyses of 11 thin sections of psammitic gneiss are summarized in Table 4. The rock appears to contain an average of about 44 per cent quartz, 30 per cent plagioclase (An_{38} avg.), 14 per cent biotite, and 8 per cent microcline; the remainder is made up of about 1 per cent pale green tremolite-actinolite, 1 per cent scapolite, 1 per cent muscovite (after biotite and plagioclase), and less than 1 per cent epidote (after plagioclase). Common accessory phases are graphite, apatite, zircon, and sphene. In some sections chlorite has partly replaced biotite.

The microfabric of the paragneiss consists of a rather homogeneous distribution of fine- to medium-grained quartz, feldspar, and biotite. Quartz and feldspar are xenoblastic and equant; biotite flakes are randomly oriented or define a weak foliation. Quartz commonly displays irregular, sutured boundaries and undulose extinction bands. In summary, thin sections of psammitic gneiss are rather unremarkable both mineralogically and texturally.

The protolith of psammitic gneiss probably was a coarser facies of clastic sediment than that of pelitic gneiss. The starting material may have been an arkose or arkosic wacke. The gneiss appears to occur at various structural or stratigraphic horizons within the group; in addition it appears to grade laterally into both calcium-silicate gneiss and pelitic gneiss.

Calcium-silicate Gneiss (APcs, APnc, APce)

Calcium-silicate gneiss forms a significant part of the Penrhyn Group in the map area. It occurs in several distinctively different field aspects, viz. interbedded diopside-rich calcium-silicate with marble laminae

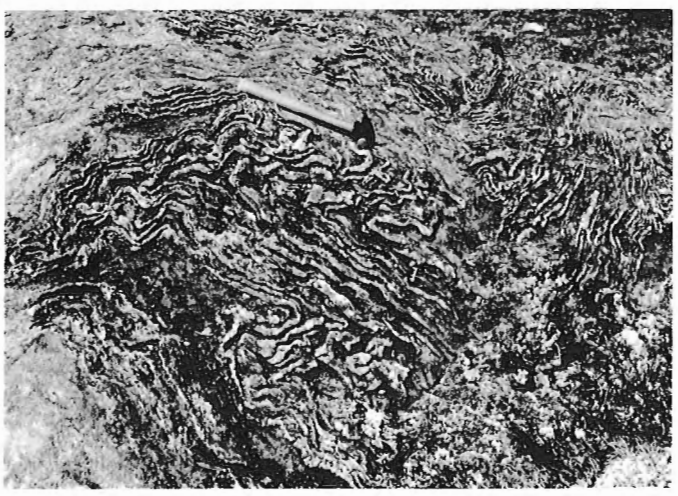

Figure 8. *Fold mullions warping axial surfaces of recumbent isoclines in calcium-silicate and marble beds. Width of photo area is 3.3 m. (GSC 203542-E)*

Figure 9. *Refolded recumbent isoclines and flattened mullions in interlayered calcium-silicate and marble. Width of photo area is 1 m. (GSC 3-8-73)*

(map unit APcs), massively bedded diopside-poor calcium-silicate gneiss (map unit APnc), and saussuritized calcium-silicate gneiss (map unit APce). Interbedded calcium-silicate and marble is the most widespread and abundant variety. Massive calcium-silicate gneiss is found mainly north of Lyon Inlet and west of Tasers Lake; in both areas it appears to grade laterally into both interbedded calcium-silicate and marble and psammitic gneiss. Saussuritized calcium-silicate gneiss is found east of Lyon Inlet; the northern occurrence passes westward into unaltered massive calcium-silicate gneiss. Of the three varieties, massive calcium-silicate gneiss generally is best exposed, but unless diopside can be identified in hand specimen it is difficult to tell from light grey psammitic gneiss (map unit APqb). Saussuritized calcium-silicate (map unit APce) has a distinctive pink-and-green mottled weathered surface due to almost complete alteration of plagioclase to epidote, chlorite, muscovite and calcite, as well as alteration of diopside to green actinolite-tremolite. Microcline weathers pink and appears to be unaltered in the thin sections examined. Interbedded calcium-silicate and marble (map unit APcs) is readily identified in the field due to the differential weathering characteristics of the two lithologies (Fig. 8, 9), but problems in designation as either marble or calcium-silicate gneiss occurred in a few places where the proportion of each lithology is about the same.

The most common mineral assemblage in calcium-silicate gneiss is plagioclase-microcline-diopside-quartz. Scapolite, calcite and tremolite-actinolite also are common locally. Generally the rock is medium- to coarse-grained granular with pale green diopside-rich and light grey quartzo-feldspathic laminae. Mineral foliation commonly is absent. In thin section feldspar, calcite, and scapolite grains generally are equant with straight-line-segment boundaries, quartz grains are irregularly-shaped, and diopside is subidioblastic. Tremolite-actinolite occurs as marginal or patchy replacement of diopside, but small subidioblastic grains occur also. The only signs of postcrystallization strain in most sections are undulose extinction bands in quartz and bent twin planes in feldspar.

A summary of modal compositions of 11 sections of diopside-poor calcium-silicate gneiss and 25 sections of diopside-rich calcium-silicate gneiss are given in Table 4. Most sections contain four or five major constituents (excluding obvious replacement minerals). The large ranges and standard deviations of the minerals listed in the table

should be noted. Calcium-silicate gneiss has more variable modal mineral abundances than the pelitic or psammitic gneisses examined. The major mineral averages given in the table show the chemical differences between the two physically distinct varieties of calcium-silicate gneiss; viz. the massive diopside-poor gneiss is more quartzofeldspathic, as well as less calcitic and diopsidic than the diopside-rich gneiss interbedded with marble. Note also that the average composition of plagioclase (optical determinations) is An_{36} in the diopside-poor gneiss and An_{60} in the diopside-rich variety. In addition to the minerals listed in Table 4, the following minerals were identified in calcium-silicate rocks: tourmaline (abundant locally), fluorite, vesuvianite (scattered occurrences of coarsely crystalline aggregates), prehnite (mostly after scapolite), and corundum (one identification).

The stratigraphic positions of calcium-silicate gneiss within the Penrhyn Group generally are unknown due to the complicated folding of the rocks and the absence of primary-facing indicators. Northwest of Aua River, calcium-silicate with marble interbeds appears to overlie the basal quartzite and to be older than a thick sequence of pelitic and psammitic gneiss in a complexly refolded and cross-faulted isoclinal anticline (Fig. 27, 28, 29). West of Tasers Lake, in an overturned, south-dipping homocline (Fig. 14), a thick section of both massive calcium-silicate gneiss (map unit APnc) and interbedded calcium-silicate and marble (map unit APcs) overlies the basal quartzite. Elsewhere, the stratigraphic position of calcium-silicate gneiss is more uncertain, and many occurrences seem to grade laterally into marble or psammitic gneiss.

The protoliths of calcium-silicate gneiss probably were quartz, feldspar, calcite psammites in places rhythmically interbedded with thin limestones (stromatolitic?). Perhaps the cyclic alternation of siliceous and calcareous beds resulted from periodic storm-driven currents depositing continental detritus in an offshore shallow-marine carbonate environment. The massive, diopside-poor calcium-silicate gneiss may have been derived from mixed siliceous and calcareous clastic sediment deposited in shallow water nearer to shore. Unfortunately, any attempt to reconstruct the depositional environment of Penrhyn Group rocks is hindered by the destruction of their sedimentary fabrics by regional metamorphism and deformation.

Marble (APc)

Numerous layers and lenses of marble (map unit APc) occur throughout the Penrhyn Group in the region mapped. Marble tends to be well exposed, and generally forms smooth, rounded, lichen-free outcrops. Where it occurs in large masses it forms ridges or buttes. Commonly the rock is very massive, coarse grained, granular, unfoliated, white- or cream-weathering calcite (rarely it is buff-weathering dolomite). A few thin, planar concentrations of calcium-silicate minerals can be found in most outcrops, and in places tightly folded calcium-silicate interbeds or marble beds with scattered, coarse grained scapolite or diopside porphyroblasts occur. Nearly all marble outcrops in the region are more-or-less permeated by white pegmatitic granite sills, dykes, and pods.

The microfabric of marble ordinarily consists of a coarse grained calcite matrix with scattered, finer grained scapolite, diopside, phlogopite, and graphite inclusions. In 50 thin sections examined the calcite grains generally form complexly intergrown sutured mosaics. Less commonly, calcite grains are polygonal or slightly flattened parallel to the foliation. Rarely, fine grained cataclastic and mortar textures occur. Calcite and dolomite grains in all of the sections examined contain deformation twins to some degree, and in many sections bent twin planes were observed.

Figure 10. *Boudinaged and folded calcium-silicate beds in marble. Width of photo area is 1.1 m. (GSC 3-10-73)*

Commonly, graphite, phlogopite and talc cleavages are bent or kinked, and feldspar, quartz, and scapolite exhibit undulose extinction.

Most marble contains more than 90 per cent calcite (generally with exsolved blebs or small interstitial grains of dolomite). Scapolite, diopside, graphite, and sphene are almost ubiquitous minor or accessory phases. Forsterite, yellow clinohumite and chondrodite (all partly altered to antigorite in most sections) are widespread, as are talc, tremolite, microcline, quartz, plagioclase (An_{35} avg.), and chlorite. A few sections examined contain purple fluorite; blue-grey tourmaline was seen also. Separate unique occurrences of the rare boron-bearing minerals serendibite and szajbelyite were observed also[1].

Large masses of coarse grained, unfoliated calcite marble with widely scattered, planar calcium-silicate laminae give the impression that the rock has undergone relatively little internal deformation. However, where calcium-silicate interbeds occur, the extent of deformation generally is revealed by sets of isoclinal folds, as well as boudinaged folds and folded boudins (see Fig. 8, 9, 10, 24, 25). Late-stage shearing of marble is indicated in a few places by foliated cataclastic textures, but the common occurrence of coarse, crystalloblastic, mosaic textures suggests that the major part of the deformation occurred prior to a late period of static grain-growth. Boudinaged and folded sills and dykes of granitic pegmatite intrude nearly all marble outcrops to some extent. Where the pegmatite occurs as extensive masses it has been mapped separately (map unit Ag).

The sedimentary texture and fabric of Penrhyn Group marble apparently has been destroyed completely by deformation and metamorphism. However, by analogy with unmetamorphosed carbonate sediments of Aphebian age found elsewhere (e.g. in the Coronation geosyncline, Hoffman, 1973) it is likely that some Penrhyn Group marble was deposited as stromatolite and oölite beds in a warm, shallow ocean. The widespread occurrence of chlorine, fluorine, sulphur, and (rarely) boron-bearing minerals in Penrhyn marble suggests that the environment may have been hypersaline. In addition the relative scarcity of interbedded pelitic and psammitic gneiss with marble indicates a depositional environment with clear water and little influx of fluvial sediment.

Generally the stratigraphic position of marble in the Penrhyn Group is not apparent. Commonly it is found in contact with granitoid basement gneiss, but at these

[1] These occurrences are described in the section on metamorphism.

localities marble or basement gneiss may be allochthonous. In areas where the basal quartzite is present (e.g. west of Tasers Lake and northwest of Aua River, Fig. 14, 27) a thick marble is the second or third lithologic unit in the succession overlying quartzite or a lower pelitic gneiss. In the belt of Penrhyn Group rocks extending from southwest of Mierching Lake to the northeast corner of the map area, marble, calcium-silicate gneiss, psammitic gneiss, and pelitic gneiss appear to be interbedded, but their relative stratigraphic positions are unknown because the geometry of the macroscopic structures in the belt is not known.

Ultrabasic Rocks (Aub)

A few lenses of mafic and ultramafic rocks (map unit Aub) occur in the centre of the map area near the Penrhyn Group-granitoid gneiss contact. The ultrabasic bodies are single lenses a few tens of metres wide and a few hundreds of metres long, except one larger mass on the shore of Norman Inlet about 7 km long and 1 km wide that contains some intermixed amphibolite and pelitic gneiss. Exposure of the ultrabasic rocks tends to be poor. They weather dark brown, and are dark green on fresh surfaces.

Textures seen in thin sections are mainly unfoliated, medium- or coarse-grained subidioblastic granular. Several thin sections from the Norman Inlet body display very coarse grained, symplectic intergrowths (Fig. 34) of hornblende, hypersthene, garnet, and plagioclase (An_{55}). Other mineral assemblages noted in ultrabasic rocks are as follows: hypersthene-olivine-hornblende, clinopyroxene-hornblende-biotite-magnetite, hypersthene-hornblende-plagioclase (An_{80})-magnetite, and hornblende-garnet-biotite. In several sections hornblende is altered marginally to cummingtonite. The unfoliated, granular, and symplectic textures of the ultrabasic rocks indicate that their final crystallization was postkinematic: supporting a similar conclusion drawn from textural studies of most other rocks in the map area.

The origin and relative age of the ultrabasic rocks is not apparent. Although they seem to be stratiform and to occur at about the same stratigraphic position in the Penrhyn Group as amphibolite the two lithologic units have not been observed in lateral continuity. The rocks could be Aphebian ultramafic flows or sills.

Granitic Rocks (Ag)

Late-tectonic granitic bodies (map unit Ag) intrude all of the older rocks in the region. They are especially common intruding Penrhyn and Prince Albert group rocks; they also intrude granitoid gneisses, especially near and between contacts with the supracrustal rocks. The granites weather chalk-white and are very leucocratic where they intrude marble and calcium-silicate gneiss; where the host rock is pelitic or granitoid gneiss, they are biotitic and weather pink, orange or rust-brown. The granites vary greatly in size and texture: smaller bodies are generally pegmatitic, whereas larger intrusions have textures varying from fine grained aplitic to coarse grained granular; no porphyritic granites were seen.

The granites observed in thin section are not foliated, although one rock examined exhibits mortar texture, and most minerals show weak undulatory extinction. Plagioclase (An_{28} avg.) generally has sericitized cores and clear rims. Microcline (less than 5 per cent perthite) is unaltered and commonly is embayed by myrmekite at plagioclase contacts. The average modal mineral composition of 20 thin sections of granitic rocks examined from the map area is 31 per cent quartz (s.d. 4.8%), 41 per cent plagioclase (s.d. 13.4%), 24 per cent microcline (s.d. 14.2%), 3 per cent biotite (s.d. 2.5%), and about 1 per cent chlorite (after biotite). Accessory minerals noted are muscovite, epidote, allanite, zircon, calcite, graphite, pyrite, and iron oxide. The modal proportions of quartz, plagioclase and microcline from the thin section estimates are plotted on Figure 5: the rocks range from quartz diorite to quartz monzonite; most of them are quartz monzonites.

Contacts with country rocks ordinarily are sharp and locally discordant. Smaller intrusions generally contain abundant inclusions; some pegmatites intruding marble form dense intrusion breccias with the host rock. Large plutons are relatively inclusion-free, and marble is the most common xenolith observed. Granite that intrudes Archean granitoid gneiss is migmatitic in places and difficult to distinguish from the host rock; in general, however, the younger granite is biotitic whereas the older granitoid gneiss contains hornblende.

The wide distribution of granite in the map area suggests that many magma sources were present; the most likely origin is by partial anatexis of nearby pelitic and granitoid gneiss. Abundant quartzofeldspathic laminae in pelitic gneiss provide a small-scale example of the palingenetic process.

The granite appears to be late synkinematic to postkinematic; smaller pegmatite dykes and sills are more deformed than the larger intrusions and are older.

Diabase Dykes (NHd)

A few northwest-striking posttectonic diabase dykes (map unit NHd) intrude Archean and Aphebian rocks in the map area. They vary from 3 to 30 m wide, and have been traced continuously along strike for as much as 10 km. The dykes are more resistant to erosion than most of the rocks they intrude, and tend to form low, thick walls with horizontal columnar joints. The diabase weathers dun-brown; fresh surfaces are dark grey.

Textures observed in three thin sections are medium grained ophitic with about 60 per cent randomly oriented plagioclase laths (An_{60} avg.), and about 30 per cent interstitial augite. About 5 per cent skeletal magnetite associated with augite, and 5 per cent interstitial micropegmatite occur also in the sections examined. Green amphibole and brown biotite appear to replace some of the augite in one section. Some postcrystallization strain is shown in the sections by undulose extinction and minor fracturing of pyroxene and plagioclase.

The dykes are emplaced parallel to a prominent set of northwest-striking vertical fractures: some of which offset lithologic boundaries up to 1 km. Other than the minor strain features seen in thin sections, the dykes are undeformed.

The diabase is post-Aphebian and may be correlated with either the Hadrynian Franklin dykes (Fahrig et al., 1971) common in Baffin Island or the similar-looking Neohelikian Mackenzie dykes abundant in the Coppermine area. Fahrig and Jones (1969) correlated northwest-trending diabase dykes in Rae Isthmus (northwest of the Lyon Inlet area) with the Mackenzie swarm, but Fahrig et al. (1971) assigned northwest-trending diabase dykes in east-central Melville Peninsula (northeast of the Lyon Inlet area) to the Franklinian swarm. Potassium-argon ages of the Rae Isthmus dykes range from 941 to 1010 Ma (Fahrig and Jones, 1969); the Franklinian dykes on Baffin Island are about 700 Ma old (Fahrig et al., 1971).

Bad Cache Rapids Formation (OB)

Two exposures of limestone were mapped on the valley wall west of Hoppner Inlet. The northern exposure lies between 100 and 130 m above sea level, and the southern exposure is between 70 and 120 m above sea level; the

surrounding Precambrian upland surface rises to about 300 m above sea level. The limestone overlies an east-dipping unconformity developed on Archean granitoid gneiss. The unconformity dips in the same direction as the present valley wall. Because the limestone occurs more than 150 m below the present Precambrian upland surface, it must have been deposited in a similar deep, narrow valley.

The limestone is about 10 m thick; bedding is finely (1-5 cm) and irregularly developed. Weathered surfaces are mottled grey and fresh surfaces are light brown. The limestone exposed in Hoppner Inlet is similar in appearance to the upper unit of the Bad Cache Rapids Formation from Hall Lake (late Middle Ordovician) described in section 13 and pictured in Figure 17 of Bolton et al. (1977, p. 4 and p. 19). Fossils collected from exposures at Hoppner Inlet as described by T.E. Bolton (in Bolton et al., 1977, p. 5) are:

"GSC loc. 91955

Most northern Paleozoic exposure west side of Hoppner Inlet, approximately 66°55'N, 84°W (see GSC Map 14-1966), J.E. Reesor 1973 collector. Bad Cache Rapids Formation: 20+ ft exposed at top of long ridge, 40+ ft high; fossils collected from foot of exposure include **Receptaculites** sp., **Plasmoporella lambei** (Bolton, this bulletin, p. 30, Pl. 6, figs. 3, 4), **Catenipora** sp., columnal debris, **Strophomena**(?) sp., **Trochonema** sp., calymenid and encrinurid trilobite fragments, and **Krausella** sp.

GSC loc. 66758

Top of southern exposure west side of Hoppner Inlet, 66°55'N, 83°55'W (see GSC Map 14-1966), B.G. Craig 1964 collector. Bad Cache Rapids Formation: 4- to 6-ft exposure; fossils collected include crinoidal debris, **Resserella** sp., **Maclurites** sp., **Trochonema** sp., **Illaenus lacertus** (Bolton, this bulletin, p. 37, Pl. 18, fig. 4) and leperditiid ostracodes indet.

GSC loc. 66725

Central-east shore of Hoppner Inlet, 66°51'N, 83°50'W (see GSC Map 14-1966), W.W. Heywood 1964 collector. Bad Cache Rapids Formation: 25 ft of rubbly limestone exposed; fossils collected include **Receptaculites** sp., **Dinorthis** sp., **Sowerbyella** sp., **Zygospira** sp., **Maclurites** sp., **Gorbyoceras baffinense** and leperditiid ostracodes indet.

GSC loc. 66726

Red Point, southeastern end of Hoppner Inlet, 66°47'N, 83°54'W (see GSC Map 14-1966), W.W. Heywood 1964 collector. Bad Cache Rapids Formation: fossils collected include **Grewingkia** sp., **Calapoecia** sp., **Catenipora aequabilis**, **Dinorthis** sp., **Rhynchotrema** sp., **Hormotoma** sp., **Maclurites** sp., **Trochonema** sp., **Cyclendoceras** sp., **Metaspyroceras**(?) sp., **Gorbyoceras** sp., isotelid trilobite fragment and leperditiid ostracodes indet."

STRUCTURAL GEOLOGY

The rocks of the Lyon Inlet area reveal fragments of a complex strain history, most of which is recorded in the Hudsonian structural fabric of Penrhyn Group paragneiss. Although radiometric results (Table 15) indicate Kenoran metamorphism affected granitoid basement gneiss in the area, signs of any pre-Hudsonian structures seem to have been completely obliterated.

The earliest secondary structure recognized in Penrhyn Group rocks is a platy mineral foliation that parallels bedding in many paragneissic units. Originally this may have been an axial-plane foliation but subsequent deformation apparently has obscured any related folds in bedding. Several phases of recumbent isoclinal folds (D_1) mapped in Penrhyn Group paragneiss represent the oldest macroscopic structures recognized in the Lyon Inlet area. Emplacement of basement gneiss nappes into the succession of Aphebian supracrustal rocks occurred early in the D_1 event. The original trend of the recumbent fold hinges may have been at a large angle to the strike of the Foxe Fold Belt.

The northeast-southwest structural grain characteristic of Foxe Fold Belt resulted from the last major deformation (D_2) of the rocks in the region. Geometries of transposed earlier structures indicate that the D_2 strain is characterized mainly by intense horizontal elongation: early fold axes are folded isoclinally and elongated parallel to the strike of the fold belt; limbs and axial surfaces of early folds commonly are deformed into open, upright, low-amplitude folds plunging at a few degrees, but isoclinal, upright, inclined and reclined folds occur also. Widespread intrusion of granitic plutons occurred mainly after the penetrative D_2 strain.

Predominantly static conditions have prevailed in the region since the peak of metamorphism more than 1750 Ma ago. Postkinematic aplitic to pegmatitic granite plutons occur throughout the region, and coarse grained mosaic and delicate symplectic textures of high grade mineral parageneses are nearly ubiquitous. Lower grade shearing was confined to local zones mainly in the augen gneiss near the north margin of the map area. Sometime before or during intrusion of Helikian or Hadrynian diabase dykes the crust fractured and faulted along steeply dipping northwest-striking surfaces. By Middle Ordovician time Foxe Fold Belt had been eroded to about the present level and subsequent down-warping permitted marine limestone to be deposited on an irregular unconformity. Recently the region has been subjected to glacial isostatic adjustments of elevation: since the depression of the area by Pleistocene ice, about 100 m of rebound has occurred.

Structural Fabric Elements

Several structural fabric elements composing part of the mesoscopic fabric of the gneissic units were recorded systematically in the field. Some of these elements are symbolized on the geologic map; all of them have been useful to interpret the structural history and macroscopic geometry of the gneisses in the region.

Bedding

Primary stratification is preserved in some paragneiss as interfaces between calcium-silicate and marble (Fig. 8, 9, 10, 24, 25), and between psammitic and pelitic gneiss. It is assumed that bedding surfaces originally were nearly horizontal and planar; bedding now is folded isoclinally.

Gneissosity

Surfaces between compositionally differentiated layers in plutonic granitoid rocks probably developed during metamorphism. When differentiation took place, gneissosity may have been plane-parallel in large volumes of rock, but its original attitude cannot be assumed. Gneissosity now is folded isoclinally.

Mineral Foliation

Parallel arrays of platy mineral grains are aligned with bedding or gneissosity in most rocks of the area. It may be assumed that mineral foliation cuts across bedding and gneissosity in some fold hinges, but this relationship seems to have been obscured completely by several sets of folds superimposed on the foliation. Figure 6 shows a typical

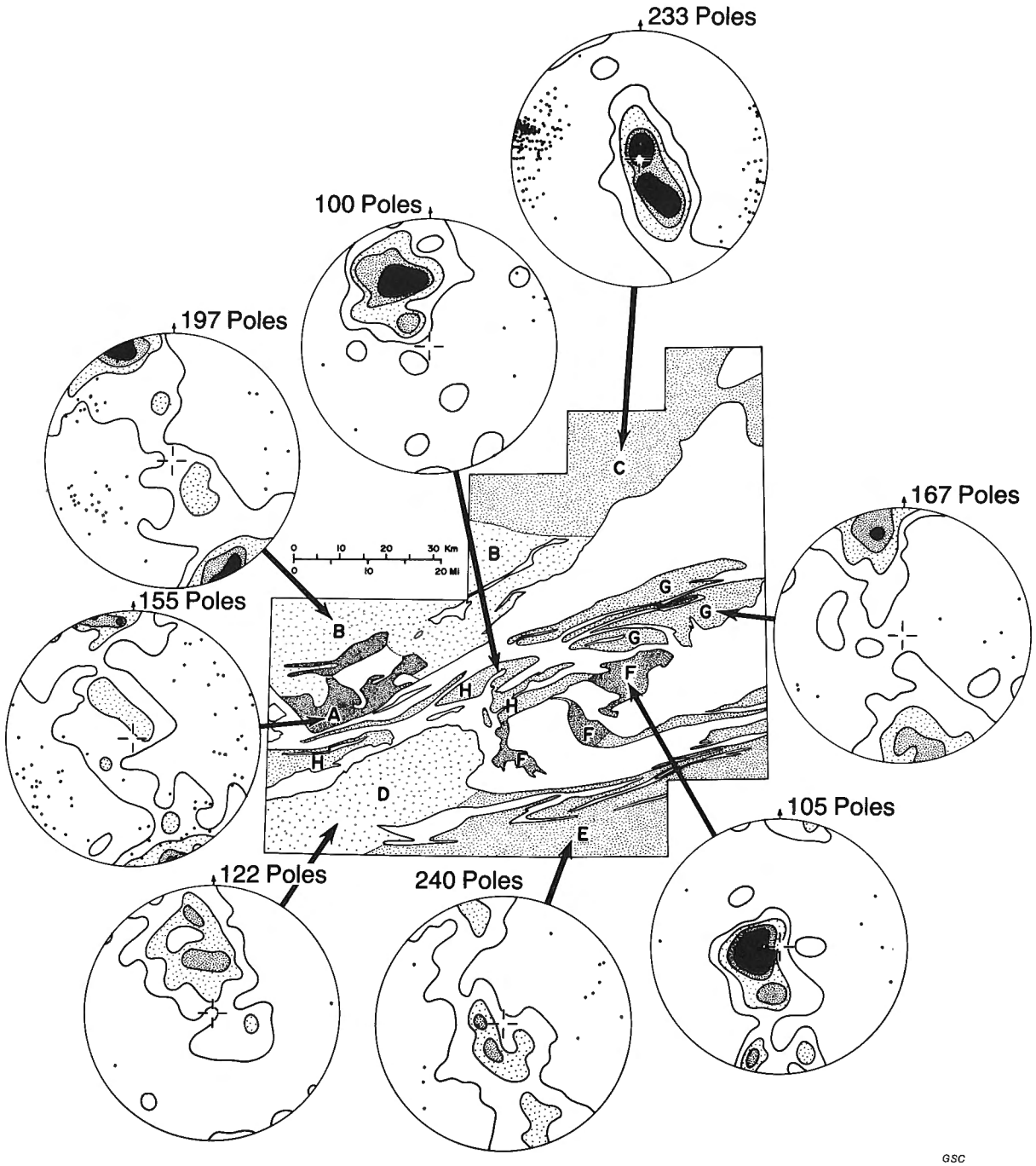

Figure 11. *Macroscopic geometry of Prince Albert Group paragneiss (domain A) and Archean granitoid gneiss (domains B through H) in the Lyon Inlet area. Mesoscopic structural fabric elements are displayed on the lower hemisphere of the equal-area projection. Bedding, gneissosity, and foliation poles are contoured (contour values 1, 3, 5, 7 per cent/unit area); fold axes and mineral lineations are shown by dots.*

microscopic-scale fold in mineral foliation. Because foliation regularly parallels bedding and gneissosity on the outcrop, and was not observed to parallel axial planes of mesoscopic folds, mineral foliation is not designated by a separate symbol on the geologic map.

Mullions and Fold Mullions

Low-amplitude crêpe-like corrugations commonly are developed on one or both surfaces of calcium-silicate beds in contact with marble. Ordinarily one set of parallel mullions occurs, but intersecting sets of mullions were seen in a few places (Fig. 7). Low-amplitude folds with semi-circular profiles are referred to as fold mullions (Fig. 8). Mullions, fold mullions and open folds generally are associated spatially and have parallel axes.

Mesoscopic Folds

Small folds occur in layered gneiss throughout the region; they are abundant in thinly interbedded sequences of calcium-silicate gneiss and marble, and are least evident in homogeneous or massively layered rocks. Fold elements most commonly measured are the orientations of the axial surface

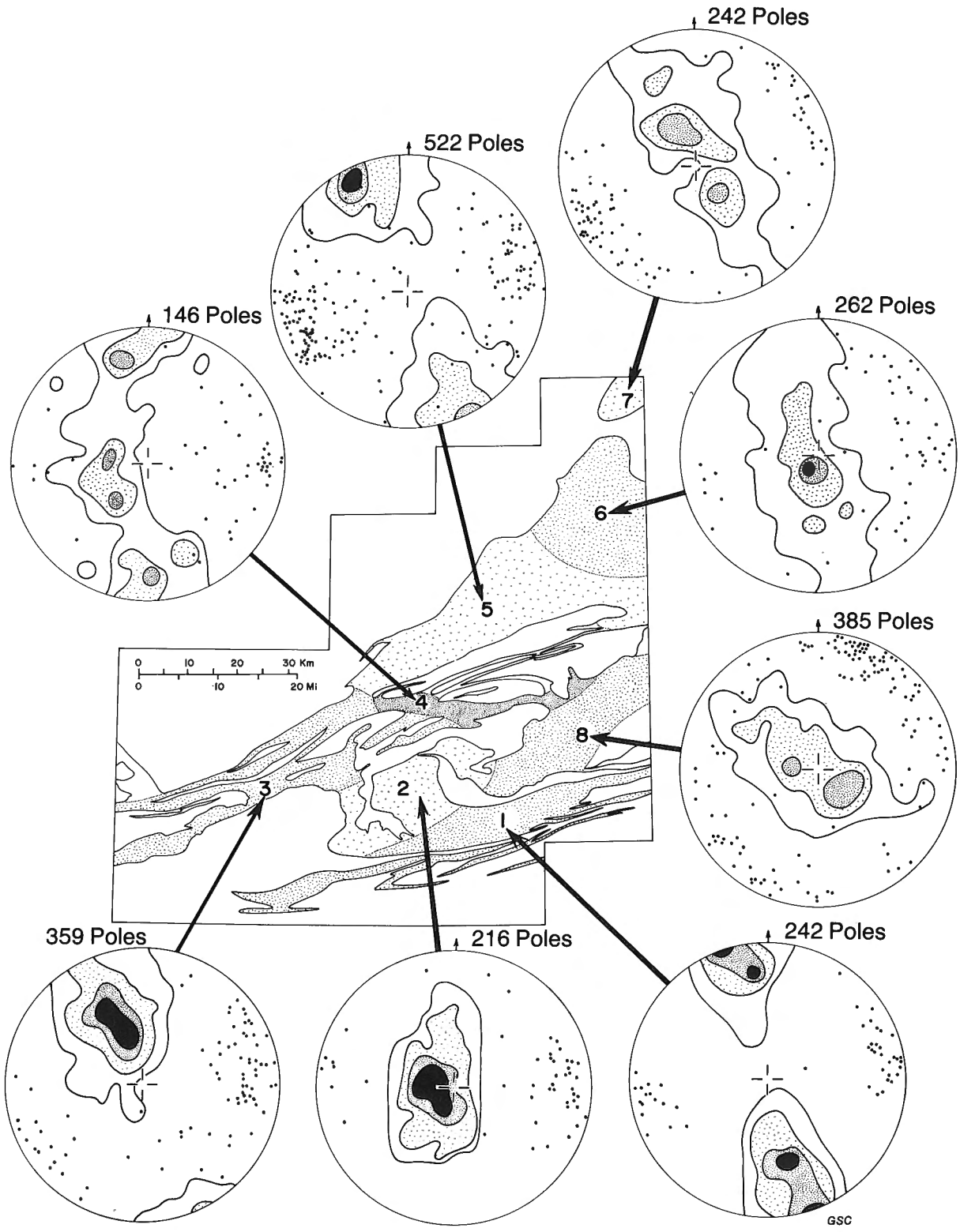

Figure 12. *Macroscopic geometry of Penrhyn Group paragneiss in the Lyon Inlet area. Mesoscopic structural fabric elements from domains 1 through 8 are displayed on the lower hemisphere of the equal-area projection. Bedding and foliation poles are contoured (contour values 1, 3, 5 and 7 per cent/unit area); fold axes and mullions are shown by dots.*

and fold axis. In a few exposures two or more antiformal or synformal crests or troughs defined the orientation of an enveloping surface. The majority of mesoscopic folds are either isoclinal folds or low-amplitude fold mullions. In some outcrops fold mullions were seen to deform recumbent isoclinal folds (Fig. 8). Rare examples of intersecting recumbent isoclinal folds also were observed (Fig. 9).

Mineral Lineations

Parallel arrays of elongate mineral grains occur in some rocks in the area: they are most common in Archean augen gneiss where prolate and triaxial-ellipsoidal feldspar megacrysts occur. In the Prince Albert Group rocks, linear alignment of hornblende prisms occurs in some amphibolite and paragneiss, and in Penrhyn Group rocks, aligned scapolite rods are found in some marble occurrences. Mineral lineations ordinarily parallel mullions and fold axes in the same outcrop.

Boudins

Boudinage structures most commonly occur in calcium-silicate beds enclosed by marble. Boudins were observed also in granitic layers in both marble and pelitic gneiss, as well as amphibolite layers in granitoid gneiss. In places boudinaged beds have been folded (Fig. 10), and some previously folded or mullioned beds have been boudinaged.

Joints

All rocks in the area are jointed. Most outcrops show one or two sets of variably-spaced fractures, but because of time limitations, coupled with a greater concern for determining the complex geometry of structures developed when the rocks were more plastic, joint orientations were not measured systematically.

In the northwest of the area, especially around Mierching Lake, the topographic expression of northwest-striking joints is emphasized by parallel valleys, lakes (Mierching Lake included), and rivers. This set of fractures also parallels the Hadrynian or Helikian diabase dykes, and in some places parallels minor faults.

Macroscopic Geometry of Structural Fabric Elements

Figures 11 and 12 show orientation patterns of planar and linear structural fabric elements displayed on lower hemisphere, equal-area projections. The data in each equal-area plot were collected from the structural fabric domains outlined on the figures. The purpose of the figures is to summarize subregional variations in the symmetry and orientation patterns of mesoscopic structures.

In dividing the map area into structural fabric domains, variations on two orientation patterns of poles (normals) to bedding and gneissosity were sought: a point maximum or a great-circle locus. On the equal-area net a circular cluster (point maximum) of poles to bedding or gneissosity indicates that the surfaces are parallel within the fabric domain; the element may be summarized by the plane whose pole is located in the apparent centre of the cluster[1]. Considering that bedding and gneissosity display abundant mesoscopic isoclinal folds in the Lyon Inlet area, point-maximum symmetry indicates the axial surfaces of isoclinal folds are plane parallel in the fabric domain.

A great-circle locus of poles to bedding or gneissosity indicates that the surfaces have more variable orientations than the point-maximum symmetry. In this symmetry pattern the family of surfaces has a common line of intersection normal to the planar distribution of poles. Considering once more that bedding and gneissosity are folded isoclinally, a complete great-circle locus or "girdle" of poles describes a system of open coaxial folds in the axial surfaces of early isoclinal folds. A partial great-circle locus of poles is a third common symmetry pattern of planar fabric data. This pattern in the Lyon Inlet area results from either weakly developed coaxial warps or tight coaxial folds in the axial surfaces of early isoclinal folds. The correct interpretation is apparent from field observations of the planar element within the fabric domain.

With one exception, the structural fabric domains on Figures 11 and 12 were outlined by inspection of the geologic map and adjustment of the domain boundaries by trial-and-error plotting of bedding or gneissosity poles until the best-looking example of one of the desired fabric symmetry patterns was achieved. The exceptional domain is the principal outcrop area of Prince Albert Group rocks, domain A on Figure 11: in this domain bedding, rather than gneissosity, is the planar fabric element displayed on the equal-area net.

Structural Fabric Geometry of Prince Albert Group Rocks and Granitoid Gneiss Units

Archean rocks outlined in Figure 11 comprise eight structural fabric domains: domain A is the principal outcrop area of Prince Albert Group rocks, B through H compose granitoid gneiss domains where equigranular layered gneiss is common, except in domains B and C where some lineated augen gneiss occurs.

In domain A, contoured bedding poles from Prince Albert Group paragneiss describe a broad great-circle locus in the stereonet. The best-fit great circle summarizing the wide bedding-pole girdle is vertical and strikes about 340°; fold axes and mineral lineations are scattered around the periphery of the net and bear no symmetrical relationship to the bedding-pole pattern. The complete great-circle girdle of bedding poles indicates that axial surfaces of mesoscopic isoclines in bedding are bent into open folds with horizontal axes trending northeast-southwest: parallel to the pole of the plane summarizing the locus of bedding normals. Because the linear structural elements in domain A are dispersed widely, it appears that the strain (D_2) producing the northeast-southwest axial plane folding was not sufficient to align them.

Gneissosity surfaces measured in granitoid gneiss in domain B display a broad great-circle girdle of poles that resembles the bedding-pole pattern in domain A. The girdle of gneissosity poles is summarized by a vertical great-circle striking northwest-southeast; most of the poles in the stereonet are horizontal and indicate a predominance of vertical gneissosity surfaces. Mineral lineations are bimodally distributed: one broad cluster is centred near the line normal to the gneissosity-pole girdle; the other more dense cluster is asymmetrical to the gneissosity fabric pattern, and plunges northwest at about 10°. The northwest-plunging lineations are part of the population displayed more abundantly in domain C.

The macroscopic geometry of the fabric elements in domain C is dominated by a dense cluster of mineral lineations plunging northwest at less than 10°. This anomalous plunge direction in the Lyon Inlet area is related to local development of cataclastic augen gneiss in the northwest of the region. The cataclastic textures characteristic of these rocks postdate the high temperature annealed textures common in gneiss to the south. The gneissosity poles in domain C lie in a great-circle girdle roughly parallel to the girdles in domains A and B, but with a dominance of subhorizontal attitudes. The orientation of the best-fit great circle suggests the gneissosity was deformed during the

[1] Poles to bedding and gneissosity are density contoured on the equal-area nets in Figures 11 and 12 to facilitate interpretation of fabric geometry.

Figure 13. *Outline geologic map of the Lyon Inlet area showing the location of regions discussed in detail.*

1. *The region west of Tasers Lake,*
2. *The region north of Lyon Inlet,*
3. *The region north of Hoppner Inlet,*
4. *The central gneiss massifs,*
5. *The region west of Aua River,*
6. *The northeast corner of the Lyon Inlet area.*

Areas of random dot pattern are underlain by Aphebian rocks. Areas of Archean rocks are unpatterned.

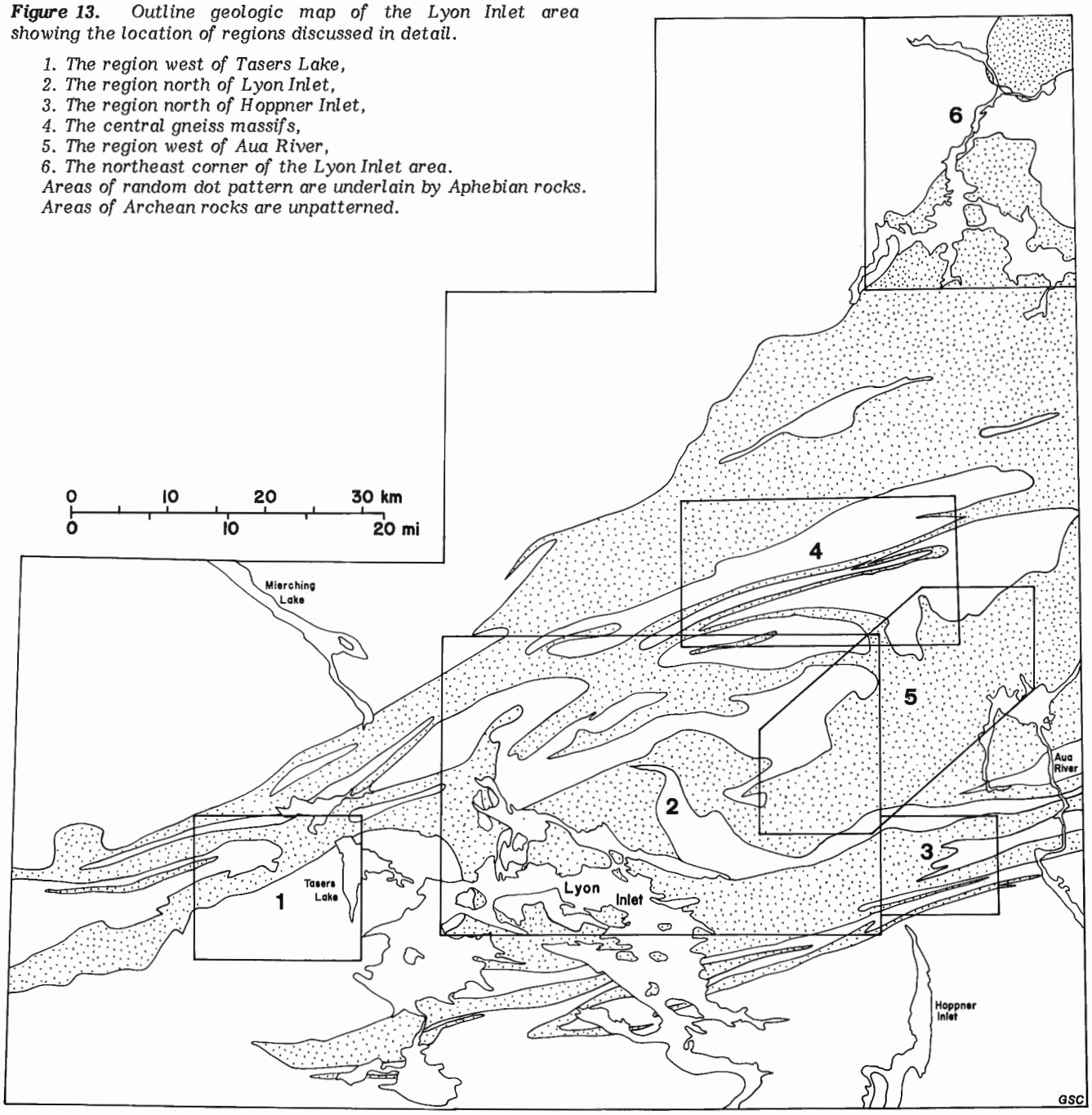

northeast-southwest folding (D_2), but was not effectively re-oriented by the later (post-D_2?) shearing that produced the elongate augen plunging northwest.

Granitoid gneiss bordering the south margin of the map area mostly strikes northeast: in domain D the partial great-circle locus of poles indicates that most of the gneiss dips southeast between 20 and 70°; in domain E, gneissosity poles describe a full great-circle pattern with the pole to the best-fit great-circle plunging northeast at about 10°. Mineral lineations plotted in both domains are few and scattered.

Basement gneiss massifs surrounded by Penrhyn Group supracrustal rocks compose domains F, G and H. Domain F is dominated by gneiss dipping east at about 10°, but some north-dipping gneiss occurs also. In contrast, gneissosity surfaces in domain G are mainly vertical or nearly so, and strike northeast. In domain H, most of the gneiss dips southeast at 45°. Mineral lineations in domains F, G and H are developed insignificantly.

The macroscopic fabrics in Archean basement rocks appear to be influenced most strongly by D_2 folding which produced the characteristic grain of the Hudsonian Foxe Fold Belt. The best-fit great circles summarizing the distributions of bedding and gneissosity are mainly vertical, indicating the late folds are mostly horizontal. Linear structures in basement gneisses generally are very heterogeneous, and show the symmetry of the late northeast-southwest folds much less than the gneissosity and bedding. Although D_2 folds dominate the macroscopic geometry and symmetry of the basement gneiss, the mesoscopic fabric indicates a history of earlier penetrative deformation that includes

development of gneissosity and foliation followed by isoclinal folding of these surfaces. Formation of cataclastic textures in augen gneiss near the northwest margin of the Lyon Inlet area probably postdates the D_2 folding in Foxe Fold Belt.

Structural Fabric Geometry of Penrhyn Group Rocks

Aphebian Penrhyn Group paragneiss in the Lyon Inlet area comprises eight structural fabric domains shown in Figure 12. The contoured bedding pole equal-area plots indicate symmetry patterns and orientations similar to the gneissosity-pole fabric diagrams shown in Figure 13. The imprint of the D_2 folding on the bedding geometry is pronounced. Fold axes and mullions reflect the late folding less definitively: they show considerable scatter around the periphery of the diagrams. In interpreting the significance of the equal-area plots of mesoscopic fabric elements, it must be noted that mesoscopic isoclinal folds occur in Penrhyn Group rocks throughout the Lyon Inlet area. In domains where the isoclines are oriented similarly, bedding-pole plots will tend to show point-maximum symmetry, and in domains where axial surfaces of isoclines are folded about parallel axes bedding-pole plots will show partial or complete great-circle girdle patterns.

Bedding poles in domains 1, 2, and 3 (Fig. 12) show limited scatter in the equal-area plots, and may be summarized within each domain by the dominant orientation of the axial surfaces of the isoclinal folds: in domain 1, the surfaces are mainly vertical and strike nearly east-west; in domain 2, they dip east at about 10°, and in domain 3 they dip southeast at about 45°. Fold axes and mullions in the three domains tend to plunge northeast or southwest at a few degrees; in domain 2 linear elements mainly plunge down the dip of reclined folds, but in domains 1 and 3 they do not indicate a regional plunge direction.

Bedding poles in domain 4 fall along a complete great-circle locus on the stereonet; the pole to the best-fit great circle plunges east at about 20°. Linear elements are scattered, but mainly plunge east at 20° or less. The fabric patterns of bedding poles and lineations in domain 4 indicate that axial surfaces of early isoclines are folded about east-plunging axes. The fabric geometry within domain 4 is very similar to the combined structural fabrics of domains 1, 2, and 3.

In domain 5 bedding poles show a pronounced point-maximum symmetry pattern which may be summarized by a surface dipping southeast at 80°. This dominant attitude of bedding in the domain reflects a pronounced preferred orientation of the axial surfaces of isoclinal folds. Fold axes and mullions cluster around the strike of the dominant axial surface, and indicate a slight preference to plunge southwest at about 10°. Inspection of the geological map shows that plunge reversals occur throughout domain 5, and the region cannot be divided into smaller east- and west-plunging segments. Note the strong similarity between the bedding-pole fabric of domain 5 and the gneissosity-pole fabric of domain G in Figure 11. Considered together, the two domains outline a large region of upright horizontal isoclinal D_2 folds in bedding and gneissosity.

Bedding poles in domain 6 indicate a partial great-circle girdle pattern with the pole to the best-fit great circle plunging east at 10° or less. The bedding-pole fabric also shows a clear preference for beds and axial surfaces in the domain to strike north-south and dip east at 10° or less, indicating that the folds mainly are reclined. Linear elements are scattered widely; most of them plunge in the east quarter of the hemisphere.

Domain 7 is the southwest end of an elliptical belt of Penrhyn Group rocks extending about 70 km northeast (Fig. 31); Archean basement gneiss along the margins of the paragneiss belt dips away from the breached antiformal core of Aphebian rocks. The equal-area plot of mesoscopic structural fabric data from the domain does not define clearly a regional plunge direction: bedding poles are spread along a vertical great-circle locus; linear elements mainly plunge southwest, but northeast-plunging folds occur also. Inspection of the geological map, however, reveals several west-dipping marble units that wrap-around parallel to the southwest margin of the domain, and indicate clearly the structure is an open D_2 antiform plunging southwest at a few degrees. Paragneiss in domains 6 and 7 plunges in opposite directions; the strip of basement gneiss separating the domains marks the zone of plunge reversal and overlies the Aphebian rocks.

The fabric symmetry of mesoscopic structures in domain 8 is difficult to summarize because both planar and linear elements are too widely scattered. The only generalizations apparent from the equal-area plot are that dips and plunges are low, and strikes are more northerly than in other domains.

The macroscopic geometry of structural elements in Aphebian paragneiss, like the Archean rocks, is strongly influenced by the D_2 folding characteristic of Foxe Fold Belt. The late folds plunge northeast at about 10° in domains 2, 4 and 6; in domains 1, 3, 5 and 8 no regional plunge is indicated, and in domain 7 the regional plunge is southwest at 10° or less. It is interesting that the late folds do not display a consistent vergence; axial surfaces and limbs of early isoclines vary from horizontal to vertical as a result of the northeast-southwest folding. In some domains axial surfaces and bedding are nearly parallel throughout (domains 1, 2 and 5), whereas in other domains planar fabric elements are bent into open folds about northeast-southwest axes (domains 4, 6 and 7).

Comparison of Structural Fabric Geometries

Gneissosity and bedding fabrics in adjacent domains (cf. Fig. 11, 12) indicate close similarities in patterns and orientations. In domains 2 and F bedding and gneissosity dip predominantly east at about 10°; in domains 3 and H they dip predominantly southeast at about 45°, and in domains 5 and G they are nearly vertical and strike northeast-southwest. The close correspondence between bedding and gneissosity fabrics indicates that either the planar elements were parallel prior to the D_2 deformation or they were transposed into nearly identical patterns during the D_2 deformation.

In contrast to the strong influence of the D_2 strain on the planar fabric elements, linear elements in nearly all domains show a wide scatter. It is not clear whether the present orientations of linear structural elements resulted from dispersion of originally parallel lineations or partial transposition of originally more randomly oriented lineations. Considering, however, that the fabrics of planar elements clearly show the geometry of the D_2 folds, it seems reasonable to assume early linear elements originally were more variable in trend and transposition parallel to the northeast-southwest D_2 fold axes was incomplete in most domains.

Structural Studies in Parts of the Lyon Inlet Area

Details of the macroscopic geometry of specific structures are more clear in parts of the Lyon Inlet area than in others; attempts are made in six regions (Fig. 13) to draw logical inferences about large structural features from mesoscopic structural fabrics and local stratigraphic relations. In some parts of the map area the superposition of structures is more apparent than in others; perhaps by drawing attention to specific parts of the region that are more amenable to structural interpretation, a clearer understanding of the development of this complex fold belt will emerge.

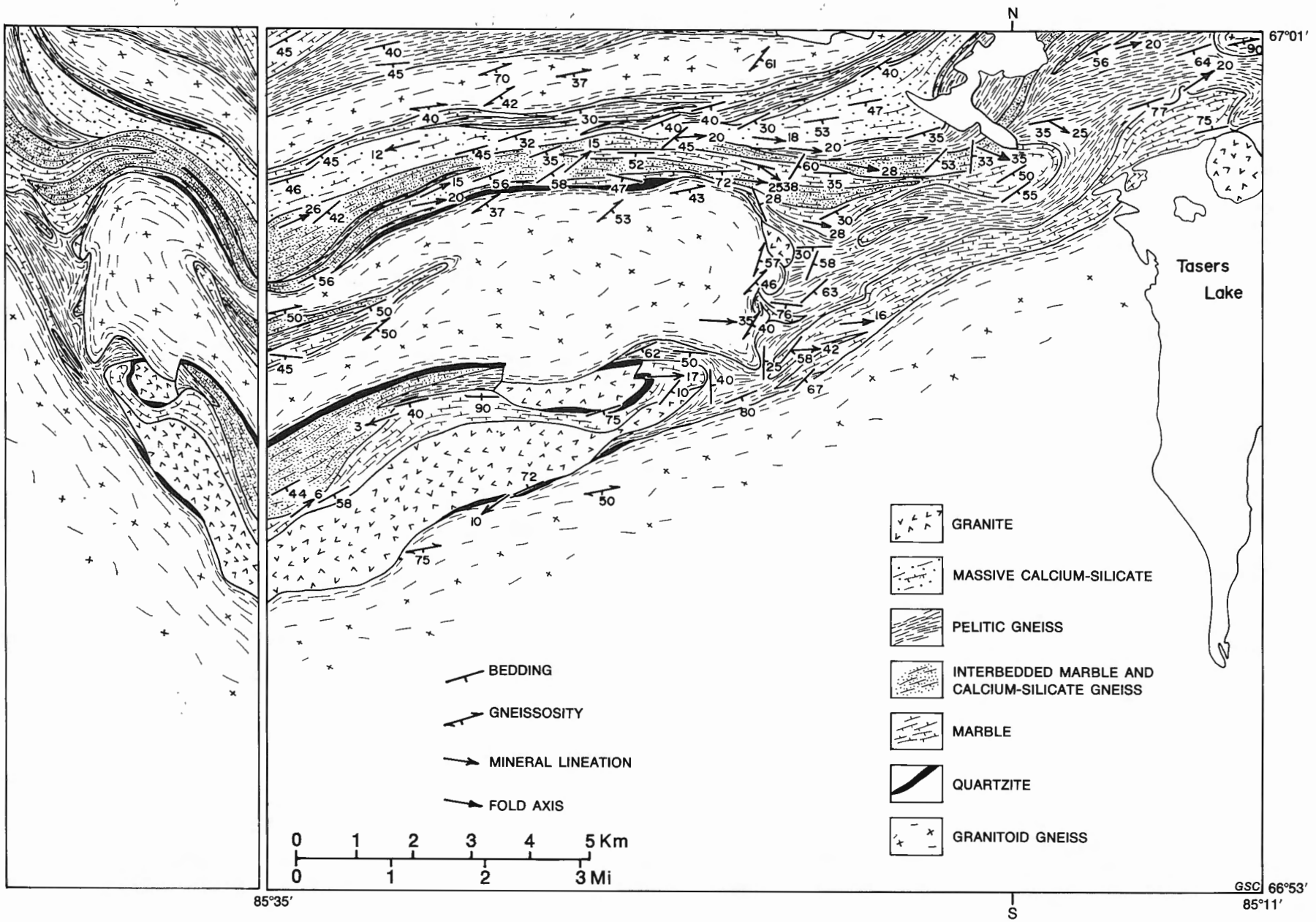

Figure 14. *Geologic map and up-plunge tectonic profile of the region west of Tasers Lake, Lyon Inlet area. The profile shows the part of the map west of the N and S marks on the margins projected onto a surface dipping 70° west; the projection plane is normal to the dominant regional plunge (20° east) indicated by mesoscopic structural elements in the area.*

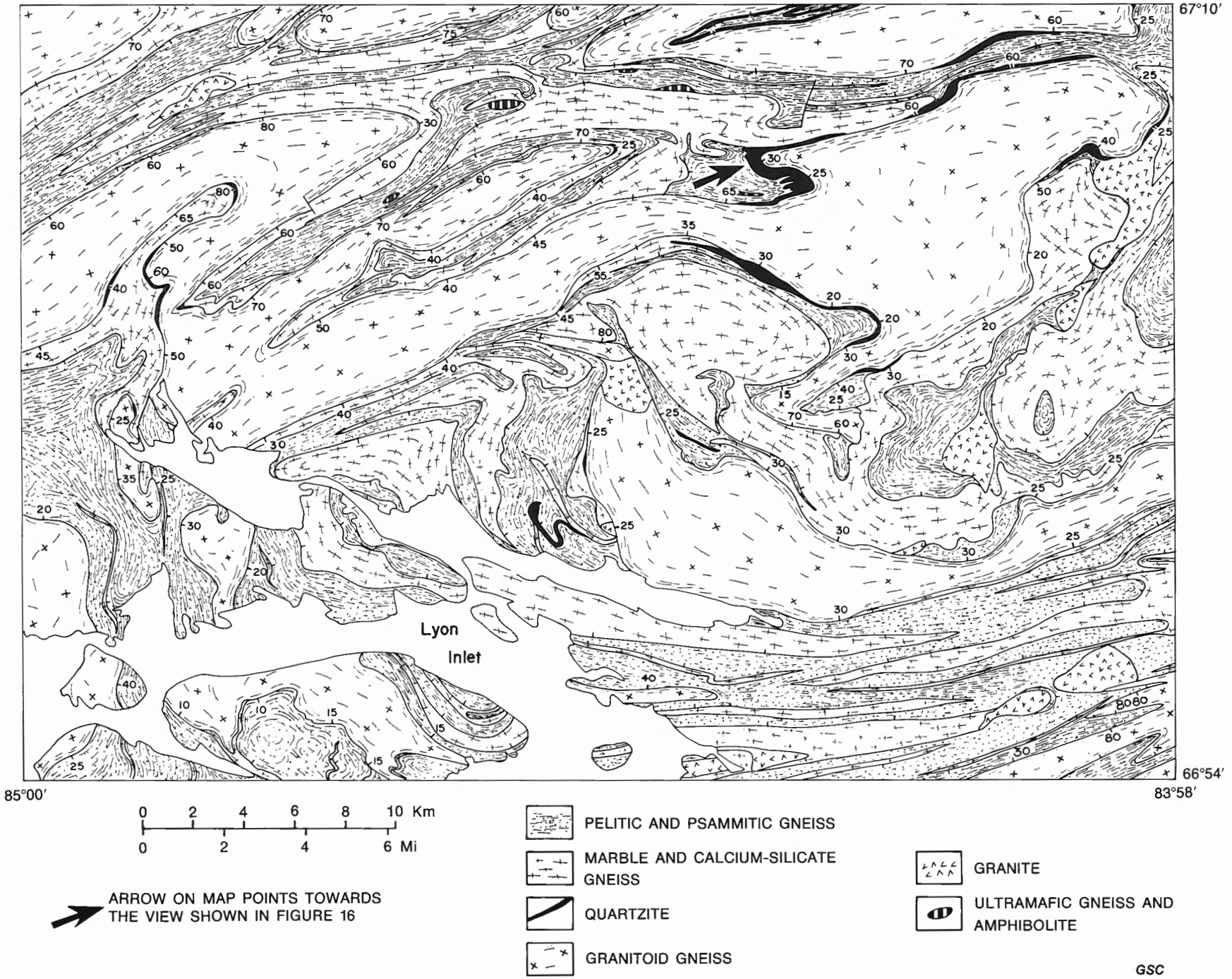

Figure 15. *Geologic map of the region north of Lyon Inlet.*

Where mesoscopic structural elements indicate a regional plunge direction, tectonic profiles are drawn to provide a two-dimensional perspective that is less distorted than the map projection (analysis of mesoscopic fabric elements in the preceding section showed that regional plunges commonly are less than 20°). The profiles are drawn by projecting the geologic map onto the plane perpendicular to the dominant regional plunge line. The tectonic profiles more-or-less distort the true structural geometry, depending upon the degree of variation in fold plunge: these artifacts are apparent on the profiles especially where contacts dip in a direction opposite to that indicated on the map. In the Lyon Inlet map area tectonic profiles aid in visualizing macroscopic D_1 recumbent and reclined folds, whereas the patterns on the geologic map tend to emphasize the macroscopic northeast-southwest striking upright folds characteristic of the D_2 deformation.

The Region West of Tasers Lake

A geologic map and tectonic profile of part of the map area west of Tasers Lake are shown in Figure 14. The region is near the southwestern margin of the Lyon Inlet area, and the figure shows the basement and cover rock relations near the southwest end of Foxe Fold Belt. The tectonic profile is a right-normal section constructed by projecting the part of the map west of the N and S marks on the map margins up-plunge onto a plane dipping 70° west. (A similar view can be obtained by viewing the geologic map down-plunge from the west at a 20° angle[1].)

Within the area (Fig. 14) few macroscopic folds were recognized in the Penrhyn Group: the Aphebian rocks and Archean basement gneiss dip uniformly south or southeast at about 45°; mesoscopic folds and mineral lineations dominantly plunge east at about 20°. An overturned homoclinal sequence of basal quartzite, marble, and calcium-silicate gneiss occurs in the northwest of the area. Within the Penrhyn Group succession a ridge of basement gneiss with quartzite and marble on its flanks apparently has pierced through the basal sequence and intruded a thick section of pelitic gneiss. Gneissosity and foliation in the basement gneiss follow the margin of the ridge. The core of Aphebian rocks in the centre of the gneiss ridge is puzzling. This feature on the geologic map is a long narrow ellipse enclosed by basement gneiss. If the paragneiss is antiformal in the core of the ridge, the basement gneiss would be an isoclinally

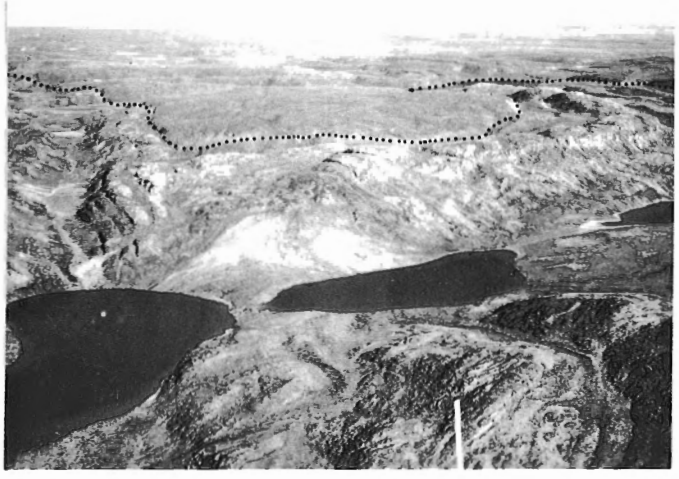

Figure 16. *Down-plunge view of the contact (dotted line) showing Penrhyn basal quartzite overlain by Archean basement gneiss. The photo is taken in the direction of the arrow in the north-centre of Figure 15. (GSC 203251-H)*

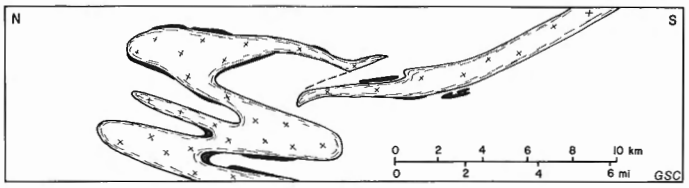

Figure 17. *Diagrammatic tectonic profile of the region north of Lyon Inlet. The basement gneiss and Penrhyn Group basal quartzite are shown. Note that the quartzite occurs above and below the folded gneiss sheet. See text for discussion of inferred structural history.*

folded sheet rather than a diapiric ridge. A stratiform sheet of basement gneiss occurs north of the gneiss ridge near the north margin of the area shown in Figure 14. The sheet is about 1 km wide and extends more than 40 km along strike; it dips south along its entire length, and shows no evidence of being folded.

A macroscopic anticline south of the ridge of basement gneiss is the only large fold recognized within Penrhyn Group paragneiss in the area of Figure 14. The anticline plunges east and is outlined by Penrhyn basal quartzite; it is cored and partially replaced by pegmatitic granite, and is pierced on its north limb by Archean basement gneiss.

The Region North of Lyon Inlet

A geologic map of part of the map area located north of Lyon Inlet is shown in Figure 15. (Part of the area covered in the figure is shown also in the frontispiece.) Many of the folds in the contact between basement gneiss and Penrhyn Group rocks in this region are reclined isoclines plunging east at about 10° (cf. Fig. 11, domain F, and Fig. 12, domain 2). Attention is focused in the direction of the arrow in the northeast of the map (Fig. 15). The tip of the arrow points to the contact between basement gneiss and Penrhyn basal quartzite. An oblique aerial photograph taken in the direction of the arrow is shown in Figure 16. Opposite the tip of the arrow the contact dips 30° east and the basement gneiss overlies the quartzite, but around the bend to the north of the arrow tip the contact dips 60° northwest, and the quartzite overlies the basement gneiss. It is clear that the hinge of an east-plunging reclined anticline pierces the ground surface near the arrow tip, and the basement gneiss is a folded sheet enclosed by supracrustal rocks.

A down-plunge tectonic profile of the folded basement gneiss sheet is shown in Figure 17. The 1- to 2-km thick gneiss layer forms several reclined antiforms and synforms. The upper limb of the top-most antiform is folded into an open synform and is broken by a contraction fault.

It can be seen in Figure 17 that the Penrhyn basal quartzite occurs on both sides of the isoclinally folded basement gneiss sheet. This suggests strongly that the gneiss was emplaced originally into the core of an attenuated anticline: the tight reclined isoclines shown in Figure 17 occurred subsequently.

Although the Penrhyn basal quartzite occurs exclusively along the basement gneiss contacts, there is a general lack of stratigraphic symmetry on opposite sides of basement gneiss massifs in the Lyon Inlet area. In addition, basement gneiss massifs commonly are regionally discordant. These observations suggest that imbrication of basement and supracrustal rocks resulted from thrusting as well as recumbent isoclinal folding. This early phase of deformation involving recumbent folding and thrusting is designated D_1. It is recognized that D_1 comprises several folding phases: at least one phase

[1] See Mackin (1950) for a general review of the method of viewing maps "down-structure".

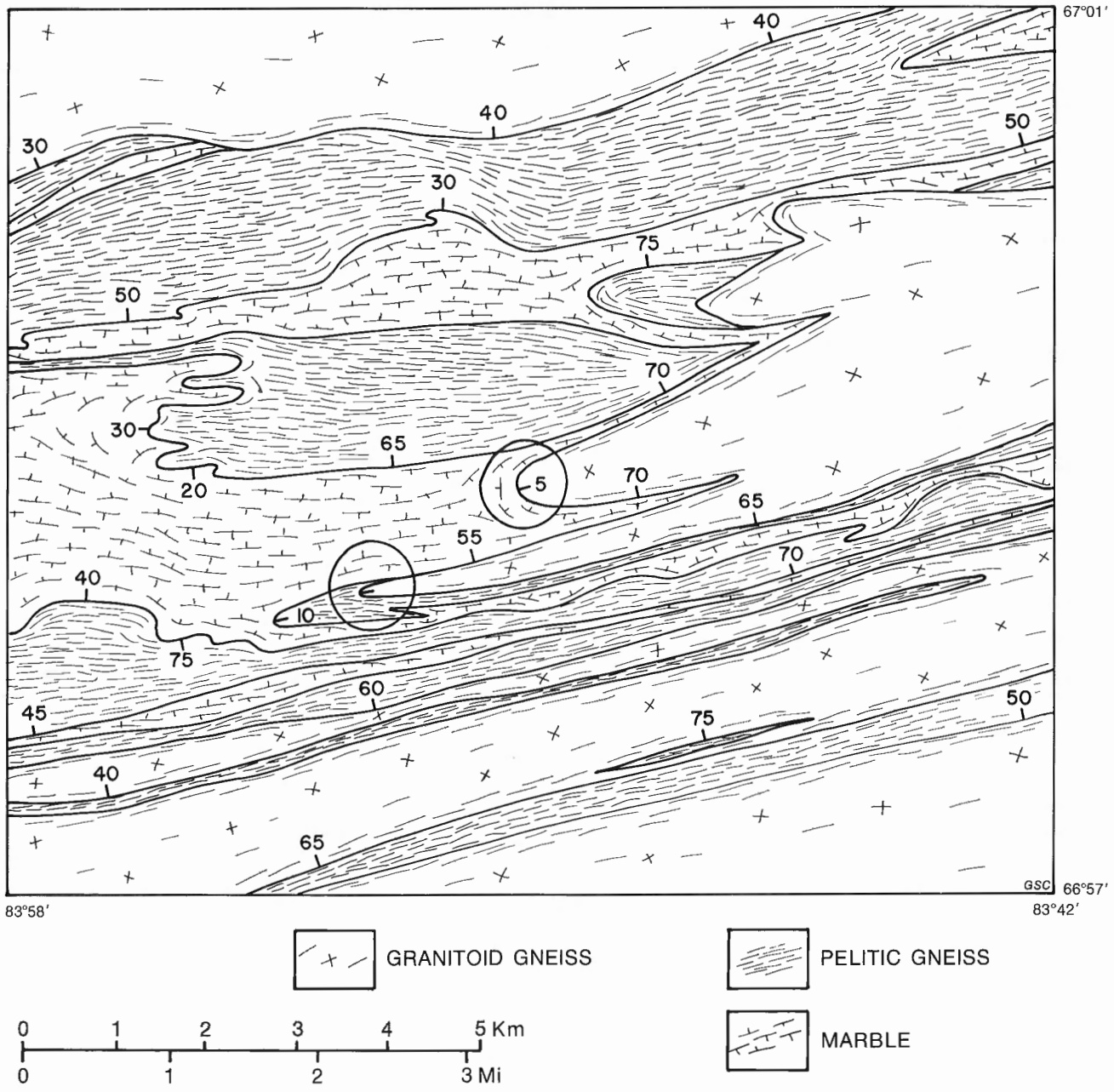

Figure 18. *Geologic map of the region north of Hoppner Inlet, Lyon Inlet area. Shallow, east dips in the circled areas indicate that the basement gneiss overlies the Penrhyn Group. See text for discussion.*

involved emplacement of basement gneiss sheets into cores of recumbent anticlines, and another phase involved recumbent folding of the basement gneiss sheets.

The Region North of Hoppner Inlet

The geology of part of the Lyon Inlet area located north and east of Hoppner Inlet is shown in Figure 18. The area is significant because it can be shown that along the south margin of Foxe Fold Belt granitoid gneiss occurs as plicated sheets overlying Penrhyn Group paragneiss with angular discordancy.

Bedding and gneissosity in the area (Fig. 18) commonly dip northwest at 40 to 80°; mullions and fold axes (see Fig. 12) trend northeast-southwest and plunge at a few degrees in either direction. The conclusion to be drawn from the patterns and orientations of mesoscopic structural fabrics is that the rocks are folded isoclinally about subhorizontal axes with axial surfaces dipping northwest between 40 and 80°. The late (D_2) northeast-southwest folds completely dominate the macroscopic geometry of the structural fabric elements in the area.

A principal problem in the area of Figure 18 is whether the basement gneiss that terminates with four digitations in the centre of the figure is below or above the surrounding supracrustal rocks. Outcrops in two critical localities (circled on Figure 18 near the centre) showed that the basement gneiss overlies paragneiss. Overstepping of several paragneiss contacts by the west margin of the gneiss sheet occurs also, indicating that the basement gneiss was emplaced into a folded supracrustal sequence. This 3- to 5-km wide sheet of basement gneiss overlies the supracrustal rocks for about 55 km to the east where it joins the main body of gneiss to the south by closing off the 1- to 2-km wide paragneiss band south of it in Figure 18 (see also Fig. 31).

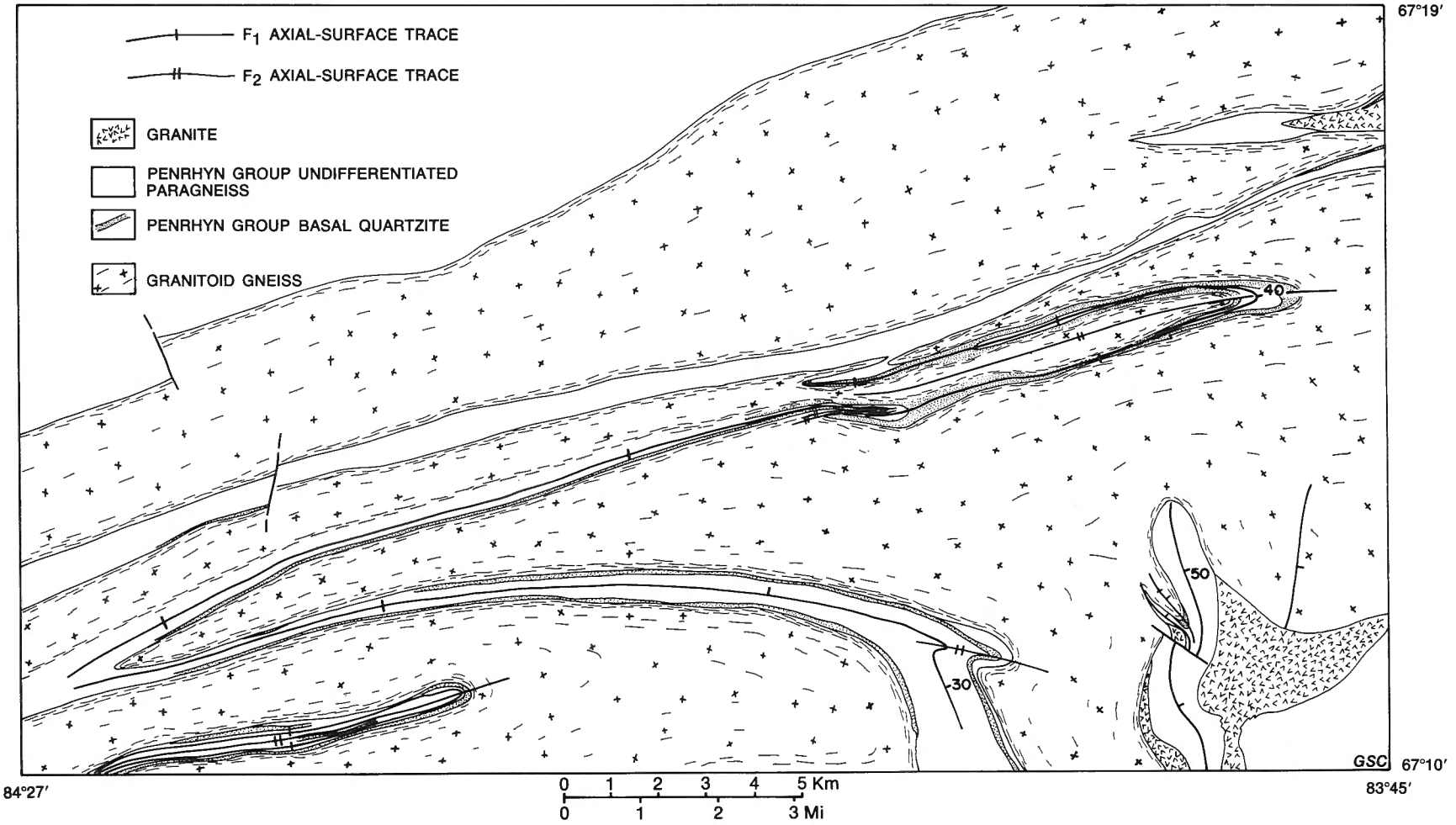

Figure 19. *Geologic map of part of the central gneiss massifs, Lyon Inlet area. See the text and Figures 20–26 for discussion of the structural geometry and strain history of the narrow refolded paragneiss belts between the granitoid basement gneiss massifs.*

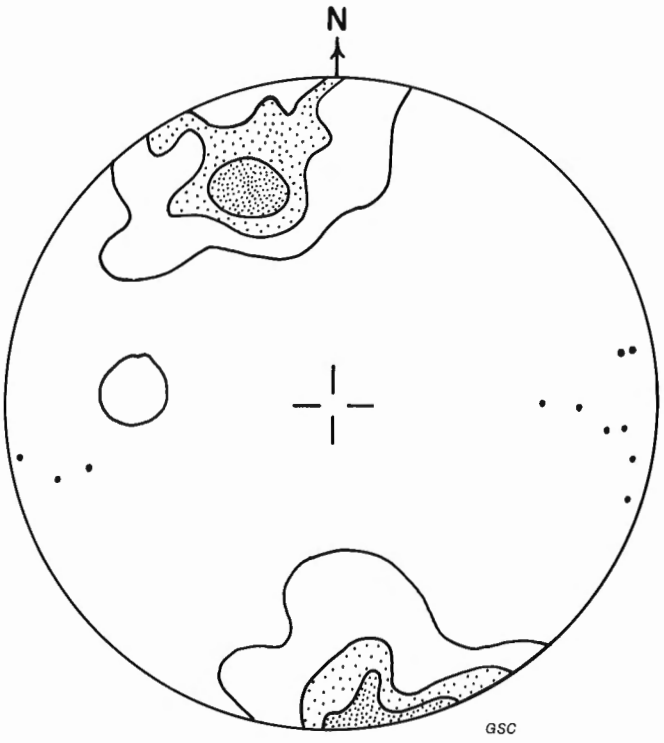

Figure 20. Macroscopic geometry of bedding and fold axes in synclinal belts bounded by basement gneiss massifs in the central gneiss terrane (Fig. 19). Lower-hemisphere, equal-area projection; 78 bedding-poles: contours are 1, 5, 10 per cent/unit area. Dots are fold axes. The fabric geometry indicates horizontal upright isoclinal folds.

The Central Gneiss Massifs

Figure 19 shows part of the basement gneiss terrane near the centre of the map area: here, four Archean gneiss massifs are separated by three narrow belts of Aphebian supracrustal rocks. Of particular interest is the three-dimensional geometry of the massifs and the structural significance of the belts of supracrustal rocks.

Analysis of mesoscopic fabric elements (Figs. 11 and 12) showed that rocks in the central part of the Lyon Inlet area contain upright horizontal isoclinal folds. Figure 20 is a plot of bedding poles and fold axes taken from the three narrow belts of Penrhyn Group gneiss shown in Figure 19; the diagram indicates that mesoscopic structures within the paragneiss are upright, subhorizontal isoclines trending east-northeast. In terms of stratigraphic superposition, all of the paragneiss belts can be considered to be F_1* synclines (perhaps down facing). The gneiss massifs may be autochthonous ridges resulting from diapiric upwelling of basement rock in a folded sedimentary succession (Heywood, 1967, p. 16), or they may be folded sheets of semi-concordant basement gneiss allochthons. The folded sheet hypothesis is most consistent with the structural geometry of basement gneiss elsewhere in the fold belt (Fig. 15, 18), but evidence of some diapiric intrusion of basement into the supracrustal sequence is indicated by the gneiss ridge west of Tasers Lake (Fig. 14). The massifs (Fig. 19) may be rooted in place or floating in the paragneiss: without a consistent regional plunge direction it is not possible to determine the structural superposition by projecting the map patterns onto a tectonic profile. Locally, however, near the southeast corner of the area of Figure 19, Penrhyn Group rocks plunge beneath the basement gneiss in several reclined and down-facing F_1 folds.

Figure 21 draws attention to an F_1 syncline and F_2 antiform near the middle of the central gneiss terrane (Fig. 19). The axial surface of the F_1 syncline apparently is folded into an upright isoclinal F_2 antiform plunging east-northeast at 40° or less. No penetrative planar structures occur in the rocks parallel to the F_2 axial surface: mineral foliation, gneissosity and bedding in paragneiss and basement gneiss parallel the 180° closure. Within the area shown in Figure 21 the hinge line of the F_1 syncline must remain

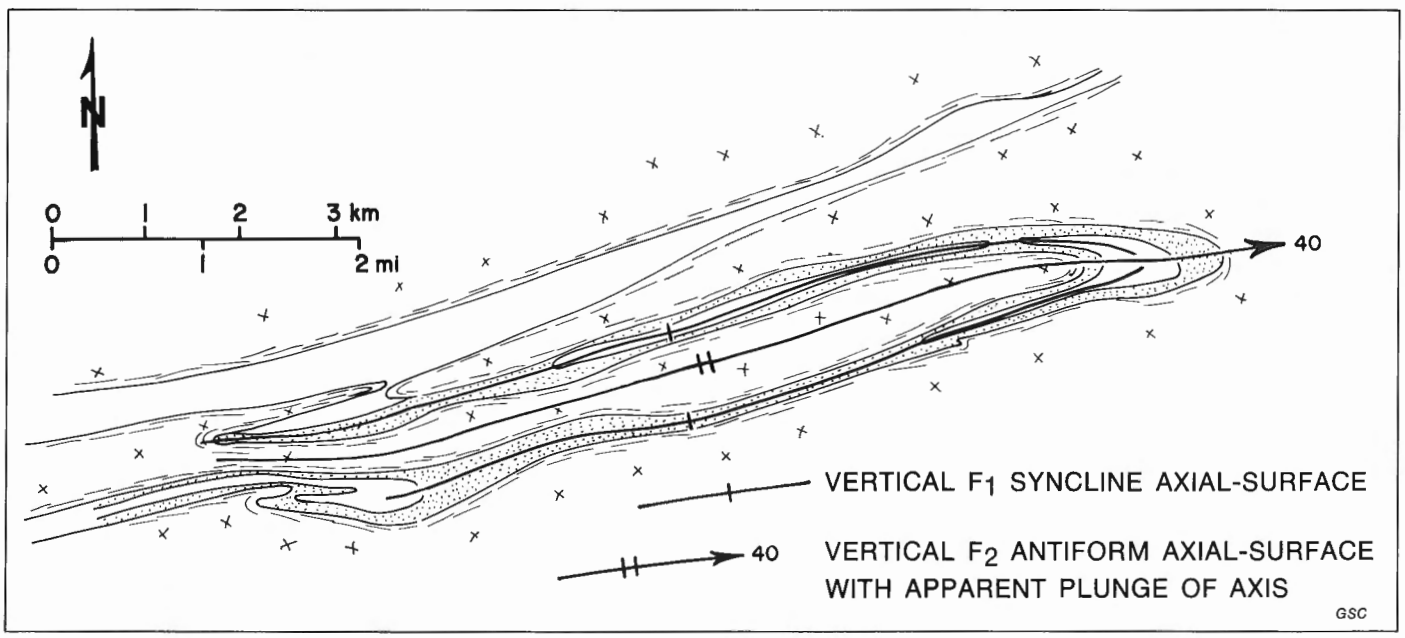

Figure 21. Map of the deformed F_1 syncline in the area of the central gneiss massifs. Penrhyn Group basal quartzite shown by dot pattern; other patterns are the same as Figure 19.

* Superposed folds are designated F_1, F_2, F_3, etc., based on crosscutting relations of axial surface traces.

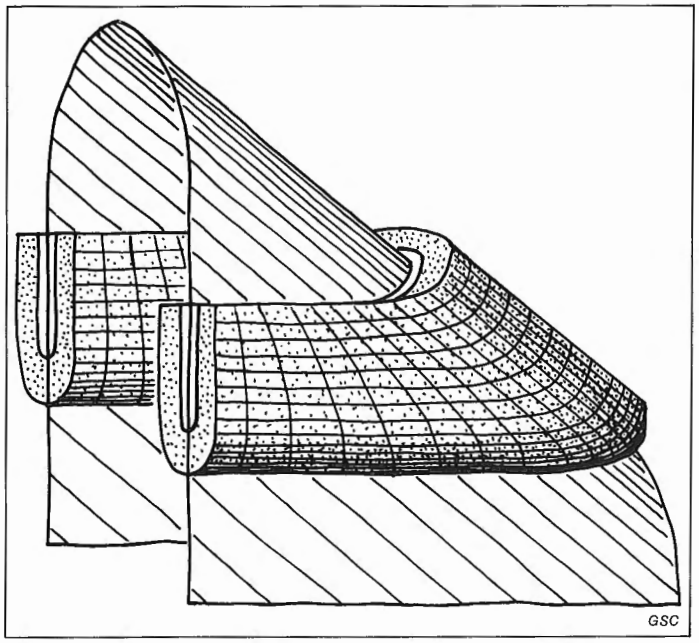

Figure 22. *Three-dimensional model of an F_1 syncline with a horizontal hinge, and an axial surface forming a plunging F_2 antiform suggested by the geometry of mesoscopic structures observed in the region shown in Figure 21.*

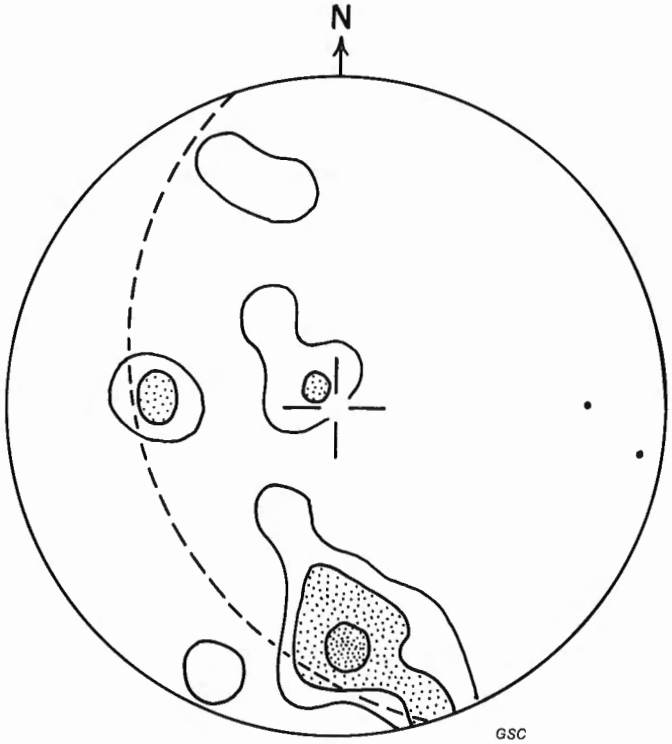

Figure 23. *Macroscopic geometry of bedding and gneissosity measured in the area around the 180° bend in the F_1 syncline axial surface (Fig. 21); lower-hemisphere, equal-area projection: 25 poles (contours 2.5, 10, 20 per cent/unit area). Dots are mesoscopic fold axes. The 40° great circle (dashed line) indicates that the maximum plunge angle of the F_2 antiform is 50°.*

Figure 24. *Sectional views of an involuted paraboloidal fold in interbedded calcium-silicate and marble. The pen, oriented 070° (to the top of the photo), parallels the subhorizontal central axis of the fold. Width of photo area is 41 cm. (GSC 203249-J)*

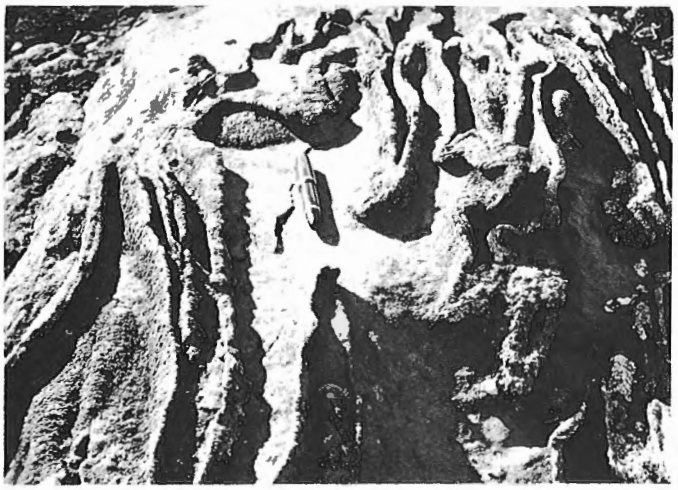

Figure 25. *Isoclinally folded hinges of recumbent F_1 isoclines revealed by calcium-silicate beds in a marble matrix exposed on a horizontal outcrop surface. The horizontal pen, oriented 070° (to the top), parallels the elongation direction (X). Width of photo area is 80 cm. (GSC 203542-B)*

nearly horizontal on both limbs of the F_2 antiform because the thin Penrhyn basal quartzite generally fills the space between the enclosing gneiss massifs. Figure 22 shows the inferred geometry of the macroscopic F_1 and F_2 folds. The F_1 syncline is shown to be up-facing (synformal), but it could be regarded equally well as a down-facing (antiformal) syncline. The F_2 antiform is drawn as a plunging cylindrical fold in the F_1 syncline's axial surface.

At first glance it looks like the F_1 syncline may have been rotated over the hinge of the plunging F_2 antiform. However, only a vertical F_2 rotation axis allows the F_1 hinge to remain horizontal on both limbs of the F_2 fold, and does not require that the F_1 fold close and reverse its facing direction as it crosses the F_2 fold hinge. Mesoscopic fabric data collected from the region of the F_2 fold hinge (Fig. 23) show a maximum possible plunge of less than 50° for the fold and the vertical F_2 rotation axis hypothesis may be rejected. No evidence was seen elsewhere in the mesoscopic structural

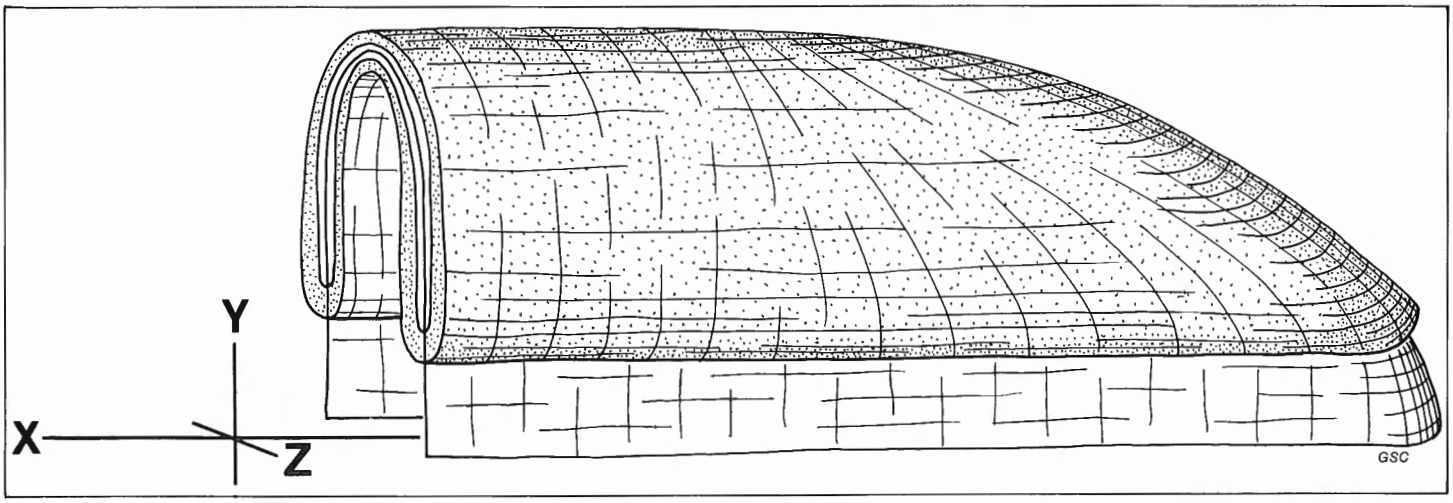

Figure 26. *Three-dimensional model of an involuted paraboloidal fold oriented relative to principal finite strain directions X, Y and Z. The model represents the apparent geometry and finite strain of Penrhyn Group rocks mapped in the area shown in Figure 21.*

fabric of the rocks of the Lyon Inlet area to support a vertical F_2 fold axis model; on the contrary, the fabric data indicate mainly subhorizontal F_2 fold axes in the region.

The geometry of some mesoscopic folds observed in Foxe Fold Belt support the macroscopic fold model described in Figure 22. These folds possess the geometrical form of paraboloids. Figure 24 shows sections of an involuted paraboloidal fold in calcium-silicate and marble beds. Observe the crimped, doughnut-shaped beds in the subvertical section (to the right of the pen tip) as well as the parabolical bedding trace closing on the subhorizontal section of the photograph (behind the pen). The pen parallels the central axis of the fold.

Figure 25 shows a bunch of paraboloidal folds exposed on a horizontal outcrop surface. An arrowhead-shaped fold pointing east-northeast (north of the pen in the centre of the photograph) is the lower half of an elliptical paraboloidal fold. Vertical bedding in a thin calcium-silicate layer outlines a parabola and parallels the hinge of an isoclinally refolded recumbent F_1 fold. The upper limb of the refolded recumbent fold is eroded, but the three-dimensional geometry of the structure can be imagined. Observe the crease in the centre of arrowhead-shaped lower limb where the recumbently folded bed buckled vertically. Except for a few crêpe-like fold mullions such as this, no upright folding is evident in the vertical plane normal to the east-northeast trending paraboloids shown in the photograph. The bulbous, thickened beds at the apices of the paraboloidal folds (Fig. 25) appear to be characteristic of the place where the hinges of the F_1 and F_2 folds interfere. In parts of the outcrop shown in the photograph the bulbous apices of the paraboloidal folds are eroded to different levels and the apparent plunge direction can be seen to vary, depending upon whether the upper, lower, or mid-section of the fold is exposed, whereas in fact the central axes are horizontal. Ray (1974, Fig. 3) described analogous interference folds formed by plunge inversion of early horizontal upright folds. Carey (1962, p. 128) noted that paraboloidal folding occurs within salt domes. In this environment tongue-shaped folds result from differential upwards motion of individual flow lobes within the salt diapir.

The mesoscopic paraboloidal folds shown in Figures 24 and 25 suggest a paraboloidal geometry for the refolded F_1 syncline in the central gneiss terrane (Fig. 21). The complete structure is modelled in Figure 26. It probably resulted from a triaxial strain (D_2) of an originally recumbent F_1 syncline in the contact between basement and supracrustal rocks. The hinge of the early (D_1) recumbent syncline originally was at a large angle to the present trend of the fold belt, and the D_2 strain exerted shortening components along the syncline's hinge and axial surface. Maximum shortening occurred normal to the F_2 axial surface (parallel to Z*) and maximum elongation occurred parallel to the strike of the F_2 axial surface (parallel to X). The F_1 syncline folded in two directions: horizontal folding occurred in the XZ plane and vertical folding occurred in the YZ plane. In the model of the involuted paraboloid (Fig. 26) the crest line of the fold is drawn parallel to X except in the vicinity of the apex where it plunges steeply and inverts.

In the Lyon Inlet area horizontal central axes of paraboloidal folds mark the direction of maximum finite strain, X; Y and Z are vertical and horizontal, respectively, in the plane normal to X. Vertical axial surfaces of F_2 folds indicate the ratio Y:Z is more than unity. The extreme elongations of the paraboloidal folds (Fig. 24, 25, 26) indicate that shortening occurred parallel to both Y and Z, and the finite strain is constrictional.

The Region West of Aua River

Some macroscopic folds within the Penrhyn Group are well exposed in the region west of Aua River (Fig. 27). In this area the Penrhyn Group can be divided into two stratigraphic units: a lower sequence of discontinuous basal quartzite, rusty paragneiss and pelitic gneiss with abundant marble and calcium-silicate gneiss; and an upper unit consisting mostly of pelitic gneiss with several psammitic gneiss lenses near the base. Very little pelitic gneiss occurs in the lower unit and very little marble or calcium-silicate gneiss occurs in the upper unit.

Based upon the recognition of lower and upper units of the Penrhyn Group and cross-cutting axial-surface traces, a three-phase sequence of macroscopic folds was mapped in the region (Fig. 27). The earliest folds (F_1) consist of a syncline-anticline pair rooted in the basement; the second phase (F_2) is represented by a single isocline refolding the F_1 anticline; the third phase fold (F_3) is a synform deforming the F_2 isocline's axial surface.

---

* Triaxial strain is referred to an ellipsoid with principal axes X>Y>Z.

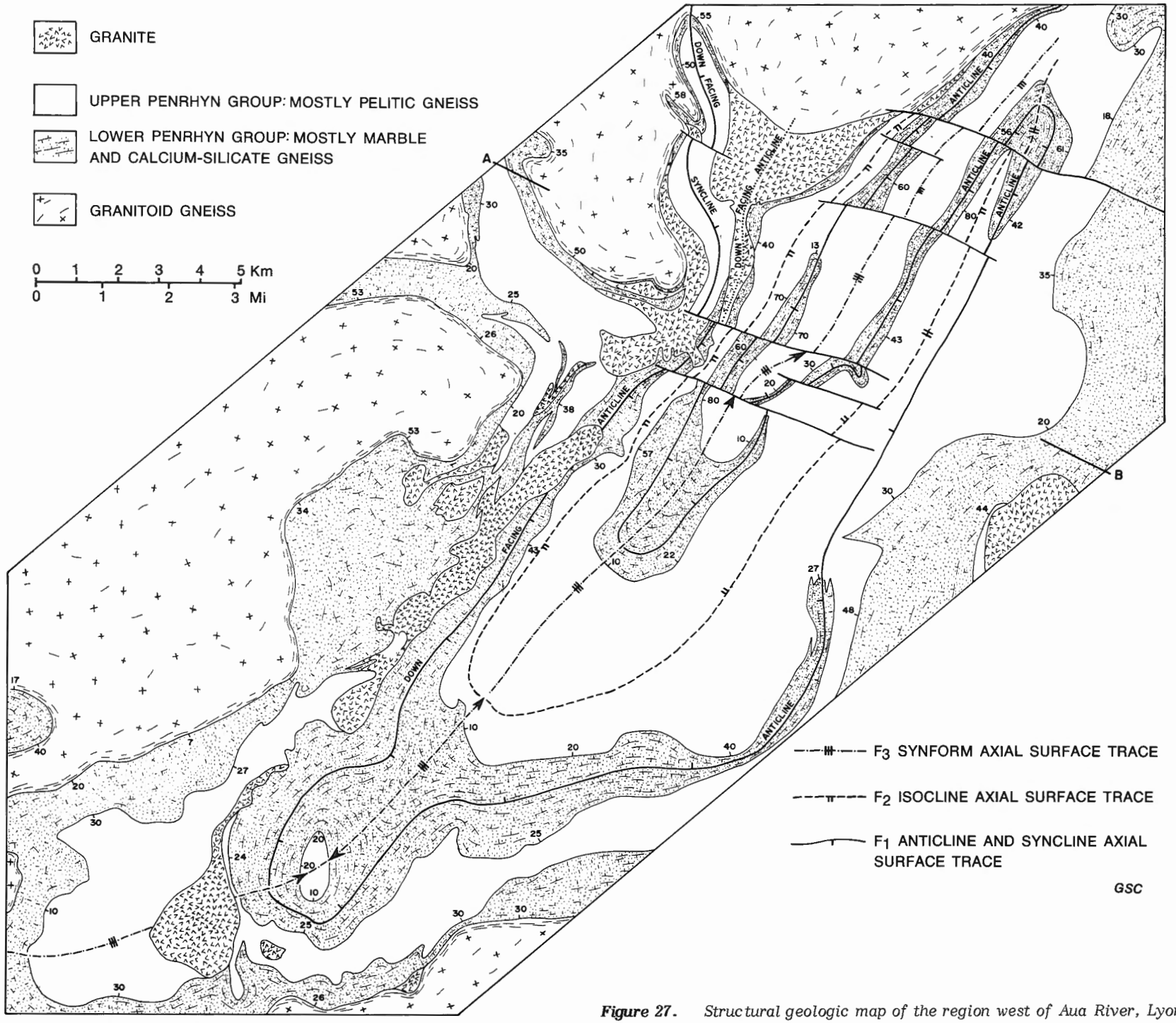

Figure 27. *Structural geologic map of the region west of Aua River, Lyon Inlet area.*

A nearly reclined, down-facing F_1 syncline is tucked deeply into the basement near the north margin of Figure 27. This fold plunges east-northeast and reveals extreme attenuation of some F_1 isoclines in the Penrhyn Group/basement gneiss contact: the isoclinal F_1 syncline is about 1 km wide near the closure at its north end, and its amplitude is at least 5 km. The fold is truncated at its south end by a fault, south of which a granite intrusion obscures the trace of its axial surface.

East of the F_1 syncline, a down-facing F_1 anticline occurs in the basement gneiss/Penrhyn Group contact. South of the basement gneiss a sheath of granite across the hinge region obscures the axial-surface trace (dotted on Fig. 27), but farther southwest, across two right-hand fault offsets, the axial surface of the down-facing anticline can be followed in the centre of a belt of lower Penrhyn rocks on the southeast-dipping limb of the F_3 synform. Near the southwest corner of the area (Fig. 27), the F_1 anticline's axial-surface trace curves around a 180° bend, where it crosses the axial-surface trace of the F_3 synform. Note the parallel trace of the F_2 axial-surface northeast of the F_1 fold on the F_3 synform: the F_2 axial-surface, like the F_1 axial-surface, apparently is folded into a northeast-plunging open synform in the southwest half of the area (Fig. 27).

The lower Penrhyn sequence in the core of the F_1 anticline plunges beneath the ground surface on the southeast limb of the F_3 synform (see Fig. 28). The anticline apparently persists northeast, because the lower Penrhyn rocks reappear about 10 km northeast along strike of the F_1 axial-surface. Here the axial-surface trace of the F_1 anticline curves around another 180° bend in the core of the F_2 isocline, and continues southwest for about 15 km contained within the narrow belt of lower Penrhyn rocks. In this region (Fig. 28) the F_1 anticline is cut by five faults; south of the southernmost fault the lower Penrhyn rocks disappear and reappear within 100 m of the fault. The axial surface of the F_1 anticline continues southwest and closes again around the hinge of the northeast-plunging F_3 synform.

Northeast along the axial-surface trace of the F_1 anticline, and across two right-hand fault offsets, the lower Penrhyn sequence disappears for the fourth time (Fig. 28). North of the next fault to the northeast, the sequence reappears along strike, and the F_1 anticline can be traced across two more fault offsets before it reaches the north margin of the area shown in Figures 27 and 28. Along this

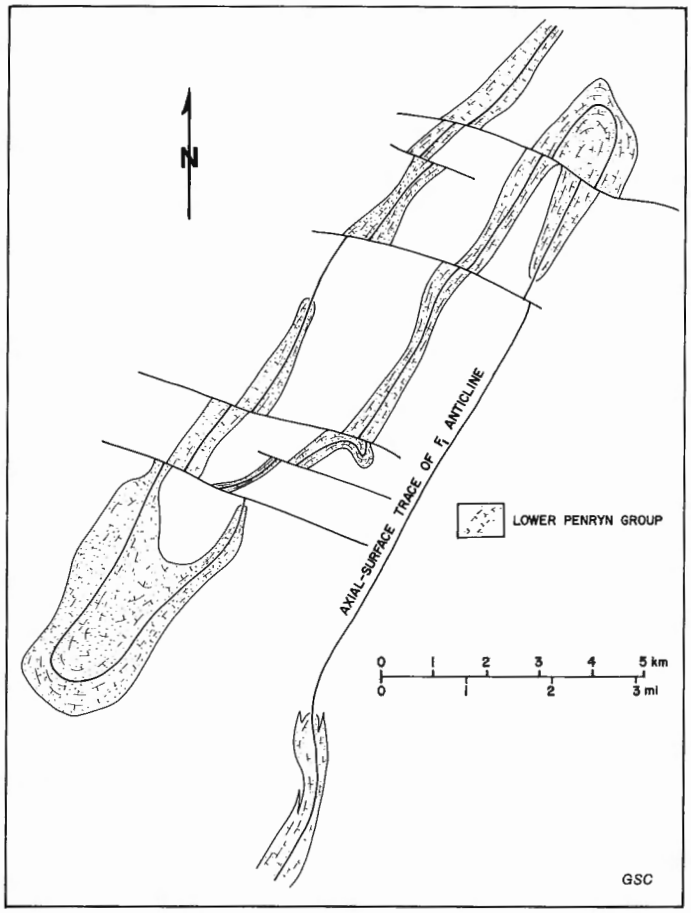

Figure 28. *Map of the folded axial surface of the F_1 anticline in the region west of Aua River. The hinge of the anticline apparently remains close to the horizontal ground-trace of the axial surface, and the map shows the D_2 strain of the F_1 anticline in the XZ principal plane of the finite strain ellipsoid.*

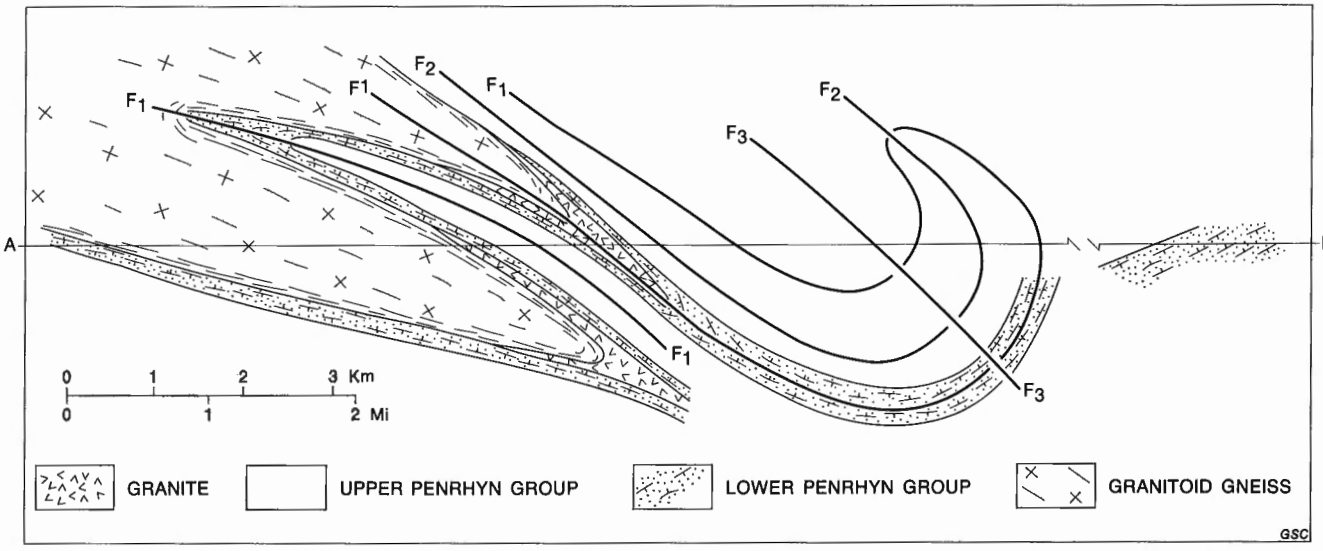

Figure 29. *Vertical structure section through the region west of Aua River, Lyon Inlet area. The section is drawn along line A-B on Figure 27, and projects above and below the horizon.*

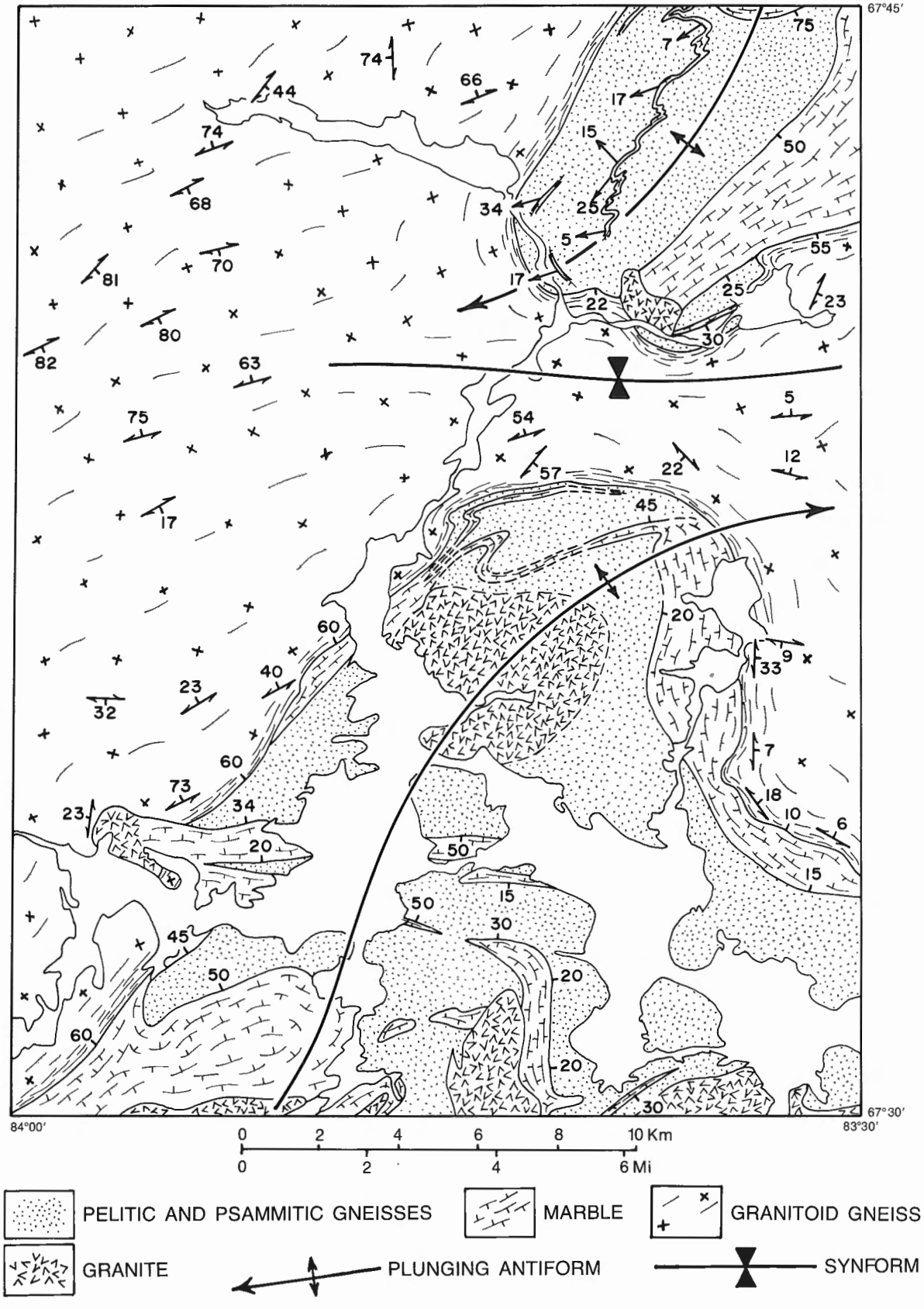

Figure 30. *Structural geologic map of the northeast corner of the Lyon Inlet area. Local attitudes of bedding, fold axes, and gneissosity are shown. The two gently plunging open folds apparently are F_2 antiformal synclines cored by Aphebian Penrhyn Group rocks and overlain by an immense sheet of Archean granitoid basement gneiss. See text for discussion.*

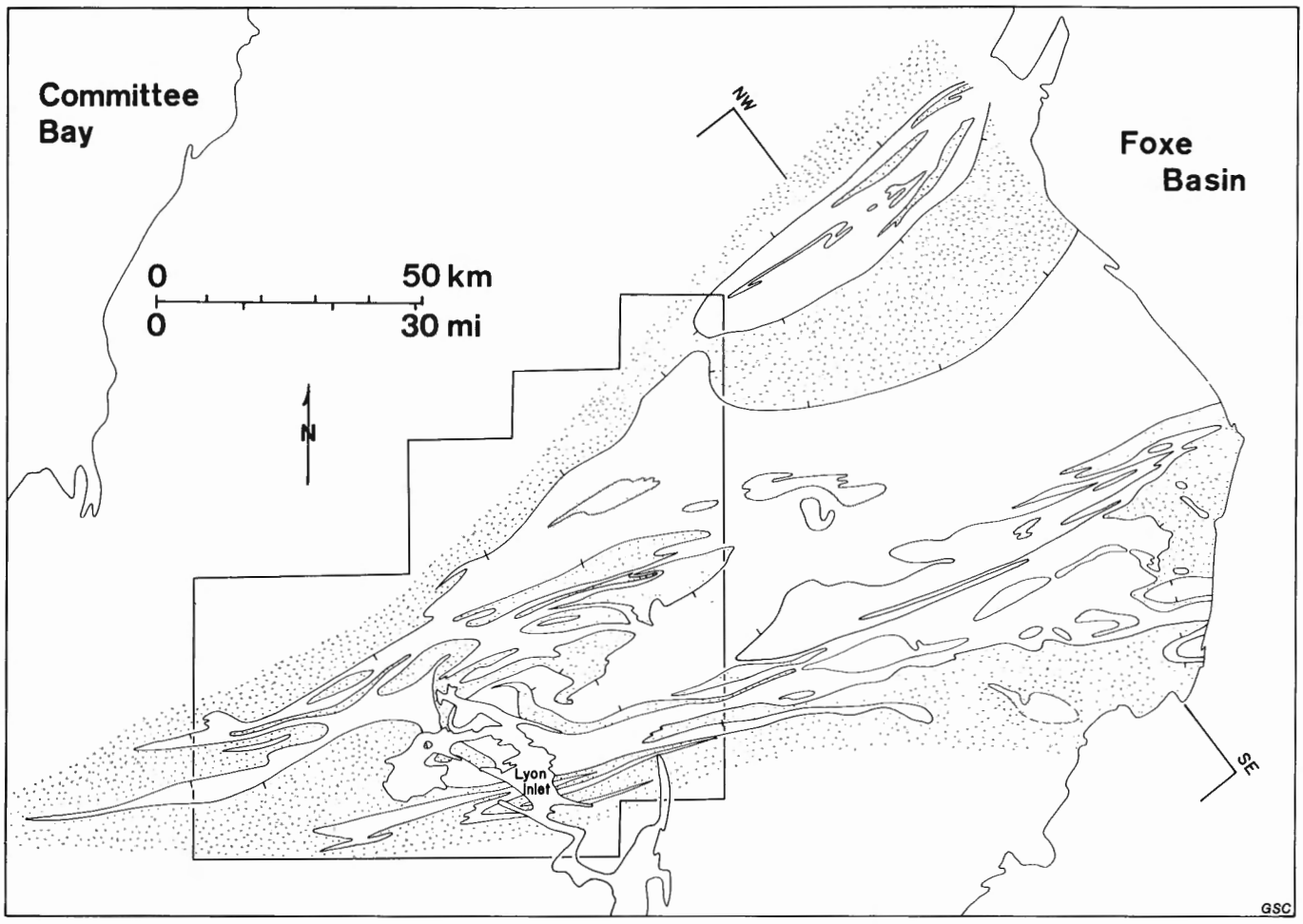

Figure 31. *Map of southern Melville Peninsula showing the distribution of Archean and Aphebian rocks in Foxe Fold Belt. Areas of probable allochthonous Archean gneiss cover on Aphebian supracrustal rocks are indicated by the dot pattern. The northwest-southeast section line of Figure 32 is shown. Geology east of Lyon Inlet area is from Okulitch et al. (1977, 1978). See text for discussion of allochthonous rocks in Foxe Fold Belt.*

last segment, the axial-surface trace of the F_1 anticline progressively encroaches upon the basement contact to the northwest, and all three folds become progressively overturned, tighter, and less distinguishable. Northeast of the area shown in Figure 27 the outcrop is very poor and a large mass of post-kinematic granite obscures the fold structures.

Figure 29 describes the apparent geometry of the axial-surface traces of the F_1, F_2 and F_3 folds in a vertical section along line A-B in Figure 27. The lower Penrhyn rocks occur continuously in the F_1 anticline's core as far as the first closure on the southeast limb of the F_3 synform (see Fig. 28). Beyond this position the lower/upper Penrhyn contact intersects the anticline's axial-surface trace five times before the three folds merge at the north margin of the map. It would appear that the hinge as well as the axial-surface trace of the F_1 anticline is deformed into the S-shape described on the map (Fig. 28), and deformation of the (originally recumbent?) F_1 anticline is shown in the horizontal plane as well as the vertical cross-section. It appears that the F_2 and F_3 folds are coeval D_2 structures representing folding in the vertical YZ plane (Fig. 29) concurrent with the folding of the F_1 hinge and axial surface in the horizontal XZ plane (Fig. 28) of the finite strain ellipsoid.

The Northeast Corner of the Lyon Inlet Area

Figure 30 shows some macroscopic structures inferred from attitudes of gneissosity, bedding and fold axes in the northeast corner of the Lyon Inlet area (map sheet 46 O/12). Throughout the area (Fig. 30) Archean basement gneiss appears to overlie disconformably Aphebian Penrhyn Group rocks. In the south half of the area basement gneiss apparently was eroded from the crest of an open, east-plunging F_2 antiform. In the northeast corner of the area shown basement gneiss was eroded from previously deformed Penrhyn Group rocks on the limbs and crest of a southwest-plunging F_2 antiform. A synformal strip of basement gneiss apparently covers Aphebian paragneiss in an east-west-trending saddle between the two breached antiforms shown in Figure 30.

Extent of Allochthonous Archean Rocks in Foxe Fold Belt

East of the Lyon Inlet area, Okulitch et al. (1978) mapped Archean basement rocks on Aphebian Penrhyn Group rocks to the Foxe Basin. They suggested that more than 3000 km^2 of supracrustal rocks may be overlain by basement gneiss along the north margin of Foxe Fold Belt in Melville Peninsula.

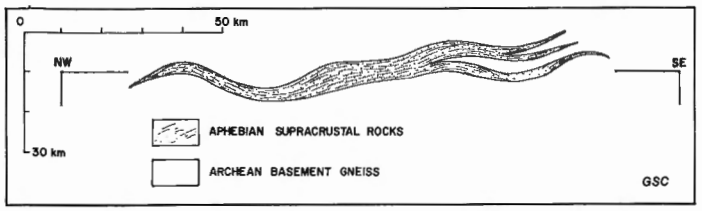

Figure 32. *Hypothetical northwest-southeast section through Foxe Fold Belt. The line of section is indicated in Figure 31. The section shows Aphebian rocks surrounded by Archean basement gneiss in the core of a paraboloidal fold nappe.*

Figure 31 shows the distribution of Archean and Aphebian gneissic rocks in Foxe Fold Belt in Melville Peninsula. The dot pattern on Archean rocks indicates areas where basement gneiss appears to cover Aphebian paragneiss. The extent of Aphebian supracrustal rocks under the basement north and south of their exposed limits may not be very great due to transposition of early structures parallel to the horizontal X direction of the finite strain ellipsoid. Within Foxe Fold Belt transported basement may be more abundant than is indicated on the map (Fig. 31) because mesoscopic structures in and around many of the elliptical Archean gneiss massifs do not reveal whether they are folded up or folded down into the Aphebian supracrustal rocks. The four basement gneiss massifs in the area shown in Figure 19 are underlain by Aphebian rocks at least along their south margins and are indicated to be allochthonous in Figure 31.

In Foxe Fold Belt in Melville Peninsula the major structure may be an elliptical paraboloidal nappe resembling the structure modelled in vertical north-south cross-section in Figure 32. The central axis of the hypothesized tongue-like fold bisects the triangular region of Penrhyn Group rocks exposed in Melville Peninsula (Fig. 31). the Archean gneiss covering envelope is preserved more extensively along the east end of the fold belt, indicating a gentle regional plunge of the central axis of the structure from west to east. The paraboloidal nappe presumably resulted from deformation of an eastward-verging synclinal nappe with a hinge oriented originally at a large angle to the present trend of Foxe Fold Belt.

Summary and Discussion

The following conclusions may be summarized from observations of structures observed in Foxe Fold Belt in the Lyon Inlet area.

1. The earliest folds are recumbent anticlines with cores of basement gneiss. These folds are inferred to exist from the distribution of Penrhyn basal quartzite, both above and below kilometre-thick sheets of basement gneiss north of Lyon Inlet (Fig. 17). Imbricate thrusting of basement gneiss sheets probably occurred during this deformation (D_1).
2. Macroscopic recumbent folds occur in kilometre-thick fold and thrust nappes north of Lyon Inlet (Fig. 17, 27).
3. The deformation characterized by recumbent folding and thrusting implies that tectonic thickening occurred in the region during D_1.
4. The last penetrative deformation of the rocks in the region (D_2) produced variably-verging open to isoclinal subhorizontal folds, crêpe-like fold mullions and paraboloidal folds with subhorizontal central axes (Fig. 24, 25, 26).
5. Both locally and regionally the finite strain indicated by the rocks may be referred to a prolate triaxial ellipsoid: the XZ principal plane of the regional strain ellipsoid is subhorizontal and the X (extension) axis parallels the strike of Foxe Fold Belt.

The last conclusion requires comment. Hobbs et al. (1967, p. 284) stated that horizontal fold axes parallel to X over large areas seems improbable because of the space problem. The writer is aware of this conceptual difficulty, but submits that regional horizontal extension is not unique to Foxe Fold Belt. Ramberg (1967, p. 159-160) noted that the difficulty of explaining the commonly encountered lineation and elongation in deep-seated crystalline schists parallel to the main trend of orogenic chains had long been recognized. He observed that fold axes in the Vestranden culmination of the western Scandinavian Caledonides parallel a strong stretching axis for more than 200 km. He suggested that Vestranden achieved its tight homoaxial folding and strong axial stretching because it is located along the crestal region between two superdomes of remobilized Precambrian basement gneiss, viz. the More and Namsos culminations. Eclogite inclusions in the More gneiss suggest that the complex rose from about a 30 km depth. Ramberg (1967, p. 160) held that the deep-seated horizontal elongation and lineation represent a true stretching caused by nearly horizontal flow, from a laterally distributed buoyant quartzofeldspathic source, towards domal culminations which are close enough for their source zones to overlap.

Foxe Fold Belt is about the same scale as the Vestranden. If the belt was a deep-seated source region between two superdomes, the culminations must lie outside the area mapped. The region southwest of Lyon Inlet area mainly consists of granitoid gneiss with very variable foliation attitudes (Heywood, 1967, Map 14-1966); northeast of Melville Peninsula the Precambrian rocks are covered by Paleozoic strata and are submerged beneath the Foxe Basin.

METAMORPHISM

Regional metamorphism throughout the Lyon Inlet area reached a climax corresponding to the upper amphibolite facies of Turner (1968) and the (cordierite-almandine) high grade of Winkler (1974). Comparisons of mineral assemblages and compositions from the map area with several calibrated geothermometers and geobarometers indicate that climactic conditions during metamorphism may have been 700-749°C and 4.9-5.4 kb[1]. P_{H_2O} was less than P_{total}. Retrograde compositional zoning in nine garnets from three samples analyzed suggests that Fe-Mg exchange of garnet with cordierite and biotite continued to $T < 600°C$ and $P_{total} < 4$ kb. Rock textures indicate that near peak metamorphic conditions prevailed after penetrative deformation ceased. Small quantities of granitic liquids crystallized before the end of penetrative deformation, but the largest granitic plutons crystallized under static conditions. Mineral and whole-rock radiometric studies in the Lyon Inlet area indicate that granitic batholiths composing the basement complex were emplaced more than 2500 Ma ago. The final high grade regional metamorphism occurred more than 1800 Ma ago.

Textures

Most metamorphic rocks in the Lyon Inlet area exhibit postkinematic annealed textures. Aggregates of feldspars, quartz, cordierite, or calcite generally form coarse grained mosaics with straight-line-segment grain boundaries. Garnets commonly are skeletal idioblasts mantled by finer grained aggregates of cordierite and quartz. Scapolite occurs in places as randomly oriented prismatic idioblasts. Biotite, sillimanite (fibrolite and prismatic varieties), and graphite

[1] 1 kb (kilobar) = 100 MPa.

Table 5

Mineral Assemblages from metamorphic rocks of the Lyon Inlet Area.
Number in parentheses refers to the number of thin sections in which the assemblage was observed.
Only primary principal phases are listed in main table. See Table 6 for key to mineral abbreviations.

Pelitic Gneiss (AAn, APn)

Bi-Qz in all assemblages
Kf-Pc-Co-Ga-Si (12)
Kf-Pc-Ga (9)
Kf-Pc-Ga-Si (9)
Kf-Pc-Si-Gr (9)
Kf-Pc-Co-Si (8)
Kf-Pc-Co (6)
Kf-Pc-Si (5)
Kf-Pc (5)
Pc-Hb (5)
Pc (5)
Kf-Co-Ga-Si (5)
Pc-Co-Si (3)
Pc-Co-Ga-Si (3)
Pc-Ga-Si (3)
Ga (2)
Kf-Si (2)
Kf-Pc-Gr (2)
Pc-Co-Ga-To (2)
Kf-Pc-Ga-Si-Gr (2)
Kf-Pc-Co-Ga (2)
Kf-Pc-Tc-Gr (2)
Pc-Gr (2)
Kf-Ga-Si (2)
Pc-Co (2)
Pc-Tc
Kf-Pc-Hb
Kf-Co
Kf-Pc-Co-To
Kf-Hb
Pc-Co-Si-To
Pc-Co-Ga
Pc-Co-Ga-Si-Gr
Pc-Si-To
Kf-Pc-Co-Si-To
Kf-To-Gr
Pc-Si-Gr

Calcium-silicate Gneiss (APcs; APnc)

Di-Kf-Sc-Qz-Cc (6)
Di-Kf-Pc-Qz-Cc (5)
Di-Kf-Sc-Cc (4)
Di-Hb-Sc-Qz-Cc (3)
Di-Pc-Qz-Cc-Gr (3)
Di-Sc-Qz-Cc-To (2)
Di-Kf-Sc-Qz-Cc-Gr (2)
Di-Sc-Qz-Cc-Gr (2)
Di-Kf-Pc-Hb-Qz (2)
Di-Kf-Pc-Cc (2)
Di-Kf-Pc-Cc-Gr (2)
Di-Kf-Pc-Sc-Qz (2)
Di-Pc-Qz
Di-Kf-Pc-Sc-Qz-Cc-Ga
Di-Kf-Sc
Di-Kf-Sc-Qz-Cc-Bi-Gr
Di-Kf-Pc-Hb-Cc-Bi
Di-Kf-Qz
Di-Kf-Pc-Qz
Di-Sc-Qz-Cc
Di-Kf-Pc-Bi
Di-Pc-Cc-Gr
Di-Sc-Qz-Cc-Ga
Di-Kf-Sc-Cc-Do-To-Gr
Di-Kf-Pc-Sc-Qz-Cc-Gr
Di-Fo-Pc-Sc-Cc-Hu-Gr
Hb-Sc-Qz-Bi-To
Di-Pc-Cc
Di-Vs-Kf-Pc-Cc
Di-Pc-Qz-Bi
Di-Kf-Sc-Qz-To-Gr
Di-Pc-Sc-Qz-Cc
Di-Pc-Bi
Di-Pc-Bi-Gr
Di-Pc-Qz-Cc-Bi-To
Di-Vs-Cc
Di-Kf-Pc-Sc-Cc-Bi-To
Vs-Qz-Cc
Kf-Sc-Cc-To

Marble (APc)

Cc in all assemblages
Di-Sc-Kf-Qz (5)
Di-Sc (3)
Di-Kf-Qz (3)
Di-Sc-Gr (2)
Ph-Do-Gr (2)
Di-Ph (2)
Hu-Do (2)
Hu (2)
Di-Sc-Qz (2)
Di-Ph-Pc-Gr
Di-Sc-Kf-Ga-Qz
Di-Sc-Hu-Do-Qz
Di-Ph-Sc-Kf
Di-Ph-Fo-Hu
Di-Ph-Hu
Do-Gr
Di-Sc-To
Di-Sc-Gr
Ph-Hu
Ph-Sc-Fo-Hu-Gr
Ph-Kf-Ga-Gr
Di
Di-Ph-Sc-Gr-Qz
Ph-Hu-Do-Gr
Di-Ph-Sc
Ph-Kf
Ph-Do-Gr
Di-Sc-Do
Di-Ph-Gr
Sc-Kf-Gr
Sc-Kf
Di-Sc-Kf-Gr
Bi-Pc
Ph
Kf-Pc-Qz
Di-Pc-Qz
Do-To
Ph-Do
Di-Kf-Gr-Qz
Di-Kf-Gr

Hornblende Paragneiss (AAn)

Hb in all assemblages
Pc-Qz (2)
Kf-Pc-Qz-Bi-Di (2)
Kf-Pc-Qz-Bi (2)
Pc-Qz-Bi (2)
Kf-Pc-Qz
Pc-Bi-Cg-Mt
Pc-Bi-At-Ga-Mt

Psammitic Gneiss (APq, APqb)

Qz in all assemblages
Kf-Pc-Bi-Gr (8)
Pc-Bi (7)
Bi-Ga (5)
Kf-Pc-Bi (2)
Kf-Pc-Bi-Hb (2)
Bi-Si (2)
Kf-Bi (2)
Kf-Bi-Si-Co-Ga (2)
Kf-Pc-Bi-To
Hb
Gr
Bi
Cg
Ga
Kf-Bi-Ga
Pc-Bi-Ga
Kf-Bi-Si
Kf
Bi-Gr
Kf-Pc-Bi-To-Si
Pc-Hb
Bi-Hb

Granite and Granitoid Gneiss (Agdn, Aqmn, Aqdn, Ag)

Pc-Qz in all assemblages
Kf-Bi (28)
Kf-Bi-Hb (8)
Bi (2)
Kf (2)
Kf-Hb
Hb
Bi-Hb
Hb-Px

Iron formation (AAif)

Qz-Mt-Cg (9)
Qz-Mt-Cg-Op-Fa-Ga (2)
Qz-Mt-Cg-Bi
Qz-Mt-Cg-Ga
Qz-Mt-Cg-Pc-Bi
Qz-Mt-Cg-Px-Op-Hb-Ga
Qz-Mt-Cg-Hb
Qz-Mt-Cg-At
Qz-Cg-Pc-Bi
Qz-Mt
Mt-Cg-Pc-Bi-Ga
Cg-Pc-Bi-At

Quartzofeldspathic Gneiss (APnc)

Kf-Pc-Qz-Bi (6)
Kf-Pc-Qz-Bi-Di-Gr (5)
Kf-Pc-Qz (4)
Kf-Pc-Qz-Bi-Hb-Sc (2)
Kf-Pc-Qz-Bi-Di-Gr (2)
Kf-Oz-Hb (2)
Kf-Pc-Qz-To (2)
Qz-Hb
Kf-Pc-Bi-Hb
Pc-Qz-Bi-Cq
Kf-Pc
Kf-Bi
Kf-Pc-Ga
Pc
Kf-Pc-Gr
Pc-Qz-Bi-To-Gr
Kf-Pc-Qz-Bi-Hb-Di
Pc-Qz-Di-Gr

Amphibolite and Ultramafic Rocks (AAm, APm, Aub)

Hb in all assemblages
Pc (5)
Pc-Bi (5)
Pc-Mt (3)
Pc-Qz (2)
Pc-Qz-Bi
Pc-Hy-Mt
Pc-Qz-Bi-Ga
Pc-Bi-Px-Mt
Pc-Bi-Px
Pc-Px-Mt
Bi-Cg-Ga
Cg-Px-Mt
Bi-Cg-Px-Ga-Mt
Bi-Px-Mt
Bi-Px-Mt
Px-Hy-Ga
Px-Ol
Hy-Ol

Common Accessory Minerals

Pelitic and Psammitic gneiss	Sp,Zr,Ap,Mt,Sl
Marble and Calc-silicate gneiss	Sp,Ap,Mt
Amphibolite and Ultramafic rocks	Sp,Ap
Granitic rocks	Ap,Sp,Zr,Mt,Al

Common Secondary Minerals

Secondary Mineral	Primary Host
Mu	Co,Pc,Kf,Bi,Si
Ep	Pc,Di,Sc
Ch	Bi,Hb,Sc,Di,Hu,Ol
Tc	Di,Hb
Sr	Ol,Hu
Ta	Ol,Hu
Ht	Mt,Sl
Ru	Bi
Pr	Pc,Sc

Rare occurrences

Andalusite (5), Spinel (twice), Corundum, Edenite, Sphalerite, Wollastonite, Szajbelyite, Serendibite.

Table 6

Key to Mineral Abbreviations

Al	Allanite	Mt	Magnetite
Ap	Apatite	Mu	Muscovite
At	Anthophyllite	Op	Orthopyroxene
Bi	Biotite	Ol	Olivine
Cc	Calcite	Pc	Plagioclase
Cg	Cummingtonite-grunerite	Ph	Phlogopite
Ch	Chlorite	Pr	Prehnite
Co	Cordierite	Py	Pyrite
Di	Diopside	Px	Clinopyroxene
Do	Dolomite	Qz	Quartz
Ed	Edenite	Ru	Rutile
Ep	Epidote Group	Sc	Scapolite
Fa	Fayalite	Sl	Sulphide mineral
Fl	Fluorite	Si	Sillimanite
Fo	Forsterite	Sp	Sphene
Ga	Garnet Group	Sr	Serpentine
Gr	Graphite	Ta	Talc
Hb	Hornblende	Tc	Tremolite-actinolite
Ht	Hematite	To	Tourmaline
Hu	Humite Group	Vs	Vesuvianite
Hy	Hypersthene	Zr	Zircon
Kf	Potassium feldspar		

commonly define a weak foliation which parallels the gneissosity deformed in hinges of microscopic folds (Fig. 7): foliation parallel to fold axial surfaces was not observed. In some metamorphosed mafic rocks delicate postkinematic symplectic intergrowths of hypersthene, plagioclase, hornblende, and garnet occur (Fig. 34).

Cataclastic textures are restricted to a few shear zones near the south margin of the map area, the Archean basement gneiss adjacent to Aphebian paragneiss contacts, and Archean augen gneiss near the north margin of the area. Very minor postcrystallization regional strain is indicated by bent twin planes in feldspars, undulose extinction in quartz grains, and deformation twins in calcite. Microscopic to mesoscopic kink folds occur locally in coarse grained biotite-graphite-sillimanite schist adjacent to basement gneiss contacts.

Mineral Assemblages

Minerals observed in thin sections of rocks from the map area are listed in Table 5; a key to mineral abbreviations used in the text appears in Table 6. Accessory phases are less than 5 per cent of the totals of modal analyses, and are not listed with the major minerals for the sake of brevity in Table 5. Some minerals occur only as alteration products of higher grade phases and are listed separately in Table 5, along with their principal hosts. Several rare minerals are present: szajbelyite, $H_2(Mg,Mn,Zn)_2B_2O_6$, occurs as grey bladed crystals more than 60 cm long in a skarn with serpentine, talc, and brown tourmaline (U.T.M. co-ordinate location 385120E-7451920N); serendibite[1], $Ca_2(Mg,Fe)_4Al_6B_2O_{10}Si_4O_{16}$, occurs as coarse grained, granular, blue crystals with diopside and tourmaline in a 20 cm wide layer in marble and calcium-silicate gneiss (U.T.M. co-ordinate location 568840E-7427420N).

The paragenesis Bi-Qz-Pc-Kf (mineral abbreviations in Table 6) is widespread in Penrhyn Group pelitic and quartzo-feldspathic rocks. In pelitic rocks the seven-phase assemblage Bi-Qz-Kf-Pc-Co-Ga-Si occurs throughout the map area except in the northeast where cordierite was not observed. Muscovite was seen only as a late phase, commonly replacing sillimanite, plagioclase, K feldspar, biotite, or cordierite. Andalusite was noted in five thin sections from widely separated localities: it occurs as rare subidioblasts in association with biotite and appears to have formed late; sillimanite is abundant in several of these rocks. Kyanite was never observed. Graphite is ubiquitous to all Penrhyn Group rocks, but it is especially abundant in rusty-weathering pelites containing abundant iron sulphides.

In calcium-silicate rocks the assemblage Di-Kf-Pc (or Sc)-Qz-Cc is most common. Scapolite is widespread and abundant; it commonly occurs without plagioclase, but coexisting scapolite and plagioclase were noted. Humite and clinohumite occur as porphyroblasts in marble; the minerals are widespread, but they are not common. Forsterite is similarly widespread, but uncommon in marble. Vesuvianite is abundant locally in marble and calcium-silicate rocks. Prehnite and epidote occur as uncommon alteration of plagioclase and scapolite in calcium-silicate gneiss.

Prince Albert Group iron formation most commonly contains quartz, magnetite, grunerite, with or without additional phases. Fayalite and iron-rich orthopyroxene occur in association with quartz, magnetite, and grunerite-bearing ironstones in several localities. In addition to grunerite, hornblende and anthophyllite occur in iron formation. Pelitic iron-rich rocks contain Qz-Mt-Cg plus garnet, biotite, or plagioclase.

Mafic rocks in the region generally have either Hb-Pc or Hb-Pc-Bi assemblages; a few garnet-, clinopyroxene-, or orthopyroxene-bearing assemblages were observed also. Ultramafic rocks are rare; the few thin sections observed contain hornblende, olivine, and/or pyroxene.

Mineral Chemistry

Specimens chosen for microprobe analysis of minerals were selected for their usefulness in regional thermobarometry. In the Lyon Inlet area the two bulk compositional groups chosen were (1) metapelites with the assemblage Bi-Qz-Kf-Pc-Co-Ga-Si, and (2) meta-ironstones containing grunerite, fayalite and orthopyroxene. Three thin

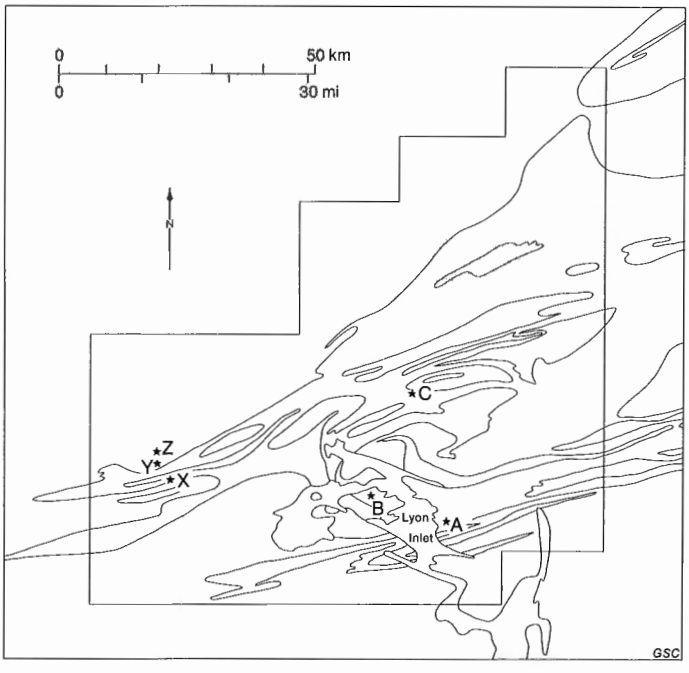

Figure 33. *Outline map of the Lyon Inlet area showing location of microprobed assemblages in metapelitic rocks A, B, and C, and meta-ironstones X, Y, and Z.*

[1] See Hutcheon et al. (1977) for an analysis of the optical, chemical and physical parameters of serendibite from this occurrence.

Table 7

Microprobe analyses of selected garnets, cordierites, and biotites in metapelitic rock A.
Analyses by G. Pringle, Mineralogy Section, Geological Survey of Canada

	Bi(avg. of 3)	Co1	Ga1(rim)†	Ga1(core)	Co2	Ga2(rim)†	Ga2(core)	Co3	Ga3(rim)†	Ga3(core)
SiO_2	35.72	47.05	37.50	37.67	47.31	39.71	37.22	47.23	37.36	37.25
Al_2O_3	15.96	33.61	20.85	20.82	33.69	20.67	20.66	33.83	20.89	20.52
TiO_2	4.39	0.05	0.03	0.03	0.07	0.08	0.02	0.04	0.00	0.06
Cr_2O_3	0.10	0.00	0.07	0.08	0.02	0.10	0.05	0.04	0.05	0.09
*FeO	17.12	6.74	35.03	33.11	7.00	34.79	31.57	6.90	34.12	33.72
MnO	0.00	0.02	0.60	0.45	0.05	0.53	0.47	0.04	0.57	0.53
MgO	11.32	9.06	5.19	6.56	9.11	5.30	6.64	9.14	5.03	5.45
CaO	0.05	0.00	1.05	1.29	0.00	1.20	1.44	0.00	1.35	1.18
Na_2O	0.34	0.46	0.02	0.00	0.50	0.03	0.00	0.33	0.17	0.00
K_2O	9.05	0.01	0.00	0.00	0.01	0.00	0.00	0.01	0.00	0.00
Total Wt. %	94.05	97.00	100.34	100.01	97.76	100.61	98.07	97.56	99.55	98.79
No. of oxygens	22	18	12	12	18	12	12	18	12	12
Si	5.47	4.89	2.99	2.98	4.89	3.09	2.99	4.88	3.02	3.00
Al	2.88	4.12	1.96	1.94	4.10	1.88	1.96	4.12	1.99	1.95
Ti	0.51	0.00	0.00	0.00	0.01	0.00	0.00	0.00	0.00	0.00
Cr	0.00	0.00	0.01	0.00	0.00	0.01	0.00	0.00	0.00	0.01
Fe	2.19	0.59	2.33	2.19	0.60	2.24	2.12	0.60	2.31	2.27
Mn	0.00	0.00	0.04	0.03	0.00	0.03	0.03	0.00	0.04	0.04
Mg	2.58	1.40	0.62	0.77	1.40	0.61	0.80	1.41	0.61	0.65
Ca	0.01	0.00	0.09	0.11	0.00	0.10	0.12	0.00	0.12	0.10
Na	0.10	0.09	0.00	0.00	0.10	0.00	0.00	0.07	0.01	0.00
K	1.77	0.00	0.00	0.00	0.00	0.00	0.00	0.00	0.00	0.00
Total Cations	15.51	11.09	8.04	8.02	11.10	7.96	8.02	11.08	8.10	8.02
X_{Mg}	0.54	0.70	0.21	0.26	0.70	0.21	0.27	0.70	0.21	0.22
Mg:Fe	1.178	2.373	0.266	0.352	2.333	0.272	0.377	2.350	0.264	0.286

†Immediately adjacent to analyzed cordierite.

*Total Fe as FeO.

sections from rocks of each group were selected: metapelite specimens A, B, and C, and meta-ironstone specimens X, Y and Z. Figure 33 shows the locations of the specimens.

Microprobe analyses of garnet, cordierite and biotite grains in metapelite specimens A, B and C are listed in Tables 7, 8 and 9; microprobe analyses of microcline and plagioclase are listed in Table 10. Fayalite, orthopyroxene, grunerite, garnet, hornblende and biotite microprobe analyses from meta-ironstone specimens X, Y and Z are listed in Tables 11, 12 and 13. Analyses were obtained at the Geological Survey of Canada using an MAC electron microprobe equipped with a Kevex energy dispersive spectrometer automated to produce simultaneous multi-element analysis and data reduction using the method of Plant and Lachance (1973). Operating conditions were: 20 kV accelerating potential, specimen current 10 nanoamperes measured on a standard kaersutite, and a 100 second counting time. Natural silicate and oxide standards were used.

Pelitic Rocks

The three thin sections (A, B, and C) selected for chemical analysis of cordierite, garnet, biotite, microcline and plagioclase (Tables 7, 8, 9, 10) are relatively free of alteration. Even so, some cordierite grains are pinitized or have yellow isotropic margins and fractures; plagioclase is "dusted" with tiny sericite flakes, and some biotites are

Table 8

Microprobe analyses of selected garnets, cordierites and biotites in metapelitic rock B.
Analyses by G. Pringle, Mineralogy Section, Geological Survey of Canada

	Bi(avg. of 3)	Co1	Ga1(rim)†	Ga1(core)	Co2	Ga2(rim)†	Ga2(core)	Co3	Ga3(rim)†	Ga3(core)
SiO_2	34.52	47.53	37.69	36.87	47.25	37.55	37.78	47.23	37.14	37.41
Al_2O_3	18.13	33.14	20.66	20.22	33.76	20.40	20.91	32.94	20.36	20.48
TiO_2	2.11	0.01	0.06	0.08	0.04	0.00	0.04	0.06	0.01	0.05
Cr_2O_3	0.11	0.02	0.10	0.06	0.02	0.10	0.03	0.01	0.07	0.03
*FeO	18.16	8.77	36.94	35.39	8.17	36.45	35.69	8.55	36.86	35.49
MnO	0.00	0.03	0.56	0.50	0.04	0.86	0.85	0.07	0.59	0.60
MgO	10.14	8.42	3.75	3.91	8.37	3.64	4.05	8.61	2.98	3.85
CaO	0.04	0.00	1.57	2.11	0.00	1.50	1.58	0.00	1.76	2.25
Na_2O	0.09	0.24	0.00	0.00	0.19	0.00	0.00	0.00	0.00	0.12
K_2O	8.81	0.00	0.00	0.00	0.00	0.00	0.00	0.02	0.00	0.00
Total Wt. %	92.11	98.16	101.33	99.16	97.84	100.50	100.93	97.49	99.75	100.28
No. of oxygens	22	18	12	12	18	12	12	18	12	12
Si	5.41	4.92	3.00	2.99	4.89	3.01	3.00	4.92	3.01	3.00
Al	3.35	4.05	1.94	1.94	4.12	1.93	1.96	4.04	1.95	1.94
Ti	0.25	0.00	0.00	0.01	0.00	0.00	0.00	0.01	0.00	0.00
Cr	0.01	0.00	0.01	0.00	0.00	0.01	0.00	0.00	0.01	0.00
Fe	2.38	0.76	2.46	2.40	0.71	2.45	2.37	0.74	2.50	2.38
Mn	0.00	0.00	0.04	0.03	0.00	0.06	0.06	0.01	0.04	0.04
Mg	2.36	1.30	0.44	0.47	1.29	0.44	0.48	1.34	0.36	0.46
Ca	0.01	0.00	0.13	0.18	0.00	0.12	0.13	0.00	0.15	0.19
Na	0.03	0.05	0.00	0.00	0.04	0.00	0.00	0.00	0.00	0.02
K	1.76	0.00	0.00	0.00	0.00	0.00	0.00	0.00	0.00	0.00
Total Cations	15.56	11.08	8.02	8.02	11.05	8.02	8.00	11.06	8.02	8.03
X_{Mg}	0.50	0.63	0.15	0.16	0.65	0.15	0.17	0.64	0.13	0.16
Mg:Fe	0.992	1.711	0.179	0.196	1.817	0.180	0.203	1.811	0.144	0.193

†Immediately adjacent to analyzed cordierite.

*Total Fe as FeO.

marginally altered to muscovite. Garnets commonly are enveloped by finer grained cordierite, and have scalloped margins. Fibrolite (specimen B) and prismatic sillimanite (A and C) are well distributed, but partly altered to muscovite. Alkali feldspar is unaltered, grid-twinned microcline.

In addition to Bi-Qz-Kf-Pc-Co-Ga-Si, minor graphite, and accessory pyrite, apatite and zircon are present in specimens A, B, and C. Specimen A also has a few grains of green spinel (hercynite?) associated with sillimanite in cordierite.

Three touching pairs of garnet and cordierite grains were analyzed in each section. The cordierite grains are not zoned and are reported as average analyses for each grain, but the garnets all show significant compositional variation from core to rim, and separate core and rim compositions are reported for each grain (Tables 7, 8, 9). Biotite is homogeneous in each section and one average analysis is reported per specimen. Both feldspars generally show internal zoning as well as compositional variation between grains; separate analyses are reported (Table 10) for each grain, and both core and rim compositions are reported for zoned grains.

Table 9

Microprobe analyses of selected garnets, cordierites, and biotites in metapelitic rock C.
Analyses by G. Pringle, Mineralogy Section, Geological Survey of Canada

	Bi(avg. of 3)	Co1	Ga1(rim)†	Ga1(core)	Co2	Ga2(rim)†	Ga2(core)	Co3	Ga3(rim)†	Ga3(core)
SiO_2	35.17	47.25	37.84	37.80	46.88	38.01	37.46	46.83	37.94	37.70
Al_2O_3	17.45	33.82	20.64	20.77	33.51	20.94	20.43	33.54	20.64	20.72
TiO_2	3.20	0.01	0.03	0.02	0.02	0.04	0.06	0.03	0.09	0.03
Cr_2O_3	0.98	0.02	0.04	0.04	0.01	0.06	0.02	0.01	0.03	0.06
*FeO	17.48	8.44	37.21	36.47	8.10	36.89	35.01	8.41	37.21	36.31
MnO	0.00	0.04	1.00	0.80	0.03	0.81	0.65	0.05	0.84	0.71
MgO	10.36	8.39	3.62	4.09	8.44	3.82	5.29	8.31	3.67	4.23
CaO	0.08	0.00	1.02	1.08	0.00	0.78	0.93	0.00	0.90	0.95
Na_2O	0.17	0.39	0.00	0.00	0.29	0.00	0.00	0.31	0.00	0.00
K_2O	9.11	0.02	0.00	0.00	0.01	0.00	0.00	0.01	0.00	0.00
Total Wt. %	94.00	98.38	101.40	101.07	97.29	101.35	99.85	97.50	101.32	100.70
No. of oxygens	22	18	12	12	18	12	12	18	12	12
Si	5.44	4.88	3.01	3.01	4.89	3.02	3.00	4.88	3.02	3.01
Al	3.18	4.12	1.94	1.95	4.12	1.96	1.93	4.12	1.94	1.95
Ti	0.37	0.00	0.00	0.00	0.00	0.00	0.00	0.00	0.01	0.00
Cr	0.11	0.00	0.00	0.00	0.00	0.00	0.00	0.00	0.00	0.00
Fe	2.26	0.73	2.48	2.43	0.71	2.45	2.34	0.73	2.48	2.42
Mn	0.00	0.00	0.07	0.04	0.00	0.05	0.04	0.00	0.06	0.01
Mg	2.39	1.29	0.43	0.49	1.31	0.45	0.63	1.29	0.44	0.50
Ca	0.01	0.00	0.09	0.09	0.00	0.07	0.08	0.00	0.08	0.08
Na	0.05	0.00	0.00	0.00	0.03	0.00	0.00	0.06	0.00	0.00
K	1.80	0.00	0.00	0.00	0.00	0.00	0.00	0.00	0.00	0.00
Total Cations	15.61	11.02	8.02	8.01	11.06	8.00	8.02	11.08	8.03	7.97
X_{Mg}	0.51	0.64	0.15	0.17	0.65	0.16	0.21	0.64	0.15	0.17
Mg:Fe	1.056	1.767	0.173	0.202	1.845	0.184	0.269	1.767	0.177	0.207

†Immediately adjacent to analyzed cordierite.

*Total Fe as FeO.

Ironstones

The specimens chosen for analysis (Tables 11, 12, 13) are nearly free of hydrous phases: sparse biotite occurs in section Y and minor grunerite and hornblende occur in sections Y and Z. Section X contains the assemblage Op-Fa-Qz-Ga-Mt in which orthopyroxene, fayalite and almandine garnet form a coarse symplectic intergrowth surrounding a pod of coarse grained quartz; magnetite grains occur throughout the slide. Section Y is mostly coarse grained granular fayalite and quartz in which smaller grains of orthopyroxene, grunerite, hornblende, biotite, and magnetite are scattered widely. Some magnetite inclusions in quartz have late reaction rims composed of radiating amphibole needles. Section Z shows alternating quartz-rich layers with finer grained fayalite and orthopyroxene inclusions, and quartz-poor layers consisting of coarse grained granular fayalite, orthopyroxene and poikiloblastic almandine garnet. Minor green hornblende occurs also, and granular magnetite is scattered throughout the slide.

Table 11 presents analyses of fayalite, orthopyroxene and garnet from section X. Rims and cores of two garnets were analyzed separately, but appear homogeneous (Table 14). Chemical data from minerals in two areas of section Y are shown in Table 12; fayalites and grunerites analyzed in both areas show no significant compositional changes. Analyses of fayalite, orthopyroxene, garnet, and hornblende from section Z are given in Table 13. Compositions of each phase are reported as averages of three grains from the section.

Table 10

Compositions of selected minerals in metapelitic rocks A, B and C

Garnet:	A1r	A1c	A2r	A2c	A3r	A3c	B1r	B1c	B2r	B2c	B3r	B3c	C1r	C1c	C2r	C2c	C3r	C3c
alm	75.7	70.7	75.2	69.1	75.0	74.2	80.1	77.9	79.8	78.0	82.0	77.5	80.8	79.7	81.1	75.7	81.0	80.4
py	20.1	24.8	20.4	26.0	19.8	21.2	14.3	15.3	14.3	15.8	11.8	15.0	14.0	16.1	14.9	20.4	14.4	16.6
spess	1.3	1.0	1.0	1.0	1.3	1.3	1.3	1.0	2.0	2.0	1.3	1.3	2.3	1.3	1.7	1.3	2.0	0.3
gross	2.9	3.5	3.4	3.9	3.9	3.3	4.3	5.8	3.9	4.2	4.9	6.2	2.9	2.9	2.3	2.6	2.6	2.7

Cordierite:		A1	A2	A3	B1	B1	B3	C1	C2	C3
Fe: (Fe+Mg+Mn)	29.6	30.0	29.9	36.9	35.5	35.4	36.1	35.1	36.1	
Mg: (Fe+Mg+Mn)	70.4	70.0	70.1	63.1	64.5	64.1	63.9	64.9	63.9	
Mn: (Fe+Mg+Mn)	0.0	0.0	0.0	0.0	0.0	0.5	0.0	0.0	0.0	

Biotite:		A	B	C
Fe: (Fe+Mg+Mn)		50.2	48.6	45.9
Mg: (Fe+Mg+Mn)		49.8	51.4	54.1
Mn: (Fe+Mg+Mn)		0.0	0.0	0.0

K feldspar:	A1r	A1c	A2r	A2c	A3r	A3c	B1r	B1c	B2r	B2c	C1r	C1c	C2r	C2c	C3r	C3c
Or	84.2	70.9	86.6	81.0	76.4	69.5	85.2	86.0	89.7	86.3	81.2	84.3	76.3	77.2	79.3	78.3
Ab	14.4	26.9	11.7	17.6	21.7	27.5	14.3	13.0	9.7	12.6	18.2	14.8	22.7	22.0	20.0	19.7
An	1.4	2.2	1.7	1.5	1.9	3.0	0.5	1.0	0.6	1.1	0.6	0.8	1.0	0.7	0.7	2.0
Ab: (Ab+An)	91.1	92.4	87.3	92.1	91.9	90.1	96.6	92.8	93.2	91.9	96.8	94.8	95.7	96.9	96.6	90.8

Plagioclase:	A1	A2	A3	B1r	B1c	B2r	B2c	B3	C1r	C1c	C2r	C2c	C3r	C3c
Ab	75.4	73.0	74.0	51.1	45.5	44.9	45.2	16.1	78.5	76.9	77.6	77.9	77.1	75.3
An	23.7	26.1	24.7	46.9	51.5	54.2	50.1	83.4	20.5	22.1	20.7	20.6	22.1	23.6
Or	0.9	0.9	1.3	2.0	2.9	0.9	4.7	0.5	1.0	1.0	1.6	1.5	0.8	1.2

Estimates of Metamorphic Conditions

Rocks exposed in the map area show no systematic mineral changes indicative of significant regional variations in climactic metamorphic conditions. The seven-phase assemblage Ga-Co-Bi-Si-Qz-Kf-Pc is widespread in metapelitic rocks, except in the northeast part of the map area where cordierite was not observed. Anatectic Kf-Pc-Qz neosome forms a subordinate component of most metapelitic rocks, but melting was incomplete because Kf-Pc-Qz mixtures occur in pelitic and psammitic paleosomes throughout the region. Muscovite was seen as an alteration of higher grade minerals. Only one wollastonite occurrence was found. Marbles and calcium-silicate rocks contain Di-Cc-Qz assemblages; tremolite occurs widely as an alteration of diopside. The assemblage grunerite, fayalite and quartz found in siliceous iron formation (specimen Y) indicates the metamorphic conditions reached the upper stability limit of grunerite; orthopyroxene, fayalite and quartz in specimens X and Z suggest that the conditions exceeded the stability limit of grunerite.

Seven-phase Assemblages

Figure 35 is a P_{total} versus T reaction grid applicable to metapelitic rocks A, B, and C. Widespread occurrence of the seven-phase assemblage Ga-Co-Bi-Si-Qz-Kf-Pc in the same outcrop with granitic neosome suggests that the metamorphic conditions were in the vicinity of the intersection of univariant reaction (4) producing garnet + cordierite and above the granite solidus curve. Presence of apparently unreacted Kf-Pc-Qz mixtures in many thin sections with cordierite, garnet and sillimanite suggests melting was incomplete.

Inspection of Figure 37 shows that if X_{H_2O}[1] = 1 the onset of water saturated melting occurs at least 50°C below the garnet + cordierite-forming reaction (4). However, with a fluid containing species other than H_2O the melting curve and reaction (4) overlap. Ubiquitous graphite in Penrhyn Group pelitic rocks indicates that any metamorphic fluid contained CO_2, CO, and CH_4 in addition to H_2O. In the presence of such a fluid phase, both the muscovite breakdown reaction (1) and the reaction producing garnet + cordierite (4) shift to lower T at constant P_{total} as X_{H_2O} decreases. Additionally, as X_{H_2O} decreases, the Kf-Pc-Qz-vapour solidus curve shifts to higher T at constant P_{total}; thus producing an overlapping of the initiation of melting of K feldspar, plagioclase and quartz mixtures, and formation of paleosomes containing garnet and cordierite.

For the garnet-cordierite-forming reaction (4) in Figure 35 X_{Mg}^{Co}[2] increases with increasing pressure and temperature. Based upon X_{Mg}^{Co} Lee and Holdaway (1977) calculated P_{total}, T, and X_{H_2O} for the assemblage Bi-Si-Qz-Co-Ga-Kf in equilibrium with granite melt (Fig. 36). They argued that if X_{H_2O} is not controlled externally by the environment, but is allowed to drop as small amounts of granite melt form and absorb water, cordierite, garnet, K feldspar, biotite, sillimanite, plagioclase, and quartz may all coexist with the melt (Lee and Holdaway, 1977). If equilibrium was closely approached in rocks A, B, and C, P_{total}, T, and X_{H_2O} can be estimated from the figure. The garnet-cordierite-forming reaction (1, Fig. 36) and the granite melt-forming reaction (2, Fig. 36) for various X_{H_2O} intersect in the steep heavy-dash line: vapour-absent melting in Bi-Si-Qz-Kf-Pc assemblages. Determination of X_{Mg}^{Co} in the assemblage (light-dash lines) establishes the unique conditions of T, P_{total}, and X_{H_2O} at which the seven-phase assemblage was in equilibrium with granite melt (Lee and Holdaway, 1977). From Figure 36, the assemblage in specimen A with average X_{Mg}^{Co} = 0.70 (Table 7) apparently formed at T = 710°C, P_{total} 5.2 kb and X_{H_2O} = 0.35, and the

[1] $X_{H_2O} = \frac{P_{H_2O}}{P_{total}}$

[2] X_{Mg}^{Co} = mole fraction $\frac{Mg}{Mg + Fe}$ in cordierite.

Table 11

Microprobe analyses of selected garnets, fayalites and orthopyroxenes in meta-ironstone specimen X. Analyses by M. Bonardi, Mineralogy Section, Geological Survey of Canada

	Fa	Op	Ga1		Ga2	
	(avg. of 4)	(avg. of 6)	rim	core	rim	core
SiO_2	30.29	47.55	36.88	36.65	36.76	36.55
Al_2O_3	0.00	0.80	19.73	19.84	19.68	19.59
TiO_2	0.06	0.08	0.00	0.08	0.00	0.04
Cr_2O_3	0.09	0.08	0.06	0.10	0.07	0.06
*FeO	66.82	45.99	37.73	37.86	37.32	37.50
MnO	0.06	0.06	0.15	0.19	0.07	0.09
MgO	2.08	5.42	1.23	1.29	1.16	1.16
CaO	0.00	0.41	4.55	4.12	4.56	4.60
Na_2O	0.00	0.04	0.05	0.21	0.02	0.00
K_2O	0.00	0.00	0.00	0.00	0.00	0.00
Total Wt. %	99.40	100.43	100.38	100.34	99.64	99.59
No. of oxygens	4	6	12	12	12	12
Si	1.01	1.99	3.01	2.99	3.01	3.00
Al	0.00	0.04	1.90	1.91	1.90	1.90
Ti	0.00	0.00	0.00	0.01	0.00	0.00
Cr	0.00	0.00	0.00	0.01	0.01	0.00
Fe	1.87	1.61	2.57	2.58	2.56	2.58
Mn	0.00	0.00	0.01	0.01	0.01	0.01
Mg	0.10	0.34	0.15	0.16	0.14	0.14
Ca	0.00	0.02	0.40	0.36	0.40	0.41
Na	0.00	0.00	0.01	0.04	0.00	0.00
K	0.00	0.00	0.00	0.00	0.00	0.00
Total Cations	2.98	4.00	8.05	8.07	8.03	8.04
X_{Mg}	0.05	0.17	0.06	0.06	0.05	0.05
Mg:Fe	0.053	0.211	0.058	0.062	0.055	0.054

*Total Fe as FeO.

assemblages in B and C with average $X_{Mg}^{Co} = 0.65$ apparently formed at T = 700°C, P_{total} = 4.9 kb and $X_{H_2O} = 0.4$. The differences in apparent conditions of formation of the three assemblages are not significant although sample localities A and C are transverse to the regional strike and 28 km apart (Fig. 33). Holdaway and Lee (1977) pointed out that Ga-Co geothermometry is subject to calibration errors, and may be incorrect by ± 50°C and ± 0.5 kb.

Retrograde Zoning in Garnet

Nine garnets analyzed in specimens A, B, and C have relatively homogeneous cores, but show Fe-enrichment and Mg-depletion of their rims (Table 10). The major zoning is between Mg and Fe (Alm + Py components average 95 per cent in the 18 analyses), but Mn-enrichment of garnet rims is shown by 5 analyses; one garnet shows Ca-enrichment, and seven show Ca-depletion of their rims. Cordierites in contact with garnets are unzoned and exhibit very little compositional variation between grains analyzed in the thin sections. Biotites are individually homogeneous and compositionally uniform in each thin section. Homogeneity of garnet interiors coupled with the restriction of zoning to the rims suggests that the garnets were homogenized at high metamorphic temperatures, and the rims re-equilibrated with cordierite and biotite by cation diffusion during cooling (Tracy, 1978).

The distribution of Fe and Mg between coexisting Ga-Bi and Ga-Co forms the basis of several calibrated geothermometers based on the temperature dependence of K, a distribution coefficient expressing the ratio of Mg/Fe in

Table 12

Microprobe analyses of selected grunerites, fayalites, orthopyroxenes, hornblendes and biotites from two parts of meta-ironstone specimen Y. Analyses by M. Bonardi, Mineralogy Section, Geological Survey of Canada

	Specimen Y1				Specimen Y2		
	Fa (avg. of 5)	Op (avg. of 3)	Gu (avg. of 2)	Hb (avg. of 3)	Fa (avg. of 4)	Gu (avg. of 4)	Bi (avg. of 6)
SiO_2	30.07	47.35	49.84	39.57	30.54	49.55	35.64
Al_2O_3	0.00	0.60	0.92	12.26	0.00	0.83	15.75
TiO_2	0.03	0.03	0.07	0.16	0.06	0.05	0.73
Cr_2O_3	0.09	0.08	0.08	0.04	0.08	0.05	0.00
*FeO	67.42	46.43	40.97	29.67	66.20	41.10	31.38
MnO	0.21	0.15	0.09	0.00	0.22	0.09	0.00
MgO	2.02	5.30	6.03	3.03	2.20	5.98	5.68
CaO	0.02	0.31	0.47	10.54	0.00	0.38	0.03
Na_2O	0.00	0.01	0.00	1.65	0.00	0.05	0.11
K_2O	0.00	0.00	0.00	1.26	0.00	0.00	8.65
Total Wt. %	99.86	100.26	98.47	98.18	99.30	98.08	97.97
No. of oxygens	4	6	23	23	4	23	22
Si	1.00	1.99	7.89	6.31	1.02	7.89	5.58
Al	0.00	0.03	0.17	2.31	0.00	0.15	2.91
Ti	0.00	0.00	0.01	0.02	0.00	0.01	0.09
Cr	0.00	0.00	0.01	0.01	0.00	0.01	0.00
Fe	1.88	1.63	5.42	3.96	1.84	5.47	4.11
Mn	0.01	0.01	0.01	0.00	0.01	0.01	0.00
Mg	0.10	0.33	1.42	0.72	0.11	1.42	1.32
Ca	0.00	0.01	0.08	1.80	0.00	0.07	0.00
Na	0.00	0.00	0.00	0.51	0.00	0.01	0.03
K	0.00	0.00	0.00	0.26	0.00	0.00	1.73
Total Cations	2.99	4.00	15.01	15.90	2.98	15.04	15.77
X_{Mg}	0.05	0.17	0.21	0.15	0.06	0.21	0.24
Mg:Fe	0.053	0.202	0.262	0.182	0.060	0.260	0.321

*Total Fe as FeO.

garnet to Mg/Fe in biotite or cordierite. The definitions of K used to estimate cation exchange equilibrium temperatures in this paper are

$$K_{Ga}^{Co} = \frac{(Mg/Fe)Co}{(Mg/Fe)Ga},$$

$$K_{Bi}^{Ga} = \frac{(Fe/Mg)Ga}{(Fe/Mg)Bi} \text{ (Nielsen, 1977), and}$$

$$K_{Bi}^{Ga} = \frac{(Mg/Fe)Ga}{(Mg/Fe)Bi} \text{ (Ferry and Spear, 1978).}$$

Table 15 reports temperatures for garnet cores and rims in specimens A, B, and C. The estimated equilibration temperatures of the cordierite-garnet touching pairs were determined from the expression of Nielsen (1977), pressures were estimated from the expression of Hutcheon et al. (1974) and from Figure 36 using Nielsen's temperatures and the average X_{Mg} of cordierite in each specimen (Tables 7, 8, and 9). The estimated equilibration temperatures of the garnets with coexisting biotite were calculated from the expressions of Nielsen (1977) and Ferry and Spear (1978).

Figure 37 summarizes the cordierite-garnet T-P results of Table 15 (pressures are from the method using Lee and Holdaway, 1977). Cores of analyzed garnets consistently show higher values than their rims. Specimens A and C indicate the highest garnet core values and specimen B indicates the lowest core values. The spread of T-P values shown in Figure 37 and Table 15 may not indicate the climactic conditions and the range of retrograde equilibration conditions of the rocks because it is very unlikely that the exact centres of the garnets were cut by the thin sections. Coexisting mineral rim compositions would not be dependent upon thin section positioning and therefore may be expected to estimate lower equilibration limits satisfactorily.

Table 14

Compositions of selected minerals in meta-ironstones X, Y and Z

Olivine:	X	Y_1	Y_2	Z
Fa	94.9	94.5	93.9	93.4
Fo	5.1	5.0	5.6	6.1
Te	0.0	0.5	0.5	0.5

Orthopyroxene:	X	Y_1		2
Of	81.7	82.3		81.2
En	17.3	16.7		17.3
Wo	1.0	0.5		1.0
Rh	0.0	0.5		0.5

Grunerite:		Y_1	Y_2	
Fe: (Fe+Mg+Mn)		79.1	79.3	
Mg: (Fe+Mg+Mn)		20.7	20.6	
Mn: (Fe+Mg+Mn)		0.2	0.1	

Hornblende:		Y_1		Z
$(Al)^4$: (Na+K)		0.63:0.68		0.62:0.77
Fe: (Fe+Mg+Mn)		84.6		83.6
Mg: (Fe+Mg+Mn)		15.4		16.4
Mn: (Fe+Mg+Mn)		0.0		0.0

Garnet:	XGa1 (rim)	(core)	XGa2 (rim)	(core)			Z
alm	82.1	83.0	82.3	82.1			79.4
peg	4.8	5.1	4.5	4.5			2.9
spess	0.3	0.3	0.3	0.3			1.9
gross	12.8	11.6	12.9	13.1			15.8

Biotite:				Y_2	
Fe: (Fe+Mg+Mn)				76.0	
Mg: (Fe+Mg+Mn)				24.0	
Mn: (Fe+Mg+Mn)				0.0	

Grunerite-fayalite-orthopyroxene-quartz Assemblages

The paragenesis of iron-rich olivine, orthopyroxene, and amphibole has been studied experimentally, and some of the results provide data to estimate equilibration temperatures and pressures of these minerals in meta-ironstone specimens X, Y and Z. Popp et al. (1977) determined that the assemblage cummingtonite-grunerite, fayalite, orthoferrosilite, quartz is invariant at T = 715°C, $P_{total} = P_{H_2O}$ = 2 kb and P_{O_2} determined by the FMQ oxygen buffer. Forbes (1977) who studied the breakdown of grunerite determined that grunerite was stable with fayalite and quartz at T = 690 ± 15°C, $P_{total} = P_{H_2O}$ = 2 kb and P_{O_2} determined by the FMQ oxygen buffer. Forbes' (1977) results indicated that grunerite decomposition temperatures increase about 12°C/kb from $P_{total} = P_{H_2O}$ = 0.5 to 3 kb. These experimental results suggest maximum stability limits of the grunerites studied: if P_{H_2O} were less than P_{total}, the upper stability limits would be reduced. The quantitative effect of Mg solid-solution on the stability of cummingtonite-grunerite is unknown but may be expected to raise the breakdown temperature at a given pressure. Smith (1971) determined experimentally that as pressure rises more iron-rich orthopyroxene is stable with olivine and quartz; he suggested that X_{Fe} in orthopyroxene was a potentially useful geobarometer provided an independent temperature estimate could be made. Jaffe et al. (1978) constructed a P-T grid showing orthopyroxene compositions stable with olivine and quartz based on the experimental work of Smith (1971), Lindsley (1965), and Bohlen et al. (1978).

Figure 38 is a P-T diagram showing the grunerite breakdown curve of Forbes (1977), and the compositions of orthopyroxene in equilibrium with olivine and quartz (after Jaffe et al., 1978). Grunerite in specimen Y occurring with olivine, orthopyroxene ($Of_{82.3}$), magnetite, and quartz suggests the maximum equilibration temperature and pressure of the assemblage was 720°C and 4.6 kb. Grunerite is absent from specimens X and Z, suggesting higher equilibration conditions, although the orthopyroxene compositions (Of_{81} and $Of_{81.2}$) are slightly less iron-rich than specimen Y (see Table 13). Specimen localities X, Y, and Z are spaced within 10 km of each other near the west margin of the Lyon Inlet area, and more than 40 km west of specimen localities A, B, and C (Fig. 33).

Table 13

Microprobe analyses of selected garnets, fayalites, orthopyroxenes, and hornblendes in meta-ironstone specimen Z. Analyses by M. Bonardi, Mineralogy Section, Geological Survey of Canada

	Fa (avg. of 3)	Op (avg. of 3)	Ga (avg. of 3)	Hb (avg. of 3)
SiO_2	30.32	47.36	37.14	40.23
Al_2O_3	0.00	0.73	19.82	12.15
TiO_2	0.05	0.07	0.04	0.49
Cr_2O_3	0.08	0.07	0.07	0.02
*FeO	66.14	45.82	36.43	29.22
MnO	0.39	0.38	0.86	0.01
MgO	2.51	5.49	0.75	3.21
CaO	0.00	0.49	5.59	10.45
Na_2O	0.00	0.02	0.00	1.49
K_2O	0.00	0.00	0.00	1.06
Total Wt. %	99.49	100.41	100.67	98.33
No. of oxygens	4	6	12	23
Si	1.01	1.98	3.02	6.37
Al	0.00	0.04	1.90	2.26
Ti	0.00	0.00	0.00	0.06
Cr	0.00	0.00	0.00	0.00
Fe	1.84	1.60	2.47	3.87
Mn	0.01	0.01	0.06	0.00
Mg	0.12	0.34	0.09	0.76
Ca	0.00	0.02	0.49	1.77
Na	0.00	0.00	0.00	0.46
K	0.00	0.00	0.00	0.22
Total Cations	2.98	3.99	8.03	15.77
X_{Mg}	0.06	0.18	0.04	0.16
Mg:Fe	0.065	0.213	0.036	0.196

*Total Fe as FeO.

Discussion of Estimates of Metamorphic Conditions

The garnet-cordierite and garnet-biotite Fe-Mg exchange geothermometry (Table 15) suggests the climactic temperature for metapelitic specimen A may have been between 733 and 841°C, and the pressure may have exceeded 5.4 kb. The 841°C maximum temperature listed in Table 15 was estimated with Ferry and Spear's Ga-Bi geothermometer; the same garnet core gave 749°C with Nielsen's Ga-Bi geothermometer, and gave 733°C with Nielsen's Ga-Co geothermometer. Nielsen's Ga-Bi calibration may be more realistic for Lyon Inlet area rocks than Ferry and Spear's because he (Nielsen, 1977) considered the effect of minor amounts of other elements on Fe-Mg partitioning. The presence of green spinel and sillimanite in cordierites of specimen A suggests the climactic temperature in the rock

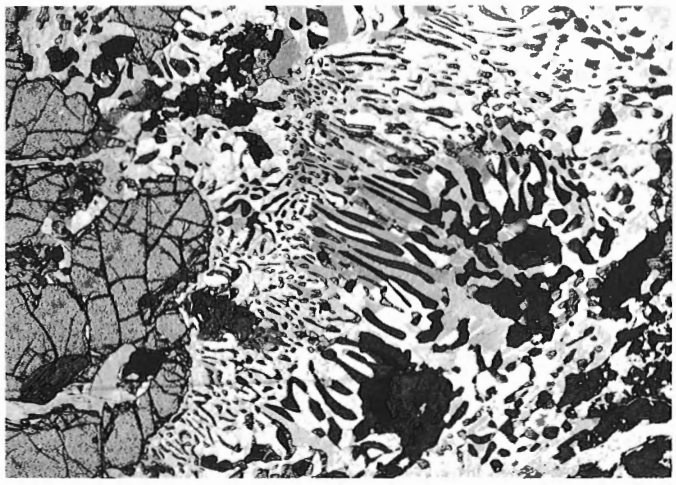

Figure 34. *Symplectic intergrowth of hornblende, hypersthene, plagioclase and garnet (large fractured grain). Partly crossed nichols. Width of photo area is 5 mm. (GSC 202949-P)*

reached the stability limit of the cordierite. Experiments by Holdaway and Lee (1977) indicated that Fe cordierite breaks down to hercynite, sillimanite, and quartz above 770°C at 3 kb $P_{H_2O} = P_{total}$.

Maximum temperatures and load pressures much in excess of 710°C and 5.2 kb are not consistent with the conclusions of Lee and Holdaway (1977) on the buffering effect of granite melt on temperature and P_{H_2O}. Their argument that X_{H_2O} is fixed locally by breakdown of biotite and absorption of water into local anatectic melts is supported by petrographic evidence from Penrhyn Group rocks: widespread occurrences of all of the solid phases in the six-phase reaction assemblage Bi-Si-Qz-Co-Ga-Kf-H_2O (Fig. 35, reaction 4), along with both Kf-Pc-Qz neosome and apparently unmelted Pc-Kf-Qz-Bi-Si mixtures, indicates that P_{H_2O} was variable, and temperature and time were inadequate to allow complete reactions to occur. For meta-ironstone specimen Y, the complete solid-phase reaction assemblage grunerite-fayalite-orthopyroxene-quartz (Fig. 38) suggests maximum equilibration conditions were near 720°C and 4.6 kb; orthopyroxene-fayalite-quartz mixtures in specimens X and Z indicate equilibration conditions coincident with specimen Y.

Widespread occurrence of scalloped and embayed garnets mantled by cordierite and quartz (Fig. 34) suggests that some cordierite formed at the expense of earlier garnet: possibly according to the reaction Ga + Si + Qz + $H_2O \rightleftharpoons$Co (reaction 3, Fig. 35). This retro-grade metamorphism is distinct from the pervasive partial alteration of high grade minerals to fine grained muscovite, epidote, actinolite, chlorite and prehnite, which signifies even lower grade conditions.

Ages of Metamorphism

Table 16 presents results of radiometric studies done on rocks from the Lyon Inlet area by the Geological Survey of Canada. Two apparent ages of batholithic magmatism in the Lyon Inlet area are indicated: 1) a 2727 Ma concordia zircon age of layered granitoid gneiss, and 2) a 2584 Ma concordia zircon age of quartz diorite augen gneiss as well as a 2527 Ma concordia zircon age of quartz monzonite augen gneiss. A 2493 Ma Rb-Sr isochron age of layered granitoid gneiss may mark the time of the Kenoran metamorphic thermal climax in the region. The granitoid gneisses appear to intrude Prince

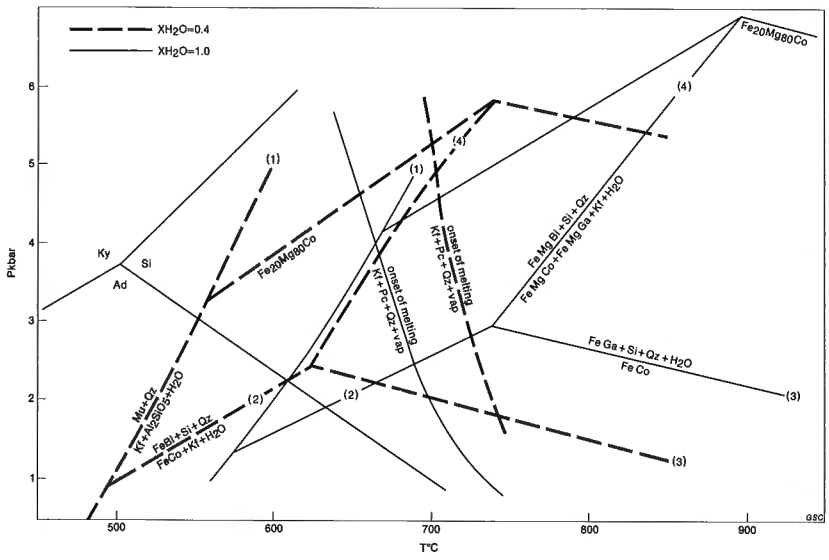

Figure 35. *P versus T diagram showing cordierite, garnet, Al_2SiO_5 and granite melt forming reactions in peraluminous rocks at $X_{H_2O} = 1.0$ and 0.4 (after Nielsen, 1978, based on data of Holdaway, 1971, Holdaway and Lee, 1977, and Lee and Holdaway, 1977). Widespread occurrence in the Lyon Inlet area of metapelitic rocks containing the seven-phase assemblage Bi-Si-Ga-Co-Kf-Pc-Qz requires that the paleosomes equilibrated with a vapour deficient in H_2O. Note that increasing pressure stabilizes more Mg-rich cordierite with garnet, biotite, sillimanite and quartz (reactions 2 and 3). See text for discussion and Table 6 for mineral abbreviations.*

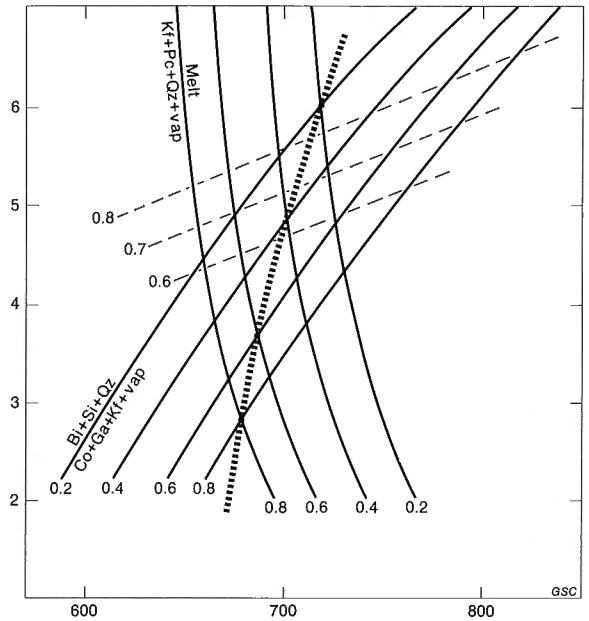

Figure 36. *Stability relations of seven-phase Bi-Si-Ga-Co-Kf-Pc-Qz assemblages (after Lee and Holdaway, 1977). The solid lines are calculated P-T curves for the reactions (1) Bi + Si + Qz ⇌ Co + Ga + Kf + vap., and (2) Kf + Pc + Qz + vap. ⇌ melt at $0.2 \leq X_{H_2O} \leq 0.8$. The light-dashed lines show the X_{Mg}^{Co} stable with the assemblage in reaction (1) at various X_{H_2O}. The steep heavy-dashed line shows vapour-absent melting of Kf-Pc-Qz-Bi-Si mixtures. A rock with the seven-phase Bi-Si-Ga-Co-Kf-Pc-Qz assemblage crystallized near the intersection of its cordierite composition line and the heavy-dashed line. See text for application to specimens A, B, and C.*

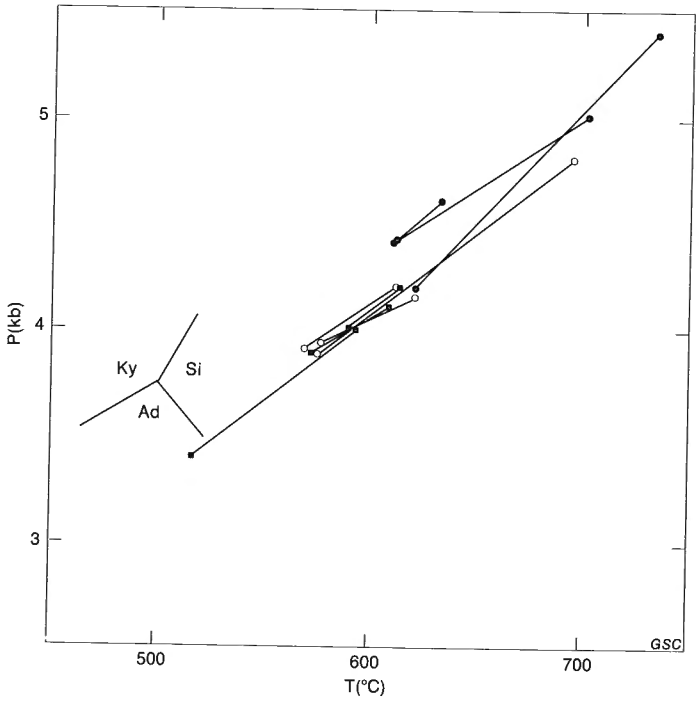

Figure 37. *Apparent retrograde P-T zoning of garnets indicated by Fe-Mg exchange between touching-pairs of garnet and cordierite grains in metapelitic rocks A, B, and C. The lines connect P-T calibrated Fe:Mg exchange ratios (Table 15) between Ga_{core}-Co (high T-P) and Ga_{rim}-Co (low T-P). The Al_2SiO_5 triple-point (after Holdaway, 1971) is shown for reference. Values plotted are derived from the temperature calibration of Nielsen (1977), and pressure data of Lee and Holdaway (1977). Solid circles are garnet-cordierite from spec. A, open circles are from B, and solid squares are from C. See text for discussion.*

Albert Group rocks whose time of formation is indicated by a 2953 Ma concordia zircon age of leucocratic orthogneiss from the group. Amphibole from Prince Albert Group leucocratic (metavolcanic?) gneiss indicates a 2657 Ma K-Ar cooling age which is surprising considering that the high grade of metamorphism suffered by nearby meta-ironstone is believed to be Hudsonian.

A Rb-Sr whole rock isochron age as well as the rest of the K-Ar mineral ages indicate that the Hudsonian regional metamorphism reached its thermal climax about 1804 Ma ago in the map area. The Rb-Sr isochron age of 1804 ± 16 Ma for Penrhyn Group pelitic rocks is somewhat older than the three hornblende K-Ar cooling ages from Archean basement granites. Biotite K-Ar cooling ages are slightly younger than the hornblende ages. One $^{207}Pb/^{206}Pb$ sphene age of 1734 Ma from Penrhyn Group paragneiss falls in the range of hornblende ages.

The youngest ages listed in Table 16 (1619 Ma biotite K-Ar, 1522 Ma muscovite K-Ar) are from a postkinematic granitic pluton intruding Penrhyn Group paragneiss. These are postcrystallization cooling ages.

Table 15

Temperature (°C) and pressure (kb) estimates of cordierite-garnet and biotite-garnet Fe:Mg partitioning in metapelitic rocks A, B and C, Lyon Inlet area

	Cordierite-Garnet				Biotite-Garnet		
Specimen		T(N)[1]	P(L)[2]	P(H)[3]		T(N)[1]	T(F)[4]
A	Co_1-Ga_1 (rim)	609	4.4	3.8	Bi-Ga_1 (rim)	631	666
	Co_1-Ga_1 (core)	701	5.1	4.6	Bi-Ga_1 (core)	723	800
	Co_2-Ga_2 (rim)	621	4.2	3.9	Bi-Ga_2 (rim)	636	671
	Co_2-Ga_2 (core)	733	5.4	4.9	Bi-Ga_2 (core)	749	841
	Co_3-Ga_3 (rim)	609	4.4	3.8	Bi-Ga_3 (rim)	629	663
	Co_3-Ga_3 (core)	634	4.6	4.1	Bi-Ga_3 (core)	653	697
B	Co_1-Ga_1 (rim)	589	4.0	3.3	Bi-Ga_1 (rim)	569	580
	Co_1-Ga_1 (core)	615	4.2	3.5	Bi-Ga_1 (core)	593	613
	Co_2-Ga_2 (rim)	573	3.9	3.2	Bi-Ga_2 (rim)	570	581
	Co_2-Ga_2 (core)	608	4.1	3.5	Bi-Ga_2 (core)	603	625
	Co_3-Ga_3 (rim)	517	3.4	2.8	Bi-Ga_3 (rim)	516	509
	Co_3-Ga_3 (core)	594	4.0	3.4	Bi-Ga_3 (core)	589	606
C	Co_1-Ga_1 (rim)	570	3.8	3.2	Bi-Ga_1 (rim)	545	547
	Co_1-Ga_1 (core)	615	4.2	3.5	Bi-Ga_1 (core)	584	601
	Co_2-Ga_2 (rim)	575	3.9	3.3	Bi-Ga_2 (rim)	560	568
	Co_2-Ga_2 (core)	695	4.8	4.3	Bi-Ga_2 (core)	668	720
	Co_3-Ga_3 (rim)	576	3.9	3.3	Bi-Ga_3 (rim)	550	555
	Co_3-Ga_3 (core)	622	4.2	3.7	Bi-Ga_3 (core)	591	610

[1] Nielsen (1977).

[2] Lee and Holdaway (1977).

[3] Hutcheon et al. (1974).

[4] Ferry and Spear (1978).

ECONOMIC GEOLOGY

During mapping of the Lyon Inlet area no mineral deposits of potential economic importance were encountered. Occurrences of magnetic iron formation in the Prince Albert Group are a few metres wide and extend a few hundred metres along strike. Magnetite generally constitutes less than 30 per cent of the rock; the other major minerals are quartz and amphiboles. Rusty-weathering graphite-sulphide-biotite-quartz-feldspar gneiss is common near the base of the Penrhyn Group (map unit APr). Limonite-capped gossans associated with the graphitic paragneiss contain pyrite and pyrrhotite veins in a white, sugary quartz matrix beneath a hard yellow caprock. Water seeping from the gossans is very acidic and bedrock down slope is iron stained.

Aquitaine Canada Limited conducted a search for base metals in Penrhyn Group rocks in the map area between 1970 and 1973. Results of their work are available in assessment reports filed with the Department of Indian and Northern Affairs, Ottawa. The company concluded that the various electrical, magnetic and electromagnetic surveys employed showed a direct correlation with graphitic and pyrrhotitic rocks, and failed to give sufficiently specific targets for the valuable base metals sought. Shallow drilling at one location (DUC claims) in graphite-pyrrhotite schist showed that the metasedimentary host-rock contained inconspicuous sphalerite (up to 8 per cent) associated with graphite and minor chalcopyrite.

The Lyon Inlet area composes part of a National Geochemical Reconnaissance survey of lake sediments and waters (Geological Survey of Canada, 1978a, b), and an airborne radiometric survey carried out under the Uranium Reconnaissance Program. Limited follow-up ground work was done by Cameron (1979) and Maurice (1979). Among the more interesting features of the data were extensive, strong and coincident Zn and Ni anomalies (Cameron, 1979). Cameron's (1979) follow-up investigations showed widespread Zn- and Ni-bearing mineralization in sulphidic-graphitic paragneiss (map unit APr). The metals occur in sphalerite and pentlandite. Also, lesser amounts of Cu, Pb, Ag, and Au were found locally. Cameron (1979) concluded that recent oxidation of base metal sulphides has been intense, and has removed all but traces of these minerals from surface exposures, thus making evaluation of the mineralization difficult.

Maurice (1979) concluded that the reconnaissance lake sediment results showed southern Melville Peninsula to be considerably enriched in uranium compared to most other areas of the Canadian Shield covered by similar surveys. He further concluded that the highest uranium values follow the Penrhyn Group rocks. In the ground follow-up he discovered a source of radioactivity to be granitic plutons (map unit Ag) intruding Penrhyn Group marble and pelitic gneiss. The metasediments in contact with the granite were not radioactive. Readings equivalent to about 2000 ppm uranium were recorded in the field (Maurice, 1979).

Table 16

Summary of radiometric studies of Lyon Inlet area rocks

Lithostratigraphic Unit	(Map unit)	Dating Method	Apparent age (Ma)	Interpretation
Prince Albert Group leucocratic quartzofeldspathic gneiss	(AAln)	Concordia zircon	2953 ± 52	Age of acid volcanism or maximum age of Prince Albert Group
		K-Ar hornblende	2657 ± 143	Argon retention age
		K-Ar biotite	1601 ± 40	Argon retention age
Layered granite to granodiorite gneiss	(Agdn)	Concordia zircon	2727 ± 33	Age of batholithic magmatism
		Rb-Sr isochron*†	2493 ± 86	Age of Kenoran metamorphic thermal climax
		K-Ar hornblende	1758 ± 51	Argon retention age
		K-Ar biotite	1595 ± 48	Argon retention age
		K-Ar biotite	1591 ± 48	Argon retention age
Quartz monzonite augen gneiss	(Aqmn)	Concordia zircon	2527 ± 10	Age of batholithic magmatism
		K-Ar hornblende	1729 ± 50	Argon retention age
		K-Ar biotite	1649 ± 40	Argon retention age
Quartz diorite augen gneiss	(Aqdn)	Concordia zircon	2584 $^{+104}_{-83}$	Age of Kenoran magmatism
		K-Ar hornblende	1687 ± 221	Argon retention age
		K-Ar biotite	1637 ± 50	Argon retention age
Penrhyn Group pelitic gneiss	(APn)	Rb-Sr isochron⊕	1804 ± 16	Age of Hudsonian metamorphic thermal climax
		$^{207}Pb/^{206}Pb$ sphene	1734	Hudsonian metamorphic cooling age
Granite	(Ag)	K-Ar biotite	1624 ± 40	Argon retention age
		K-Ar muscovite	1528 ± 39	Argon retention age

*$\lambda^{87}Rb = 1.42 \times 10^{-11}\ a^{-1}$.

†$Sr_i = 0.7070 \pm 0.0016$.

⊕$Sr_i = 0.7209 \pm 0.0010$.

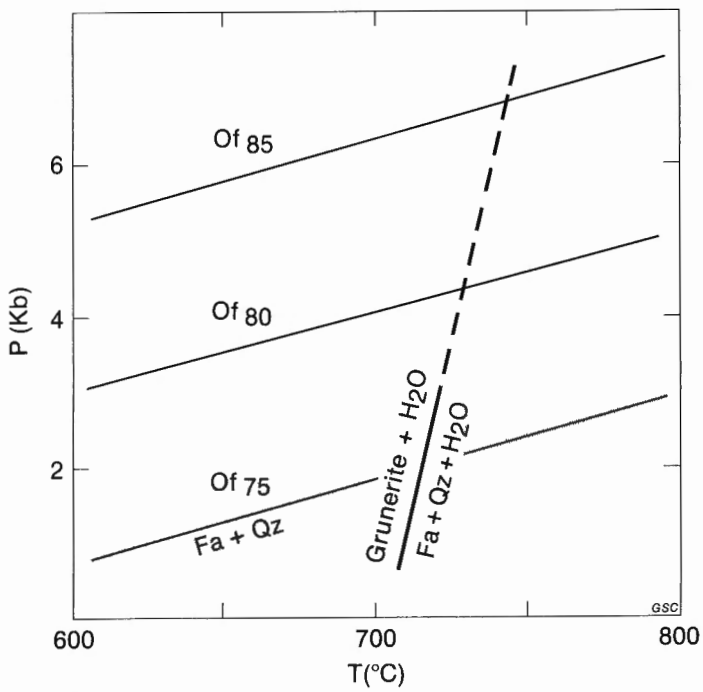

Figure 38. *P versus T diagram, showing grunerite breakdown conditions (after Forbes, 1977) and isopleths showing the compositions of orthopyroxene in equilibrium with olivine and quartz (after Jaffe et al., 1978). The coexistence in meta-ironstone specimen Y of grunerite-fayalite-orthopyroxene ($Of_{82.3}$)-quartz-magnetite indicates that the assemblage equilibrated at $T \leq 730°C$ and $P \leq 4.9$ kb.*

SUMMARY

Some inferences drawn from field and laboratory data presented in this report may be summarized.

1. Prince Albert Group, a eugeoclinal assemblage of greywacke, volcanic rocks, and iron formation, is about 2953 Ma old; older basement rocks have not been identified in the Lyon Inlet area.
2. Granitoid batholiths, intruded 2727, 2584 and 2527 Ma ago, and metamorphosed 2493 Ma ago, compose most of the basement on which Aphebian sediments were deposited.
3. Penrhyn Group sedimentation occurred between 2493 and 1804 Ma ago.
4. The preserved Aphebian sedimentary sequence is miogeoclinal; a discontinuous regolith and blanket quartz sand is overlain by a lower siliceous carbonate sequence deposited in hypersaline water, and an upper fine grained carbonaceous clastic sequence enriched in Zn and Ni deposited in stagnant water.
5. Penrhyn Group was deformed at least twice. The earliest structures recognized compose fold and thrust nappes; the last penetrative deformation, characterized by elongation of the rocks parallel to the strike of the belt, produced paraboloidal folds. The present northeast-southwest trend of the fold belt resulted from the strong horizontal elongation in that direction, and bears no a priori relationship to the orientation of the Aphebian sedimentary basin.

6. The Hudsonian metamorphic culmination occurred about 1804 Ma ago, after penetrative deformation ceased. The climactic conditions were essentially the same throughout the map area: they apparently were 700-749°C, $4.0 < P_{total} < 5.4$ kb, $0.4 \leq P_{H_2O} \leq 1.0$, and low P_{O_2}. Retrograde Fe-Mg re-equilibration of garnet with cordierite and biotite occurred until about 600°C and 4 kb total pressure.

7. During the Neohelikian or Hadrynian the rocks in the region were fractured, faulted and intruded by diabase dykes along steeply dipping northwest-southeast-striking surfaces.

8. By late Middle Ordovician the region had been denuded to the present level and shelf-type carbonate sediments were deposited on an erosion surface with several hundred metres of local relief.

9. The present climate of the region promotes oxidation and leaching of base metal sulphides from exposed rocks. Abundant gossans in Penrhyn Group graphitic gneiss contain relatively insoluble secondary iron oxides, iron sulphides, and quartz which discourage surface prospecting. Downstream lake waters and sediments are enriched in Zn, Ni, and Cu.

REFERENCES

Bohlen, S.R., Boettcher, A.L., and Essene, E.J.
1978: Experimental reinvestigation of ferrosilite-fayalite-quartz stability (abstract); EOS, v. 59, p. 402.

Bolton, T.E., Sanford, B.V., Copeland, M.J., Barnes, C.R., and Rigby, J.K.
1977: Geology of Ordovician Rocks, Melville Peninsula and Region, Southeastern District of Franklin; Geological Survey of Canada, Bulletin 269, 137 p.

Cameron, E.M.
1979: Investigation of base metal mineralization in Proterozoic metasediments, Melville Peninsula, N.W.T.; in Current Research, Part A, Geological Survey of Canada, Paper 79-1A, p. 187-196.

Carey, S.W.
1962: Folding; Journal of Alberta Society of Petroleum Geologists, v. 10, p. 95-144.

Fahrig, W.F. and Jones, D.L.
1969: Paleomagnetic evidence for the extent of Mackenzie igneous events; Canadian Journal of Earth Sciences, v. 6, p. 679-688.

Fahrig, W.F., Irving, E., and Jackson, G.D.
1971: Paleomagnetism of the Franklin diabases; Canadian Journal of Earth Sciences, v. 8, p. 455-467.

Ferry, J.M. and Spear, F.S.
1978: Experimental calibration of the partitioning of Fe and Mg between biotite and garnet; Contributions to Mineralogy and Petrology, v. 66, p. 113-117.

Forbes, W.C.
1977: Stability relations of grunerite, $Fe_7Si_8O_{22}(OH)_2$; American Journal of Science, v. 277, p. 735-749.

Geological Survey of Canada
1978a: National Geochemical Reconnaissance Release, regional lake sediment and water geochemical reconnaissance data, Melville Peninsula, N.W.T., NGR 32A-1977 or 32B-1977, NTS 46 N and part of 47 B; Geological Survey of Canada, Open File 521A or 521B.

Geological Survey of Canada (cont.)
1978b: National Geochemical Reconnaissance Release, regional lake sediment and water geochemical reconnaissance data, Melville Peninsula, N.W.T., NGR 33A-1977 or 33B-1977, NTS 46 O-P and part of 47 A; Geological Survey of Canada, Open File 522A or 522B.

Henderson, J.R., Reesor, J.E., LeCheminant, A.N., Hutcheon, I., and Miller, A.
1976: Geological maps of Penrhyn Group, Melville Peninsula, N.W.T.; Geological Survey of Canada, Open File 307.

Heywood, W.W.
1967: Geological notes, northeastern District of Keewatin and southern Melville Peninsula, District of Franklin, Northwest Territories (Parts of 46, 47, 56, 57); Geological Survey of Canada, Paper 66-40, 20 p.

Hobbs, B.E., Means, W.D., and Williams, P.F.
1976: An Outline of Structural Geology; John Wiley and Sons, Inc., Toronto, New York, London, 571 p.

Hoffman, P.
1973: Evolution of an early Proterozoic continental margin: the Coronation geosyncline and associated aulacogens of the northwestern Canadian Shield; Philosophical Transactions, Royal Society of London, A 273, p. 547-581.

Holdaway, M.J.
1971: Stability of andalusite and the aluminum silicate phase diagram; American Journal of Science, v. 271, p. 97-131.

Holdaway, M.J. and Lee, S.M.
1977: Fe-Mg cordierite stability in high-grade pelitic rocks based on experimental, theoretical and natural observations; Contributions to Mineralogy and Petrology, v. 63, p. 175-198.

Hutcheon, I., Froese, E., and Gordon, T.M.
1974: The assemblage quartz-sillimanite-garnet-cordierite as an indicator of metamorphic conditions in the Daly Bay Complex, N.W.T.; Contributions to Mineralogy and Petrology, v. 44, p. 29-34.

Hutcheon, I.E., Gunter, A.E., and LeCheminant, A.N.
1977: Serendibite from Penrhyn Group marble, Melville Peninsula, District of Franklin; Canadian Mineralogist, v. 15, p. 108-112.

Jackson, G.D.
1971: Operation Penny Highlands, south-central Baffin Island; Geological Survey of Canada, Paper 71-1, Part A, p. 138-140.

Jackson, G.D. and Taylor, F.C.
1972: Correlation of major Aphebian rock units in the northeastern Canadian Shield; Canadian Journal of Earth Sciences, v. 9, no. 12, p. 1650-1669.

Jaffe, H.W., Robinson, P., and Tracy, R.J.
1978: Orthoferrosilite and other iron-rich pyroxenes in microperthite gneiss of the Mount Marcy area, Adirondack Mountains; American Mineralogist, v. 63, p. 1116-1136.

Lambert, M.B. and Reesor, J.E.
1974: A format for field and laboratory data collection; Geological Survey of Canada, Paper 74-60, p. 35-40.

Lee, S.M. and Holdaway, M.J.
1977: Significance of Fe-Mg cordierite stability relations on temperature, pressure and water pressure in cordierite granulites; American Geophysical Union, Geophysical Monograph 20, p. 79-84.

Lindsley, D.H.
1965: Ferrosilite; Carnegie Institute of Washington Yearbook, 64, p. 148-150.

Mackin, J.H.
1950: Studies for students: the down-structure method of viewing geological maps; Journal of Geology, v. 58, no. 1, p. 55-72.

Maurice, Y.T.
1979: A preliminary assessment of the uranium potential of southern Melville Peninsula, N.W.T.; in Current Research, Part A, Geological Survey of Canada, Paper 79-1A, p. 281-287.

Nielsen, P.A.
1977: Mineralogy and metamorphic petrology of the Arseno Lake area, N.W.T.; unpublished Ph.D. thesis, University of Alberta.

1978: Metamorphism of the Arseno Lake area, Northwest Territories; in Metamorphism in the Canadian Shield, Geological Survey of Canada, Paper 78-10, p. 115-122.

Nockolds, S.R.
1954: Average chemical compositions of some igneous rocks; Geological Society of America, Bulletin 65, p. 1007-1032.

Okulitch, A.V., Gordon, T.M., Henderson, J.R., Reesor, J.E., and Hutcheon, I.E.
1977: Geology of the Barrow River map-area, Melville Peninsula, District of Franklin; in Report of Activities, Part A, Geological Survey of Canada, Paper 77-1A, p. 213-215.

Okulitch, A.V., Gordon, T.M., Henderson, J.R., Hutcheon, I.E., and Turay, M.
1978: Geology of the Barrow River and Hall Lake map-areas, Melville Peninsula, District of Franklin; in Current Research, Part A, Geological Survey of Canada, Paper 78-1A, p. 159-161.

Plant, A.G. and Lachance, G.R.
1973: Quantitative electron microprobe analysis using an energy dispersive spectrometer; Proceedings of the Eighth National Conference on Electron Probe Analysis (New Orleans), Paper 13.

Popp, R.K., Gilbert, M.C., and Craig, J.R.
1977: Stability of Fe-Mg amphiboles with respect to oxygen fugacity; American Mineralogist, v. 62, p. 1-12.

Preto, V.A.G.
1970: Amphibolites from the Grand Forks Quadrangle of British Columbia; Geological Society of America, Bulletin 81, p. 763-782.

Ramberg, H.
1967: Gravity, Deformation and the Earth's Crust; Academic Press, New York and London, 214 p.

Ray, S.K.
1974: Inversion of fold-hinge in superposed folding: an example from the Precambrian of central Rajasthan, India; Precambrian Research, v. 1, p. 157-164.

Tracy, R.J.
1978: High grade metamorphic reactions and partial melting in pelitic schist, west-central Massachusetts; American Journal of Science, v. 278, p. 150-178.

Turner, F.J.
1968: Metamorphic Petrology; McGraw-Hill, New York.

Winkler, H.G.F.
1974: Petrogenesis of Metamorphic Rocks, 3rd edition; Springer-Verlag, New York.

Energy, Mines and Resources Canada
Énergie, Mines et Ressources Canada